

# TRANSFER OF POLARIZED RADIATION IN ASTROPHYSICAL CONTEXT

*A Thesis*  
*submitted for the degree of*  
*DOCTOR OF PHILOSOPHY*

*In*  
*The Faculty of Science*

Bangalore University  
Bangalore

By  
SUJAN KUMAR SENGUPTA

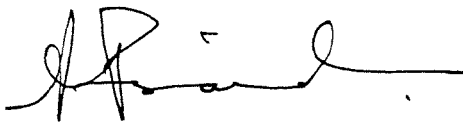


Indian Institute of Astrophysics  
Bangalore 560 034, India

*July 1996*

## DECLARATION

*I hereby declare that the matter embodied in this thesis is the result of the investigations carried out by me in the Indian Institute of Astrophysics, Bangalore, under the supervision of Professor A. Peraiah and has not been submitted for the award of any degree, diploma, associateship, fellowship, etc. of any university or institute.*



Prof. A. Peraiah  
*(Thesis supervisor)*

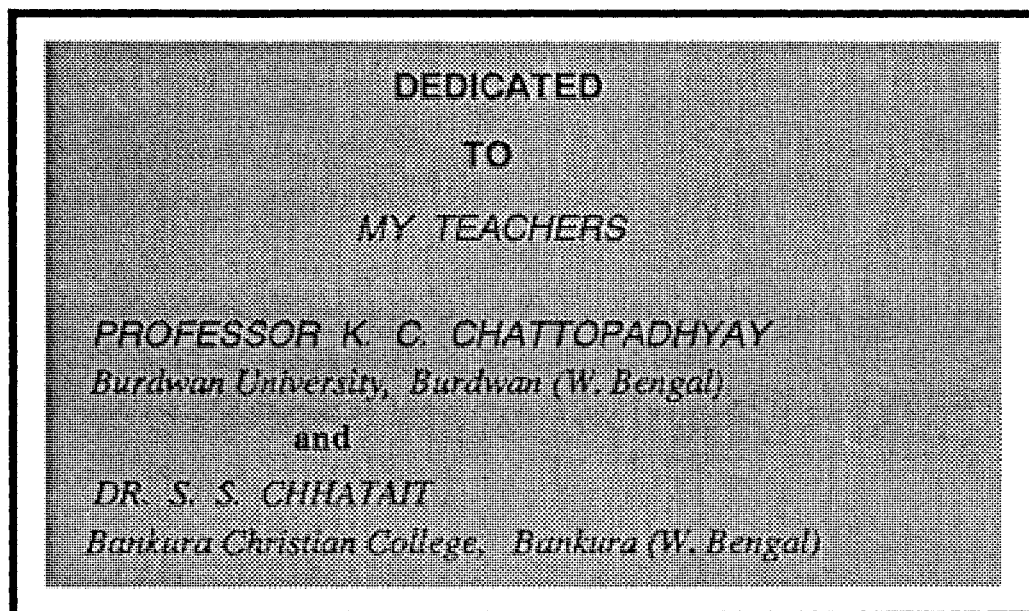


Sujan Kumar Sengupta  
*(Ph. D. Candidate)*

*Indian Institute of Astrophysics*

*Bangalore 560 034*

*16 JULY 1996*



YOU HAVE FLAGGED OFF MY JOURNEY AND

I HAVE MILES TO GO

**THIS WORK IS FINANCIALLY SUPPORTED**

*BY*

**COUNCIL OF SCIENTIFIC AND INDUSTRIAL RESEARCH  
NEW DELHI – 110 012, INDIA**

*UNDER*

**JUNIOR RESEARCH FELLOWSHIP SCHEME**

*AND*

**SENIOR RESEARCH FELLOWSHIP SCHEME**

**NO. 9 / 561 (2) / 90 EMR – I**

## ACKNOWLEDGEMENTS

*In the preface of his famous book *The Selfish Gene*, Richard Dawkins wrote "I recently learned a disagreeable fact: there are influential scientists in the habit of putting their names to publications in whose composition they have played no part. .... For all I know, entire scientific reputations may have been built on the work of students and colleagues!" If Dr. Dawkins' view is a fact of scientific community then I must say that in the very beginning of my research career I have come into touch with an exceptional scientist, my thesis supervisor Professor A. Peraiiah who provided me a very careful guidance throughout my Ph. D. programme and in a sharp contrast to Dr. Dawkins' opinion, compelled me to withdraw his name from my scientific publications. I shall be able to express my gratitude to him only if I can follow his exceptional scientific attitude in the rest of my career.*

*Another imitable person without whose help I could not have even started my research is the computer cat Mr. Baba Varghese. I am greatly indebted to him for his assistance while facing the computers*

*I am thankful to the directors of Indian Institute of Astrophysics, Prof. J. C. Bhattacharya who offered me the opportunity to work in this institute, Prof. K. R. Sivaraman, Prof. Ch. V. Sastry, Prof. A. Peraiiah and Prof. R. Cowsik for extending me the research facilities which have been more than necessary. I would also like to thank the chairman of the Physics Department, Bangalore University, for all the help extended and for clearing all administrative formalities.*

*I would like to express my gratitude to Prof. N. C. Rana and Prof. Palash B. Pal. While Prof. Rana being my friend, philosopher and teacher kindled the fire in me by influencing my perception on scientific research in a great extent, Prof. Pal has been a source of fuel for it. He has been an excellent sounding board for even of my wildest idea. I feel myself fortunate for my association with these two versatile physicists.*

*I would like to take this opportunity to thank Prof. A. R. Prasanna and Prof. C. V. Vishveshwara for their encouragement. I thank Dr. K. N. Nagendra, Dr. D. Mohan Rao and Dr. K. E. Rangarajan for many stimulating discussions. My thanks are also due to Prof. R. K. Kochhar for his pragmatic advices which enabled me to overcome several rough patches at the very initial stage of my journey towards the goal.*

*For their encouragement and assistance to me, directly or indirectly, in finishing of my Ph. D. programme, there are many people to whom I am greatly indebted -- too many to thank individually. Without my having the benefit of their help, it is unlikely that I could have embarked upon the daunting task of finishing of my thesis work. My ups and downs have been accompanied by the love and affection of Dr. Mausumi Dikpati who has indeed been a friend in need. I shall always remain indebted to her.*

*All of my friends; my batchmates, seniors and juniors, in their own ways, have contributed significantly towards making this thesis a reality. In the most crucial financial situations, Uma Gorti's generous support shall be gratefully remembered by me. I also offer my very particular warm thanks to Eshwar Reddy, Dipankar Banerjee, Sanjoy Mazumdar, Pavan Chakraborty, A. D. Jana, Gajendra Pandey, Angom Dilip, Krishna Kumar, Sankarasubramanian, R. Ramesh, T. Sivarani and others for making the environment home outside home. My sincere thanks are also due to Dr. R. T. Gangadhara for many discussions we have had.*

*The untiring job of making several xerox copies of scientific documents for me by Mr. P. N. Prabhakara is thankfully acknowledged hereby. I would also like to offer my sincere thanks to the librarian and her subordinates who always extended their helpful hands in sorting out any problem related to books, journals, reprints etc.*

*If 'Life has no blessing than true friends' then I am blessed by having two genuine friends who always appear beside me when I face the toughest hurdle in my way. I express my deepest gratitude to Dr. Prasun Kanta Moitra and Mr. Abhijit Hazra by confessing that it is beyond my capacity to repay their debt.*

*Finally, I would like to offer my most sincere thanks to my relatives, my beloved parents and my brother for their contribution, co-operation, encouragement and inspiration. I am especially grateful to my maternal uncle in law, Mr. D. N. Roy from whom I virtually inherited mental strength and self-confidence that lead me to be optimistic even in the most adverse situation. My warm thanks are due to my brother Suman who relieved me from all types of domestic responsibilities. I wish to record my great debt to my parents who unintentionally developed in me the realization that success is a journey and not a destination.*

**Bangalore, India**

**July, 1996**

**Sujan Kumar Sengupta**

# Preface

---

*“The study of stellar atmospheres is in many ways one of the most interesting and rewarding areas of modern astrophysics. It is not an exaggeration to state that most of what we know about stars, and systems of stars, is derived from an analysis of their radiation, and that this knowledge will be secure only as long as the analytical technique is physically reliable. It is therefore important to have sound theoretical framework upon which our inferences can be based with confidence.”*

— Dimitri Mihalas in *Stellar Atmospheres* (1978).

Resonance line polarization is sensitive to the magnetic field (Hanle effect), the collisional rates, interference between atomic sublevels, the frequency redistribution, the degree of angular anisotropy of the incident radiation and the geometry of the line forming region. The collisional rates are determined by various physical causes. The above mentioned processes are greatly affected by the radial expansion of the atmosphere. On the other hand it is well-known from observations that early type stars, giant and supergiant stars, symbiotic stars, luminous late type stars possess differential velocities along the radial direction in their outer layers with high velocities of tens of mean thermal units and sometimes even hundreds of mean thermal units. These objects show degree of polarization ranging from 0.1 % to 5 % in the optical band. Therefore in modelling the atmospheres of these objects it is essential to include velocity fields which may play crucial role in the formation of polarization profile.

The present study was undertaken with the goal of understanding the behavior of line polarization in an extended and radially expanding stellar atmosphere. In this thesis a

detail study of the effect of differential radial velocity on the distribution of line intensities and line polarization of an extended stellar atmosphere has been made with the two level atom approximation. They are described in the following chapters of this thesis. The contents of these chapters are briefly presented here.

The first chapter contains a brief survey of the investigations on the problem of transfer of polarized radiation in stellar atmospheres that has already been done by various authors. In the second chapter the relevant equation for the transfer of polarized radiation in an extended and expanding stellar atmosphere has been formulated. In general a linearly polarized beam is represented by the three Stoke's parameters I, Q and U. In a plane parallel or spherically symmetric medium, because of the axial symmetry of the radiation field, only two parameters are required to define the polarization state of the radiation field: the specific intensity of the radiation field  $I (= I_l + I_r)$  and the polarized intensity  $Q (= I_l - I_r)$  where  $I_l$  and  $I_r$  are the components which are perpendicular and parallel to the surface respectively. The degree of linear polarization  $p = Q/I$  gives the measure of the angular anisotropy of the diffuse radiation field.

In the rest frame calculations one can use velocities upto one to two mean thermal units only. Beyond two mean thermal units it is very difficult to get correct solution. The difficulties arise because of the fact that absorption co-efficient changes continuously due to Doppler shifts and therefore the angle frequency mesh required to solve the equation becomes enormously large and one has to take a mesh of infinite size. The calculation becomes quite involved simply because photons can be redistributed from any given point to any other point in the interval  $\nu_o(1 - V_{max}/c)$  to  $\nu_o(1 + V_{max}/c)$  where  $\nu_o$  is the central frequency of line and  $V_{max}$  is gas velocity. Hence the transfer of radiation has been considered in the comoving frame. In comoving frame it is easy to handle such large velocities. The absorption co-efficient in the comoving frame is constant as the Doppler shifts do not create problems of frequency changes in the line absorption. Therefore one can reduce the size of the angle frequency mesh considerably and the number of angles and the number of frequency points are considerably reduced in the case of comoving frame



and this can easily give exact solution for the atmosphere of stars in which the velocities are as large as 100 mean thermal units and even more. Further the phase function for the static case which gives the angular distribution of the polarized radiation can well be applied in the comoving frame calculations. The transfer equation for polarized radiation in comoving frame is presented in this chapter.

In the third chapter the methodology for the numerical solutions of the transfer equation for polarized radiation is described in detail. For solving the plane parallel and the spherical radiative transfer problems in co-moving frame the method due to Peraiah has been employed. In general the following steps are taken in obtaining the solution. (i) The medium is divided into a number of 'cells' whose thickness are less than or equal to the critical thickness that is determined on the basis of the physical characteristics of the medium. The critical thickness ensures stability and uniqueness of the solution. (ii) The integration of the transfer equation is performed on the 'cell' which is a two dimensional grid bounded by radial and angular points. (iii) The discrete equations are compared with the canonical equation of the interaction principle and the transmission and the reflection operators of the 'cell' which contains all the physical informations in the problem under consideration are obtained. (iv) Lastly, all the cells are combined by internal field algorithm and the diffuse radiation field is obtained. For a thick layer, the so called star product is used. The generalization of all the steps of this finite difference method to include the polarization state of radiation is presented in this chapter. Since a two dimensional vector  $(I, I_r)^T$  has been employed to represent the specific intensity vector, the matrices appearing in the computational algorithm get dimensions twice as much for the corresponding scalar line transfer problem.

The method can handle the problem arising out of the coupling of the comoving points across the line profile and the local velocity gradients. The stability of the solution is achieved by controlling the step size which arises in the discretization in radial, angle and frequency integrations. Choosing a proper step size, stable solution can be found. Thus the stability and the uniqueness are maintained.

Finally, the frequency-independent l- and r- components of the source vectors that have been computed in the comoving frame are used to obtain the corresponding line profiles and the polarization line profiles along the line of sight of an observer at infinity.

In the **fourth chapter** the effect of differential radial velocity on the distribution of line intensities and line polarization in a stellar atmosphere stratified in parallel planes has been presented in detail. The medium is assumed to be homogeneous and isothermal. Two different types of velocity rules have been adopted in this case. The velocity at the outermost layer is taken to be 5, 10 and 20 mean thermal units with zero velocity at the innermost layer. The results have been compared with that of the static case. The line intensity profile and the polarization profile in the comoving frame as well as in the observer's frame are discussed in detail. Two types of media have been considered: (i) purely scattering medium and (ii) partially scattering medium through which the role of the thermalization parameters is investigated.

As the stellar radius increases the curvature effect plays a dominant role and a spherically symmetric geometry becomes more relevant in that case. In the **fifth chapter** the effect of differential radial velocity in the distribution of line intensities and line polarization for a spherically symmetric, inhomogeneous and isothermal medium is presented in detail. The atmospheric models could represent the outer layers of early type stars, giant and supergiant stars as well as luminous late type stars. In the fourth chapter the role of non-zero thermalization parameter has been discussed. In the case of a spherically symmetric stellar atmosphere, a fixed value of the thermalization parameter is taken in all models and the effect of differential radial expansion to line polarization under different optical depth as well as sphericity of the medium has been discussed in detail.

Although the models employed are highly idealized, they can provide a reasonably good physical insight into the polarized line formation problem in a radially expanding and extended spherical stellar atmosphere.

Finally, in the **sixth chapter** the results of the investigation described in the thesis are summarized with specific conclusions.

# Contents

---

<b>Preface</b>	<b>i</b>
<b>1 Introduction</b>	<b>1</b>
<b>2 Equations for the transfer of polarized radiation</b>	<b>5</b>
2.1 Resonance line polarization . . . . .	5
2.2 Representation of polarized radiation by Stokes parameters . . . . .	6
2.3 Rayleigh scattering . . . . .	10
2.3.1 The explicit form of the phase matrix for Rayleigh scattering . . .	12
2.4 The phase matrix for resonance line scattering . . . . .	14
2.4.1 The explicit form of the phase matrix for resonance scattering . .	14
2.5 Equations for the transfer of polarized radiation in rest frame . . . . .	15
2.5.1 In plane parallel geometry . . . . .	15
2.5.2 In spherically symmetric geometry . . . . .	16
2.6 The comoving frame formalism . . . . .	17
2.6.1 The need for comoving frame formalism . . . . .	17
2.6.2 The transfer equation for polarized radiation in comoving frame .	20
<b>3 The numerical method for solving the transfer equations</b>	<b>24</b>
3.1 Introduction . . . . .	24
3.2 The basic theory of the numerical method . . . . .	25

---

3.2.1	Interaction principle . . . . .	25
3.2.2	Star Product . . . . .	28
3.2.3	Calculation of radiation field at internal points . . . . .	30
3.3	Application of Discrete Space Theory . . . . .	33
3.3.1	Boundary conditions . . . . .	33
3.3.2	Method of solution for spherically symmetric medium . . . . .	33
3.4	Stability condition and correctness check . . . . .	40
3.4.1	Global flux conservation . . . . .	41
3.4.2	Specular reflection at the inner boundary . . . . .	43
3.5	Calculation of the flux at the observer's frame . . . . .	47
<b>4</b>	<b>Resonance line polarization in expanding stellar atmosphere stratified into plane-parallel</b>	<b>49</b>
4.1	Introduction . . . . .	49
4.2	Model parameters . . . . .	50
4.3	Results and discussions . . . . .	52
4.4	Summary . . . . .	67
<b>5</b>	<b>Resonance line polarization in extended and expanding spherical stellar atmosphere</b>	<b>72</b>
5.1	Introduction . . . . .	72
5.2	Model parameters . . . . .	73
5.3	Results and discussions . . . . .	75
5.4	Summary . . . . .	104
<b>6</b>	<b>Conclusions</b>	<b>107</b>
	<b>References</b>	<b>113</b>

# Chapter 1

## Introduction

---

The study of the outer layers of stars is one of the most important branches of Astrophysics. A quantitative study of the nature of radiation emanating from the outer layers of stars leads to an understanding of the physical conditions, viz., the densities, temperatures, pressures, gas motions and chemical composition of the matter present in their atmospheres. The study also provides information on various stages of ionizations and excitations of different atoms and molecules constituting the atmospheres. Therefore the basic goal of radiative transfer calculation is to describe quantitatively, the flow of energy through the outermost layers of stars and to explain and predict the observational characteristics of the emergent radiation. Hence one needs to develop the relations between microscopic phenomena such as the interaction of radiation with matter and the macroscopic phenomena like the transfer of radiation, the radiative heat conduction and the mass motion in order to understand the physical nature of stars with different spectral features. Unless such a link is established, a correct theoretical modelling of the regions emitting the radiation becomes difficult. Though in the past few decades important advances have been done in this field, the exact theoretical modelling involving realistic physical processes is yet to be considered in detail.

Since on scattering (viz., by atoms or electrons) light in general, gets polarized, in order to specify the nature of the radiation field, one must allow for polarization in any

exact treatment of the scattering problems. One of the fundamental aspects of polarized radiation is "Resonance line polarization". In the absence of any external magnetic field, the absorption of an anisotropic radiation field by an atom leads to a non-uniform population of the Zeeman sublevels of the excited state of the atom and the coherences among such levels. As a consequence, the re-emitted radiation field is linearly polarized. Such a two-level atom model is a quantum analogue of the Rayleigh scattering of the continuum radiation.

The basic theory of resonance line polarization has been studied extensively by many authors. Zanstra (1941) developed a theory to calculate resonance line polarization in the solar atmosphere. Chandrasekhar (1960) introduced the Stroke's parameters to represent the polarized radiation in the equations of radiative transfer. Since then the theory of resonance line polarization has been extensively studied by Voigt (1951), Warwick & Hyder (1965), Lamb (1970), House (1971) and Stenflo (1976, 1978, 1980). Detailed theoretical discussions can also be found in Mitchell & Zemanski (1934), Hamilton (1947) and Landi degl'Innocenti (1984).

The diagnostic potential of resonance line polarization in solar observations has been studied extensively by Stenflo (1980), Stenflo & Stenholm (1976), Stenflo, Baur & Elmore (1980). Rees & Saliba (1982) have extended the formalism developed by Stenflo and co-workers to a more complicated but realistic problem of resonance line polarization with partial frequency redistribution in a static plane parallel medium. Faurobert (1987, 1988) has discussed the validity and usefulness of some approximate forms of the partial frequency redistribution functions in the polarized line transfer computations, in relation to the exact angle-dependent version of these functions. The effect of external magnetic field on resonance line polarization (Hanle effect) has also been investigated by the same author (Faurobert 1991). Detailed studies on similar lines have been carried out by McKenna (1984, 1985). Peraiah (1976) investigated the effect of rotation and tidal forces in the components of close binary stars on linear polarization with an aim to explain the observational findings of Kruszewski, Gekrels & Serkowski (1968) and Dyck &

Sandort (1971). The observations made by Brukner (1963), Stenflo (1974), Wiehr (1975, 1981) on the linear polarization in resonance lines of *Ca*, *Na* and *Mg* have been quite successfully explained by the theoretical calculations. The transfer of polarized radiation in spherically symmetric geometry has been studied in detail by Nagendra (1988).

So far all the theoretical investigations have been carried on by assuming static medium. But it is well-known from observations that early type stars, giant and supergiant stars, symbiotic stars and luminous late-type stars possess differential velocities in the radial direction in their outer layers with speeds ranging from 2 mean thermal units to 100 mean thermal units. These objects show degree of polarization ranging from 0.1 to 5 per cent in the optical band (Coyne et al. 1988).

Resonance line polarization is sensitive to the magnetic field, the collisional rates, transitions between atomic sublevels, the frequency redistribution, the degree of angular anisotropy of the incident radiation and the geometry of the medium. Except the geometry of the medium, all the above mentioned processes are greatly affected by the inclusion of radial expansion of the atmosphere. Collisional rates are determined by the density of the medium which in turn governed by the velocity field. The velocity field alters the frequency of the line photons due to Doppler shift. It is therefore necessary to include the velocity field in the study of line polarization in astrophysical context.

The present work is a continuation of the work done earlier by other authors with the consideration of the radial motion of the atmosphere. In this thesis the effect of differential radial velocity to the distribution of line intensities and line polarization along the line of sight of an extended stellar atmosphere is presented. For this purpose, the radiative transfer equation in the comoving frame (Castor 1972) is considered. The choice of comoving frame formalism is to reduce the frequency-angle mesh which becomes enormously large in rest frame calculation due to the velocity field. Further one can use the frequency redistribution function used for the static case which is significantly altered with the velocity gradient in a rest frame calculation. The scalar line formation in the comoving frame has been well studied by Mihalas, Kunasz & Hummer (1975) and Peraiah

---

(1984). In the present work, the scalar radiative transfer equation in comoving frame has been generalized into vector form in order to include line polarization. Considering plane parallel and spherically symmetric geometries the transfer equation for polarized radiation in comoving frame has been solved by using the method due to Peraiah (1984). Complete frequency redistribution is assumed with different velocity gradients and velocity rules. A large number of results have been presented along with the results for the static case for comparison. The results will be useful for obtaining a general idea about the resonance line polarization in an extended and radially expanding stellar atmosphere.



## Chapter 2

# Equations for the transfer of polarized radiation

---

### 2.1 Resonance line polarization

The quantum theory of resonance fluorescence leads to a law of scattering which is formally of the same type as the classical law of scattering by anisotropic particles.

In the context of resonance line scattering one is concerned with transitions from an initial ground state to an excited intermediate state and back to the ground state. However, in the study of these transitions the different substates of each level as specified by the magnetic quantum number  $m$  which are the eigenvalues of the z-component of the total angular momentum in units of  $\hbar$ , must be taken into consideration.

Let the relevant states of the radiating atom be designated by  $X_k$ ,  $Y_n$  and  $X_p$ , where  $X$  and  $Y$  refer to the ground state and the intermediate excited state respectively. The subscripts refer to the  $m$ -values of the different substates under consideration.

The probability of a transition from  $X_k$  to  $Y_n$  between a single pair of  $m$ -states can be calculated for any given stream of incident radiation. Similarly, the angular distribution and the state of polarization of the quantum emitted in a transition from  $Y_n$  to  $X_p$  between a single pair of  $m$ -states are also known. But in resonance fluorescence, the

different sequences of transitions which are possible starting from the same state  $X_k$  are correlated, because, when transitions from a given state  $X_k$  to different substates  $Y_n$  are possible, the wave functions belonging to these substates have phases which are related in a definite manner to the phase of the wave function belonging to  $X_k$ . The resulting transitions to  $X_p$  from the different substates  $Y_n$  cannot therefore be regarded as independent of each other. As a consequence, the reemitted radiation is polarized and is called resonance line polarization.

For a transition with  $j = 0$  and  $\Delta j = 1$ , resonance line polarization becomes similar to the Rayleigh scattering. Hence, resonance line polarization can be regarded as a quantum analogue of the Rayleigh scattering of the continuum radiation.

## 2.2 Representation of polarized radiation by Stokes parameters

In order to formulate the equations of transfer in a gaseous medium the most convenient representation of polarized radiation is by a set of four parameters called Stokes parameters. Chandrasekhar (1960) first introduced the Stokes parameters in the equation of radiative transfer with a slight modification of Stoke's representation.

In an elliptically polarized beam the vibrations of the electric and the magnetic vectors in the plane transverse to the direction of propagation are such that the ratio of the amplitudes and difference in phases of the components in any two directions at right angles to each other are absolute constants. A regular vibration of this character can be represented by

$$\xi_l = \xi_l^{(0)} \sin(\omega t - \epsilon_l), \xi_r = \xi_r^{(0)} \sin(\omega t - \epsilon_r) \quad (2.1)$$

where  $\xi_l$  and  $\xi_r$  are the components of the vibration along two directions  $l$  and  $r$  at right angles to each other (see Fig. 2.1),  $\omega$  the circular frequency of the vibration, and  $\xi_l^{(0)}$ ,  $\xi_r^{(0)}$ ,  $\epsilon_l$  and  $\epsilon_r$  are constants. If the principal axes of the ellipse described by  $(\xi_l, \xi_r)$  are

in directions making angles  $\chi$  and  $\chi + \frac{1}{2}\pi$  to the direction  $l$ , the equations representing the vibration take the simplified forms :

$$\xi_{\chi} = \xi^{(0)} \cos \beta \sin \omega t, \xi_{\chi + \frac{1}{2}\pi} = \xi^{(0)} \sin \beta \cos \omega t \quad (2.2)$$

where  $\beta$  denotes an angle whose tangent is the ratio of the axes of the ellipse traced by the end point of the electric (or magnetic) vector, and the numerical values of it lies between 0 and  $\frac{1}{2}\pi$ . The sign of  $\beta$  is positive or negative according as the polarization is right-handed or left-handed.

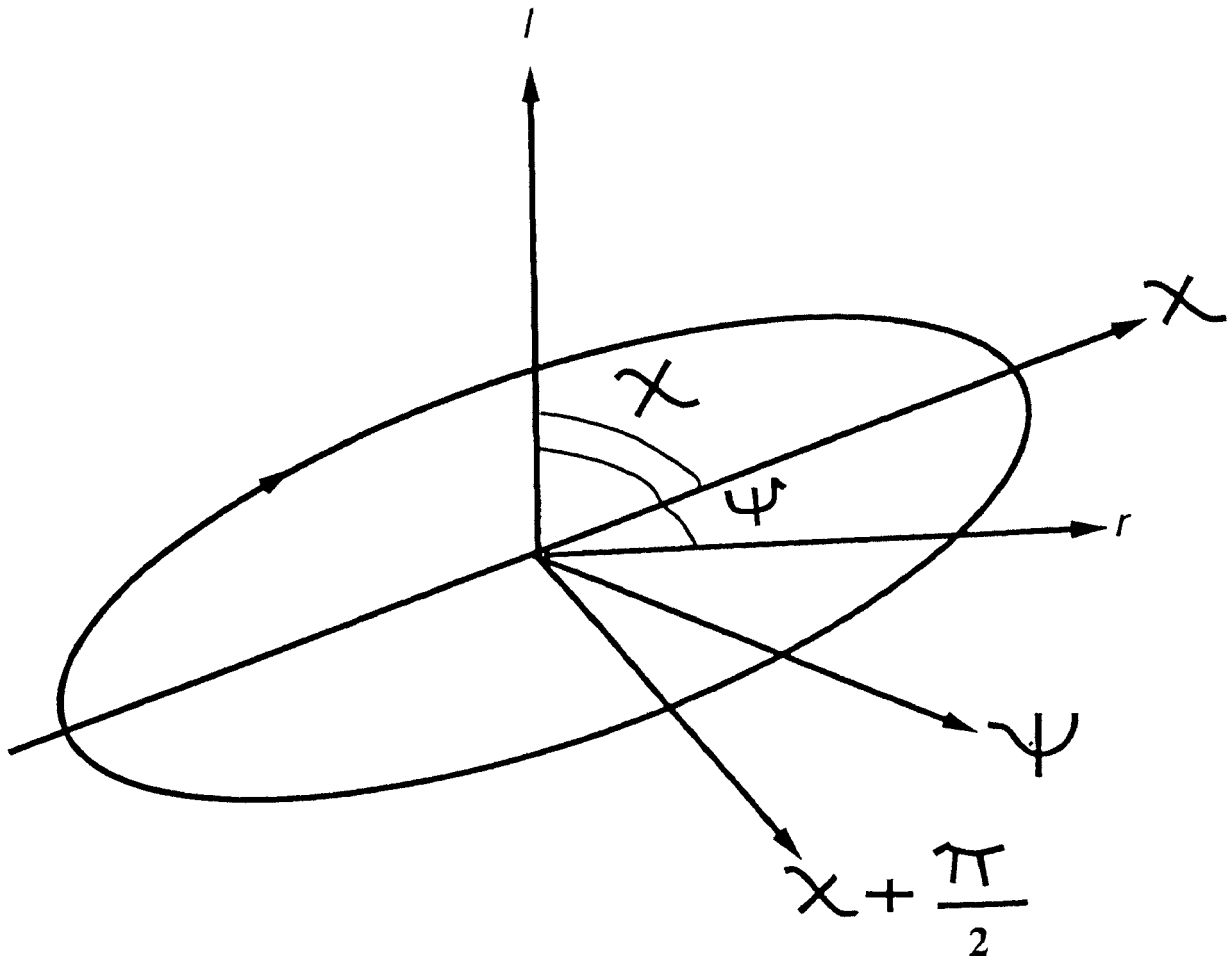


Figure 2.1: Schematic diagram representing elliptical polarization

In equation (2.2),  $\xi^{(0)}$  denotes a quantity proportional to the mean amplitude of the

electric vector and whose square is equal to the intensity of the beam:

$$I = [\xi^{(0)}]^2 = [\xi_l^{(0)}]^2 + [\xi_r^{(0)}]^2 = I_l + I_r. \quad (2.3)$$

Following the representation given in equation (2.2) one obtains for the vibrations in the  $l$  and  $r$  directions

$$\xi_l = \xi^{(0)}(\cos \beta \cos \chi \sin \omega t - \sin \beta \sin \chi \cos \omega t) \quad (2.4)$$

and

$$\xi_r = \xi^{(0)}(\cos \beta \sin \chi \sin \omega t - \sin \beta \cos \chi \cos \omega t). \quad (2.5)$$

The intensities  $I_l$  and  $I_r$  in the directions  $l$  and  $r$  can be written as

$$I_l = [\xi_l^{(0)}]^2 = I(\cos^2 \beta \cos^2 \chi + \sin^2 \beta \sin^2 \chi) \quad (2.6)$$

and

$$I_r = [\xi_r^{(0)}]^2 = I(\cos^2 \beta \sin^2 \chi + \sin^2 \beta \cos^2 \chi). \quad (2.7)$$

It follows from the foregoing equations that whenever the regular vibrations representing an elliptically polarized beam can be expressed in the form given in equation (2.1) we can write the relations

$$I = [\xi_l^{(0)}]^2 + [\xi_r^{(0)}]^2 = I_l + I_r, \quad (2.8)$$

$$Q = [\xi_l^{(0)}]^2 - [\xi_r^{(0)}]^2 = I \cos 2\beta \cos 2\chi = I_l - I_r, \quad (2.9)$$

$$U = 2\xi_l^{(0)}\xi_r^{(0)} \cos(\epsilon_l - \epsilon_r) = I \cos 2\beta \sin 2\chi = (I_l - I_r) \tan 2\chi \quad (2.10)$$

and

$$V = 2\xi_l^{(0)}\xi_r^{(0)} \sin(\epsilon_l - \epsilon_r) = I \sin 2\beta = (I_l - I_r) \tan 2\beta \sec 2\chi. \quad (2.11)$$

These are the Stokes parameters representing an elliptically polarized beam. It follows from equation (2.8) to equation (2.11) that

$$I^2 = Q^2 + U^2 + V^2.$$

Further,

$$\tan 2\chi = \frac{U}{Q}$$

and

$$\sin 2\beta = \frac{V}{\sqrt{Q^2 + U^2 + V^2}}$$

which give the plane of polarization and the ellipticity respectively.

In the above formalism the amplitudes and the phase have been considered to be constants. But in practice this is not attainable. So one has to consider the mean intensity in any direction in the transverse plane. Hence, the apparent intensities  $I_l$  and  $I_r$  in the directions  $l$  and  $r$  are given by the values of all amplitudes:

$$I_l = [\overline{\xi_l^{(0)}}]^2$$

and

$$I_r = [\overline{\xi_r^{(0)}}]^2.$$

Accordingly, one writes

$$Q = [\overline{\xi^{(0)}}]^2 \cos \beta \cos 2\chi = I \cos 2\beta \cos 2\chi, \quad (2.12)$$

$$U = [\overline{\xi^{(0)}}]^2 \cos 2\beta \sin 2\chi = I \cos 2\beta \sin 2\chi, \quad (2.13)$$

$$V = [\overline{\xi^{(0)}}]^2 \sin 2\beta = I \sin 2\beta. \quad (2.14)$$

It can be shown that the character of an arbitrary polarized light, in so far as experimental tests can reveal, is completely determined by the intensities in two directions at right angles to each other (or equivalently, the total intensity  $I$  and  $Q = I_l - I_r$ ) and

the parameters  $U$  and  $V$ . The intensities  $I$ ,  $Q$ ,  $U$  and  $V$  are the general Stokes parameters representing light. When several independent streams of light are combined, the Stokes parameters for the mixture is the sum of the respective Stokes parameters of the separate streams. For a beam resulting from a mixture of several independent streams of elliptically polarized light the Stokes parameters are therefore given by

$$\begin{aligned} I &= \sum I^{(n)}, I_l = \sum I_l^{(n)}, I_r = \sum I_r^{(n)} \\ Q &= \sum Q^{(n)} = \sum I^{(n)} \cos 2\beta_n \cos 2\chi_n \\ U &= \sum U^{(n)} = \sum I^{(n)} \cos 2\beta_n \sin 2\chi_n \\ V &= \sum V^{(n)} = \sum I^{(n)} \sin 2\beta_n \end{aligned}$$

where  $I^{(n)}$ ,  $\xi_n$  and  $\beta_n$  denote the intensity, the plane of polarization and the ellipticity of the component streams.

The necessary and sufficient condition that light be natural is

$$Q = U = V = 0.$$

## 2.3 Rayleigh scattering

One of the most important physical law of light scattering is Rayleigh's law of scattering. Rayleigh's law states that when a pencil of natural light of wavelength  $\lambda$ , intensity  $I$  and solid angle  $d\omega$  is incident on a particle of polarizability  $\alpha$ , energy at the rate (Chandrasekhar 1960)

$$\frac{128\pi^5}{3\lambda^4} \alpha^2 I d\omega \times \frac{3}{4} (1 + \cos^2 \Theta) \frac{d\omega'}{4\pi} \quad (2.15)$$

is scattered in a direction making an angle  $\Theta$  with the direction of incidence and in a solid angle  $d\omega'$ ; that the scattered light is partially plane-polarized; that the plane of polarization is at right angles to the plane of scattering and that the intensities of the scattered light in the directions (in the transverse plane containing the electric and the

magnetic vectors) parallel and perpendicular respectively to the plane of scattering are in the ratio  $\cos^2\Theta : 1$ .

According to equation (2.15) the scattering co-efficient  $\sigma$  per particle is

$$\sigma = \frac{128\pi^5}{3\lambda^4}\alpha^2. \quad (2.16)$$

For electrons, the Thomson scattering co-efficient

$$\sigma_e = \frac{8\pi e^4}{3m_e^2 c^4} \quad (2.17)$$

can be obtained by setting

$$\alpha = \left(\frac{\lambda}{c}\right)^2 \frac{e^2}{4\pi^2 m_e}$$

in equation (2.16). Here  $c$  denotes the velocity of light,  $e$  the charge of the electron and  $m_e$  the mass of electron.

In order to incorporate Rayleigh's scattering into the radiative transfer equation, Chandrasekhar (1960) modified it which can be stated as the vibrations representing the light scattered in a direction making an angle  $\Theta$  with the direction of incidence is

$$\xi_{\parallel}^{(0)} = \left(\frac{3}{2}\sigma\right)^{1/2} \xi_{\parallel}^{(0)} \cos\Theta \sin(\omega t - \epsilon_1) \quad (2.18)$$

and

$$\xi_{\perp}^{(0)} = \left(\frac{3}{2}\sigma\right)^{1/2} \xi_{\perp}^{(0)} \sin(\omega t - \epsilon_2), \quad (2.19)$$

where the phase  $(\epsilon_1, \epsilon_2)$  and the amplitude  $(\xi_{\parallel}^{(0)}, \xi_{\perp}^{(0)})$ , relations in the incident beam are maintained, unaltered, in the scattered beam. Here  $\parallel$  and  $\perp$  refer to directions in the transverse planes (of the incident and scattered light) parallel and perpendicular respectively to the plane of scattering. Accordingly, the parameters representing the scattered light are proportional to

$$\frac{3}{2}\sigma \overline{[\xi_{\parallel}^{(0)}]^2} \cos^2\Theta = \frac{3}{2}\sigma I_{\parallel} \cos^2\Theta, \quad (2.20)$$

$$\frac{3}{2}\sigma \overline{[\xi_{\perp}^{(0)}]^2} = \frac{3}{2}\sigma I_{\perp}, \quad (2.21)$$

$$\frac{3}{2}\sigma \overline{[2\xi_{\parallel}^{(0)}\xi_{\perp}^{(0)} \cos(\epsilon_1 - \epsilon_2)]} \cos \Theta = \frac{3}{2}\sigma U \cos \Theta \quad (2.22)$$

and

$$\frac{3}{2}\sigma \overline{[2\xi_{\parallel}^{(0)}\xi_{\perp}^{(0)} \sin(\epsilon_1 - \epsilon_2)]} \cos \Theta = \frac{3}{2}\sigma V \cos \Theta. \quad (2.23)$$

Therefore, denoting the incident light by the vector

$$\mathbf{I} = (I_{\parallel}, I_{\perp}, U, V)$$

we can express the scattering intensity in the direction  $\Theta$  by

$$\left(\sigma \frac{d\omega'}{4\pi}\right) \mathbf{R} \mathbf{I} d\omega \quad (2.24)$$

where

$$\mathbf{R} = \frac{3}{2} \begin{pmatrix} \cos^2 \Theta & 0 & 0 & 0 \\ 0 & 1 & 0 & 0 \\ 0 & 0 & \cos \Theta & 0 \\ 0 & 0 & 0 & \cos \Theta \end{pmatrix}$$

$\mathbf{R}$  is called the phase matrix for Rayleigh scattering.

### 2.3.1 The explicit form of the phase matrix for Rayleigh scattering

In the formulation of the equation of radiative transfer, the radiation field at each point is characterized by the four intensities  $I_l(\theta, \phi)$ ,  $I_r(\theta, \phi)$ ,  $U(\theta, \phi)$  and  $V(\theta, \phi)$  where  $\theta$  and  $\phi$  are the polar angles referred to an appropriately chosen coordinate system through the point under consideration and  $l$  and  $r$  refer to the directions in the meridian plane and at right angles to it respectively.

Therefore one writes

$$\mathbf{I}(\theta, \phi) = [I_l(\theta, \phi), I_r(\theta, \phi), U(\theta, \phi), V(\theta, \phi)].$$



The explicit form of the phase function for Rayleigh scattering in terms of  $\theta$  and  $\phi$  which is used in the transfer equation and which describes the angular distribution of the radiation field is given by (Chandrasekhar 1960):

$$P(\mu, \phi; \mu', \phi') = Q[P^{(0)}(\mu, \mu') + (1 - \mu^2)^{1/2}(1 - \mu'^2)^{1/2}P^{(1)}(\mu, \phi; \mu', \phi') + P^{(2)}(\mu, \phi; \mu', \phi')], \quad (2.25)$$

where

$$P^{(0)}(\mu, \mu') = \frac{3}{4} \begin{pmatrix} 2(1 - \mu^2)(1 - \mu'^2) + \mu^2 \mu'^2 & \mu^2 & 0 & 0 \\ \mu'^2 & 1 & 0 & 0 \\ 0 & 0 & 0 & 0 \\ 0 & 0 & 0 & \mu \mu' \end{pmatrix}$$

$$P^{(1)}(\mu, \phi; \mu', \phi') = \frac{3}{4} \begin{pmatrix} 4\mu \mu' \cos(\phi' - \phi) & 0 & 2\mu \sin(\phi' - \phi) & 0 \\ 0 & 0 & 0 & 0 \\ -2\mu' \sin(\phi' - \phi) & 0 & \cos(\phi' - \phi) & 0 \\ 0 & 0 & 0 & \cos(\phi' - \phi) \end{pmatrix}$$

$$P^{(2)}(\mu, \phi; \mu', \phi') = \frac{3}{4} \begin{pmatrix} \mu^2 \mu'^2 \cos 2(\phi' - \phi) & -\mu^2 \cos 2(\phi' - \phi) & \mu^2 \mu' \sin 2(\phi' - \phi) & 0 \\ -\mu'^2 \cos 2(\phi' - \phi) & \cos 2(\phi' - \phi) & -\mu' \sin 2(\phi' - \phi) & 0 \\ -\mu \mu'^2 \sin 2(\phi' - \phi) & \mu \sin 2(\phi' - \phi) & \mu \mu' \cos 2(\phi' - \phi) & 0 \\ 0 & 0 & 0 & 0 \end{pmatrix}$$

and

$$Q = \begin{pmatrix} 1 & 0 & 0 & 0 \\ 0 & 1 & 0 & 0 \\ 0 & 0 & 2 & 0 \\ 0 & 0 & 0 & 2 \end{pmatrix}$$

Here  $\mu = \cos \theta$ ,  $\mu' = \cos \theta'$ ,  $\theta$  and  $\theta'$  denote the direction of the photon before and after scattering. Similarly for  $\phi$  and  $\phi'$ .

## 2.4 The phase matrix for resonance line scattering

In resonance fluorescence, the Stokes parameters  $I_l$ ,  $I_r$  and  $U$  are scattered in accordance with a phase matrix of the form

$$\frac{3}{2}E_1 \begin{pmatrix} \cos^2 \Theta & 0 & 0 \\ 0 & 1 & 0 \\ 0 & 0 & \cos \Theta \end{pmatrix} + \frac{1}{2}E_2 \begin{pmatrix} 1 & 0 & 0 \\ 1 & 1 & 0 \\ 0 & 0 & 0 \end{pmatrix} \quad (2.26)$$

where  $E_1$  and  $E_2$  are certain constants depending on the initial  $j$ -value and the  $\Delta j$  ( $= \pm 1$  or  $0$ ) involved in the transition. As in Rayleigh scattering the parameter  $V$  is scattered independently of the rest and according to a phase function of the form

$$\frac{3}{2}E_3 \cos \Theta,$$

where  $E_3$  is another constant depending also on  $j$  and  $\Delta j$ . From the condition of conservative scattering

$$E_1 + E_2 = 1$$

and for  $j = 0$  and  $\Delta j = 1$ ,  $E_1 = 1$ ,  $E_2 = 0$  and  $E_3 = 1$  which implies that in this case, resonance line scattering is the same as Rayleigh scattering.

### 2.4.1 The explicit form of the phase matrix for resonance scattering

In the present work, plane parallel and spherically symmetric atmospheres have been considered. For both the cases the axial symmetry of the radiation field clearly requires that the plane of polarization be along the meridian plane (or, at right angle to it). Consequently,  $U = V = 0$  and the two intensities  $I_l$  and  $I_r$  are sufficient to characterize the radiation field.

With this consideration the phase matrix used to describe the angular distribution of

photons that undergo resonance scattering can be written as

$$P(\mu, \mu') = \frac{3}{8} E_1 \begin{pmatrix} 2(1 - \mu^2)(1 - \mu'^2) + \mu^2 \mu'^2 & \mu^2 \\ \mu'^2 & 1 \end{pmatrix} + \frac{(1 - E_1)}{4} \begin{pmatrix} 1 & 1 \\ 1 & 1 \end{pmatrix}. \quad (2.27)$$

## 2.5 Equations for the transfer of polarized radiation in rest frame

### 2.5.1 In plane parallel geometry

The two-level atom line transfer equation governing the intensities  $I_l$  and  $I_r$  in rest frame with the medium stratified into plane parallel can be written as (Chandrasekhar 1960)

$$\mu \frac{\partial}{\partial z} \begin{pmatrix} I_l(x, \mu, z) \\ I_r(x, \mu, z) \end{pmatrix} = k_L [\beta + \phi(x)] \left[ \begin{pmatrix} S_l(x, \mu, z) \\ S_r(x, \mu, z) \end{pmatrix} - \begin{pmatrix} I_l(x, \mu, z) \\ I_r(x, \mu, z) \end{pmatrix} \right] \quad (2.28)$$

where  $\mu = \cos \theta$  ( $\mu \in [0, 1]$ ) and  $\theta$  is the angle between the Stokes specific intensity vector and the axis of symmetry  $z$ ;  $x = (\nu - \nu_0)/\Delta\nu_D$ ,  $\nu$  being the frequency at any point in the line,  $\nu_0$  is the line center frequency and  $\Delta\nu_D$  is the Doppler width. The quantity  $\beta$  is the ratio  $\frac{k_c}{k_L}$  of the opacity due to continuum absorption per unit interval  $x$  to that in the line ( $k_L$  is the frequency integrated line opacity).  $\phi(x)$  is normalized absorption profile, generally represented by a Doppler profile or Lorentz profile or a Voigt function.

The total source function in its vector form is given by

$$\mathbf{S}(x, \mu, z) = \begin{pmatrix} S_l(x, \mu, z) \\ S_r(x, \mu, z) \end{pmatrix} = \frac{\phi(x) \mathbf{S}^L(x, \mu, z) + \beta \mathbf{S}^c(z)}{\beta + \phi(x)}; \quad (2.29)$$

$\mathbf{S}^L$  and  $\mathbf{S}^c$  refer to the source vectors in the line and the continuum respectively,

$$\mathbf{S}^c(z) = B(z) \mathbf{1}, \mathbf{1} = (1, 1)^T. \quad (2.30)$$

The line source vector is given by

$$\mathbf{S}^L(x, \mu, z) = \frac{1(1 - \epsilon)}{2 \phi(x)} \int_{-\infty}^{\infty} dx' \int_{-1}^{+1} \mathbf{R}(x, \mu; x', \mu') \begin{pmatrix} I_l(x, \mu, z) \\ I_r(x, \mu, z) \end{pmatrix} d\mu' + \epsilon B(z) \mathbf{1}, \quad (2.31)$$

where  $\epsilon$  is the probability per scattering that a photon is destroyed by collisional de-excitation. The redistribution matrix  $\mathbf{R}(x, \mu; x', \mu')$  is usually defined according to a hybrid model prescription by Rees & Saliba (1982) and is given by

$$\mathbf{R}(x, \mu; x', \mu') = \mathbf{P}(\mu, \mu')\mathbf{R}(x, x')$$

which retains the angular correlation in the phase matrix  $\mathbf{P}(\mu, \mu')$  that is essential for scattering polarization and mimics the frequency correlation via the angle-averaged scalar redistribution function  $\mathbf{R}(x, x')$  for isotropic scattering. Clearly the transfer equation for polarized radiation is a vector analogue of the non-LTE two-level atom line transfer equation.

### 2.5.2 In spherically symmetric geometry

Similar to the plane parallel case, the transfer equation for polarized radiation in a spherically symmetric atmosphere is a vector analogue of the non-LTE two-level atom line transfer equation in spherically symmetric geometry for the isotropic case. The equation of transfer in this case is written as

$$\begin{aligned} \mu \frac{\partial}{\partial r} \begin{pmatrix} U_l(x, \mu, r) \\ U_r(x, \mu, r) \end{pmatrix} + \frac{(1 - \mu^2)}{r} \frac{\partial}{\partial \mu} \begin{pmatrix} U_l(x, \mu, r) \\ U_r(x, \mu, r) \end{pmatrix} = \\ k_L[\beta + \phi(x)] \left[ \begin{pmatrix} S_l(x, \mu, r) \\ S_r(x, \mu, r) \end{pmatrix} - \begin{pmatrix} U_l(x, \mu, r) \\ U_r(x, \mu, r) \end{pmatrix} \right] \end{aligned} \quad (2.32)$$

where  $\mu = \cos \theta$  ( $\mu \in [0, 1]$ ) and  $\theta$  is the angle between the Stokes specific intensity vector and the symmetry axis (radius) at the radial point  $r$  in the atmosphere.

The components of the specific intensity in spherical symmetry are defined by

$$U_l(x, \mu, r) = 4\pi r^2 I_l(x, \mu, r)$$

and

$$U_r(x, \mu, r) = 4\pi r^2 I_r(x, \mu, r).$$

The total source vector, the continuum source vector and the line source vector are given as

$$\mathbf{S}(x, \mu, r) = \begin{pmatrix} S_l(x, \mu, r) \\ S_r(x, \mu, r) \end{pmatrix} = \frac{\phi(x)\mathbf{S}^L(x, \mu, r) + \beta\mathbf{S}^c(r)}{\beta + \phi(x)}, \quad (2.33)$$

$$\mathbf{S}^c(r) = B(r)\mathbf{1}, \mathbf{1} = (1, 1)^T \quad (2.34)$$

and

$$\mathbf{S}^L(x, \mu, r) = \frac{1}{2} \frac{(1 - \epsilon)}{\phi(x)} \int_{-\infty}^{\infty} dx' \int_{-1}^{+1} \mathbf{R}(x, \mu; x', \mu') \begin{pmatrix} U_l(x, \mu, r) \\ U_r(x, \mu, r) \end{pmatrix} d\mu' + \epsilon B(r)\mathbf{1} \quad (2.35)$$

respectively.

## 2.6 The comoving frame formalism

The existence of macroscopic motions (i.e., non-thermal velocities that are coherent over distances much larger than a particle mean-free path) in stellar atmospheres is well-documented by a wealth of observational evidence. These motions appear to be present on all scales, from ‘eddies’ whose sizes are small compared to a photon mean-free path, upto expansion of the whole atmosphere. Although, velocity fields have but little effect on radiative transfer in the continuum, they strongly influence line formation because even a small (Doppler) frequency shift of a line produces a major change in its absorptivity as seen by a stationary observer.

In the present work I focus on the kinematics of radiative transfer for polarized light in moving media, i.e., given the velocity field and the model atmosphere, we compute the emergent polarized spectrum.

### 2.6.1 The need for comoving frame formalism

A variety of techniques exist to attack the problem. Rest frame or observer’s frame methods can handle complicated velocity fields but are generally restricted to velocities

of the order of a few Doppler widths and hence are not well suited to handle rapid atmospheric expansion. The difficulties arise because of the fact that absorption co-efficient changes continuously due to the Doppler shifts and therefore the angle-frequency mesh becomes enormously large and one has to take a mesh of infinite size. The calculations become quite involved simply because photons can be redistributed from any given point to any other point in the interval  $\nu_0(1 - V_{max}/c)$  to  $\nu_0(1 + V_{max}/c)$  where  $\nu_0$  is the central frequency of the line and  $V_{max}$  is gas velocity. If one intends to compute profiles formed in a medium expanding with 2000 - 3000 km/s one has to consider a band width as large as 200 thermal units. This kind of size of angle-frequency mesh is impossible to handle in the case of rest frame.

When the material in the atmosphere moves with velocity  $V(r)$  relative to an external observer at rest, there is a Doppler shift of photon frequencies between the observer's frame and the frame of the atoms of which the material is composed. If the frequency in the observer's frame is  $\nu$ , then in the atom's frame the frequency at which a photon travelling in direction  $\mathbf{n}$  was emitted or can be absorbed is

$$\nu' = \nu - \nu_0(\mathbf{n} \cdot \mathbf{V}/c).$$

Thus the opacity and emissivity of the material as seen by a stationary observer, become angle dependent.

To line source function that contains a scattering term depends on the radiation field and hence it can be strongly affected by material motions. For example, an expansion at the upper surface of an atmosphere can displace a line away from a dark absorption feature, at the rest position, into a bright nearby continuum, thus raising the line source function dramatically.

Accurate calculation of the scattering integral in the expression for line source function with a quadrature sum poses a fundamental difficulty in a rest-frame solution for two reasons : (1) The line profile is shifted by an amount  $2V$  in frequency as  $\mu$  varies from -1 to +1. Thus in the frequency quadrature, an amount equal to twice the maximum flow velocity must be added to the bandwidth required to describe the static line profile.

(2) The angle quadrature scheme must employ a large number of angles. Because the argument of the profile function is  $(x - \mu V)$ , there is an inextricable coupling between the angular and frequency variations of the intensity. These two difficulties often leads to unstable solution in the rest frame calculation. In rest frame calculation the intensity can no longer be assumed to be symmetric around the line center, hence the full profile must be taken into account.

The approximation of complete frequency redistribution becomes invalid for moving media as the conditions that help validate it in static media no longer occur. Much work has been devoted to the problem of partial redistribution in moving atmospheres (see for example Mihalas 1976, Peraiah 1980a), it has been shown that to treat the problem in the rest frame the full angle-frequency dependent redistribution function must be employed.

On the other hand all the above mentioned difficulties are ameliorated by adopting comoving-frame method. The absorption co-efficient in the comoving frame is constant as the Doppler shifts do not create problems of frequency changes in the line absorption. Therefore one can reduce the size of angle-frequency mesh considerably and the number of angles and number of frequency points are considerably reduced in the case of comoving frame and this can easily give exact solution for the atmosphere of stars in which the velocities are as large as 100 mean thermal units. Further in a comoving-frame method one can employ static frequency redistribution functions for scattering in the fluid frame. That is because in the calculation of scattering integrals one needs only a frequency bandwidth enough to contain fully the line profile; this bandwidth is independent of the fluid velocity and the angle quadrature may be chosen on the basis of the angular distribution of the radiation alone. Also, the dynamical calculations in spherical flows such as expansion can be handled accurately in a Lagrangian co-ordinate system, i.e., in the comoving frame. The Lagrangian equations of gas dynamics are easy to formulate and offer many physical and computational advantages.

### 2.6.2 The transfer equation for polarized radiation in comoving frame

To obtain expression describing how the relevant physical variables change between the rest frame and the comoving frame, Lorentz transformations are applied. But a Lorentz transformation applies only when velocity  $V$  of one frame relative to the other is uniform and constant. But in stellar atmospheres we are concerned with situations where the velocity changes with the radial distance. Hence the fluid frame is not an inertial frame. One must therefore consider transformation taking place from uniformly moving frames that instantaneously coincide with the moving fluid. It is easy to show that the transfer equation is covariant under the transformation of two uniformly moving frames provided one accounts for the effects of Doppler shifts and aberration of photons when one calculates atomic properties. But for unsteady or steady differential flows, new terms appear in the equations that account, in effect, for changes in the Lorentz transformation from one point in the medium to another.

A velocity field produces a Doppler shift and aberration of photons, and give rise to advection terms describing the “sweeping up” of radiation by the moving fluid. Formally, these terms are all of the order  $\frac{v}{c}$ . However, in the case of line profiles, the effect of a frequency shift  $\Delta\nu$  becomes important not when  $\frac{\Delta\nu}{\nu} = \frac{v}{c}$  is significant, but when  $\frac{\Delta\nu}{\Delta\nu_D} = \frac{v}{v_{th}}$  is significant. As a consequence, Doppler effects are amplified a factor of  $\frac{c}{v_{th}}$  by the swift variation of the line profile with frequency.

In the present study, for simplicity, only Doppler shifts have been considered ignoring aberration and advection. This is sufficient to a first approximation of the problem under consideration.

The full transformation of the equation of transfer for a nonuniform velocity field has been derived by Castor (1972). The formulation uses the radiation quantities which would be seen by an observer moving with the fluid. The equation of transfer satisfied by the intensity  $I_\nu$ , and the moment equations satisfied by the radiation moments  $J_\nu$ ,  $H_\nu$  and  $K_\nu$  or by  $J$ ,  $H$  and  $K$  has been obtained. It has been shown that the lowest frequency



integrated moment equation has the significance of being the first law of thermodynamics as applied to the radiation and its use ensures that due account is taken of the internal energy and pressure of radiation in overall energy conservation. The formulations are based on the work by Lindquist (1966) who derived the general relativistic radiative transfer equations.

Mihalas (1978) derived the same equations by using a simple first-order expansion method that yields results correct to  $O(\frac{v}{c})$ . One dimensional flows have been considered in this derivation with the application of a local Lorentz transformation to a frame that instantaneously coincides with the moving fluid. The terms of  $O(\frac{v^2}{c^2})$  are ignored and  $\nu = (1 - \frac{v^2}{c^2})^{-1/2}$  is set as 1.

The non-LTE two-level atom line transfer equation in comoving frame for plane parallel medium can be written as (Mihalas, Shine, Kunasz & Hummer 1976)

$$\mu \frac{\partial I}{\partial z} = k_L [\beta + \phi(x)] [S(x, \mu, z) - I(x, \mu, z)] + \left\{ \mu^2 \frac{dV(z)}{dz} \frac{\partial I}{\partial x} \right\} \quad (2.36)$$

where  $\mu = \cos \theta$  ( $\mu \in [0, 1]$ ) and  $\theta$  is the angle between the ray direction and the axis of symmetry  $z$ ;  $x = (\nu - \nu_0) / \Delta \nu_D$ ,  $\nu$  being the frequency,  $\nu_0$  is the line center frequency,  $\Delta \nu_D$  is the Doppler width and  $V(z)$  is the flow velocity. Other quantities are described in section 2.5.1.

The same equations in spherically symmetric atmosphere can be written as (Peraiah 1984)

$$\left\{ \mu \frac{\partial}{\partial r} + \frac{(1 - \mu^2)}{r} \frac{\partial}{\partial \mu} \right\} U = k_L [\beta + \phi(x)] [S(x, \mu, r) - U(x, \mu, r)] + \left\{ [(1 - \mu^2) \frac{V(r)}{r} + \mu^2 \frac{dV(r)}{dr}] \frac{\partial I}{\partial x} \right\} \quad (2.37)$$

Here  $r$  is the radius and  $U(x, \mu, r) = 4\pi r^2 I(x, \mu, r)$ . Other quantities are described in section 2.5.2. Clearly the terms within the curly bracket in the right hand side of both the equations incorporate the comoving conditions.

The solutions of the above equations have been obtained numerically and discussed extensively by Mihalas (1978), Mihalas, Shine, Kunasz & Hummer (1976), Mihalas, Kunasz & Hummer (1975, 1976) as well as Peraiah (1984).

In the present work, equation (2.37) has been generalized into its vector form in order to include linear polarization. It can be written as

$$\left\{ \mu \frac{\partial}{\partial r} + \frac{(1-\mu^2)}{r} \frac{\partial}{\partial \mu} \right\} \begin{pmatrix} U_l(x, \mu, r) \\ U_r(x, \mu, r) \end{pmatrix} = k_L [\beta + \phi(x)] \left[ \begin{pmatrix} S_l(x, \mu, r) \\ S_r(x, \mu, r) \end{pmatrix} - \begin{pmatrix} U_l(x, \mu, r) \\ U_r(x, \mu, r) \end{pmatrix} \right] + \left\{ (1-\mu^2) \frac{V(r)}{r} + \mu^2 \frac{dV(r)}{dr} \right\} \frac{\partial}{\partial x} \begin{pmatrix} U_l(x, \mu, r) \\ U_r(x, \mu, r) \end{pmatrix} \quad (2.38)$$

Equation (2.38) is for spherically symmetric atmosphere. The transfer equation for the plane parallel geometry is a special case of spherical geometry and can be recovered in the limit of zero curvature. Clearly equation (2.38) is vector analogue of the non-LTE two-level atom line transfer equation in comoving frame given by equation (2.37).

The normalized absorption profile is represented either by a Doppler profile

$$\phi(x) = \frac{1}{\sqrt{\pi}} e^{-x^2}, \quad (2.39)$$

or by a Voigt function

$$\phi(x) = \frac{H(a, x)}{\sqrt{\pi}}, \quad (2.40)$$

where

$$H(a, x) = \frac{a}{\pi} \int_{-\infty}^{\infty} \frac{\exp(-y^2)}{a^2 + (x-y)^2} dy,$$

$a$  represents a constant ratio of the damping width to the Doppler width.

The expression within the curly bracket in the right hand side of equation (2.38) is due to the comoving term where  $V(z)$  or  $V(r)$  is the velocity along the axis of symmetry of the medium. Obviously, if  $V(z)$  or  $V(r)$  is zero, the equation reduces to the well known radiative transfer equation in its vector form for a static case as given by equation (2.32).

Similar to the case for a static medium, the line source vector for the spherically symmetric case is given by

$$\mathbf{S}^L(x, \mu, r) = \frac{1}{2} \frac{(1-\epsilon)}{\phi(x)} \int_{-\infty}^{\infty} dx' \int_{-1}^{+1} \mathbf{R}(x, \mu; x', \mu') \begin{pmatrix} U_l(x, \mu, r) \\ U_r(x, \mu, r) \end{pmatrix} d\mu' + \epsilon B(r) \mathbf{1}. \quad (2.41)$$

To maximize the polarization, we always assume a  $j = 0 \rightarrow j = 1$  transition, so that the quantity  $E_1$  in the phase matrix for resonance line scattering given in section 2.4.1 is equal to 1 and  $\mathbf{P}(\mu, \mu')$  takes the form of the well-known Rayleigh phase matrix given by

$$\mathbf{P}(\mu, \mu') = \frac{3}{8} \begin{pmatrix} 2(1 - \mu^2)(1 - \mu'^2) + \mu^2 \mu'^2 & \mu^2 \\ \mu'^2 & 1 \end{pmatrix}.$$

For the sake of simplicity, the complete frequency redistribution function has been considered which is given by

$$\mathbf{R}(x, x') = \phi(x)\phi(x') \begin{pmatrix} 1 \\ 1 \end{pmatrix}.$$

Now equation (2.38) can be rewritten as

$$\begin{aligned} & \left\{ \mu \frac{\partial}{\partial r} + \frac{(1 - \mu^2)}{r} \frac{\partial}{\partial \mu} \right\} \begin{pmatrix} U_i(x, \mu, r) \\ U_r(x, \mu, r) \end{pmatrix} = \phi(x) k_L \mathbf{S}^L(x, \mu, r) + k_c \mathbf{S}^c(r) - \\ & [\phi(x) k_L + k_c] \begin{pmatrix} U_i(x, \mu, r) \\ U_r(x, \mu, r) \end{pmatrix} + \left[ (1 - \mu^2) \frac{V(r)}{r} + \mu^2 \frac{dV(r)}{dr} \right] \frac{\partial}{\partial x} \begin{pmatrix} U_i(x, \mu, r) \\ U_r(x, \mu, r) \end{pmatrix} \end{aligned} \quad (2.42)$$

and for the oppositely directed beam

$$\begin{aligned} & \left\{ -\mu \frac{\partial}{\partial r} + \frac{(1 - \mu^2)}{r} \frac{\partial}{\partial \mu} \right\} \begin{pmatrix} U_i(x, -\mu, r) \\ U_r(x, -\mu, r) \end{pmatrix} = \phi(x) k_L \mathbf{S}^L(x, -\mu, r) + k_c \mathbf{S}^c(r) - \\ & [\phi(x) k_L + k_c] \begin{pmatrix} U_i(x, -\mu, r) \\ U_r(x, -\mu, r) \end{pmatrix} + \left[ (1 - \mu^2) \frac{V(r)}{r} + \mu^2 \frac{dV(r)}{dr} \right] \frac{\partial}{\partial x} \begin{pmatrix} U_i(x, -\mu, r) \\ U_r(x, -\mu, r) \end{pmatrix} \end{aligned} \quad (2.43)$$

The above equations are mixed initial-plus-boundary-value problem for coupled partial integro-differential equations.

In the next chapter the necessary boundary conditions and the method of numerical solutions of equations (2.42) and (2.43) are described in detail.

## Chapter 3

# The numerical method for solving the transfer equations

---

### 3.1 Introduction

The solution of transfer equation depends on the type of physics used. If any change in physics is contemplated, the whole system of solution will have to be modified. This requires new approach and may create new problems due to instability and non-uniqueness of the solution in any numerical treatment.

Several techniques have been developed for solving the transfer equation in the co-moving frame. Chandrasekhar (1945a, 1945b) obtained solutions of the equations for plane-parallel geometry with a linear velocity law. Lucy (1971) solved the equations in planar geometry, with coherent scattering, in the high-velocity limit, by ignoring the spatial derivative and treating the equation as an ordinary differential equation in frequency alone. An integral-equation method for planar geometry has been devised by Simonneau (1973) which can incorporate linear velocity laws only. Noerdlinger and Rybicki (1974) solved the equations in planar geometry by using a Feautrier-type elimination scheme (1968). Assuming complete frequency redistribution Mihalas (1978) solved the equation

by considering Rybicki-type solution.

Among the most notable methods of solving the equation of radiative transfer in comoving frame is the one based on a physical principle called interaction principle. The interaction principle permits one to set up exact difference equations for both reflection and transmission co-efficients for radiation field. These co-efficients are exact and can be used in the calculation of radiation field.

The work of Redheffer (1962) and Preisendorfer (1965) on the interaction principle have been formalized by Grant and Hunt (1969a, 1969b) with the introduction of the internal sources which is crucial for the stellar atmospheres. Following this work, Grant and Peraiah (1972) and Peraiah and Grant (1973) developed a method to obtain direct solution of line transfer problem. This method is called the discrete space theory of Radiative Transfer. In the frame-work of discrete space theory method, Peraiah (1984) developed a method which solves the line transfer equations in comoving frame.

In the present work the method due to Peraiah has been employed to solve the line transfer equations in comoving frame in their vector form as given in by adding polarization terms.

## 3.2 The basic theory of the numerical method

### 3.2.1 Interaction principle

The interaction principle relates the incident and the emergent radiation field from a medium of given optical thickness. In Figure 3.1, a shell of given optical thickness with incident and emergent intensities is shown. It is assumed that the specific intensities  $U_n^+$  and  $U_{n+1}^-$  are incident at the boundaries  $n$  and  $n + 1$  respectively of the shell with optical thickness  $\tau$ . The symbols with signs  $+$  and  $-$  represent specific intensities of the rays travelling in opposite directions. If  $\mu$  represents the cosine of the angle made by a ray with the normal to the plane parallel layers (in the spherical case,  $\mu$  is the angle made by

the ray direction with the radius vector) in the direction in which the geometrical depth decreases.

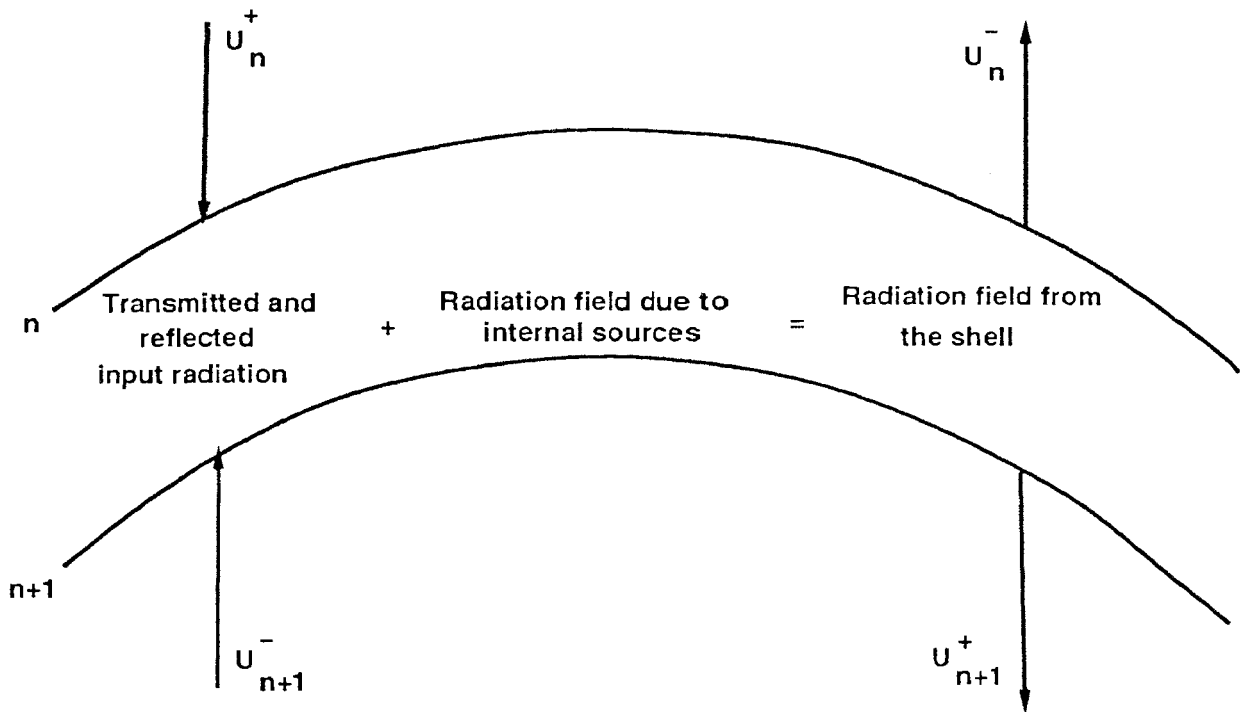


Figure 3.1: Schematic diagram showing the interaction principle.

That is,

$$U_n^+[U_n(\mu) : 0 < \mu \leq 1]$$

and

$$U_n^-[U_n(-\mu) : 0 < \mu \leq 1],$$

$U_n^+$  represents the specific intensity of the ray travelling in the direction  $\mu$  and  $U_n^-$  represents the specific intensity of the ray travelling in the opposite direction. We select

a finite set of values of  $\mu(\mu_j : 1 \leq j \leq m; 0 < \mu_1 < \mu_2 < \mu_3 \cdots \mu_m < 1)$

$$U_n^+ = \begin{pmatrix} U_n(\mu_1) \\ U_n(\mu_2) \\ \vdots \\ U_n(\mu_m) \end{pmatrix}$$

and

$$U_n^- = \begin{pmatrix} U_n(-\mu_1) \\ U_n(-\mu_2) \\ \vdots \\ U_n(-\mu_m) \end{pmatrix}$$

are  $m$ -dimensional vectors on Euclidean space.

The incident intensity vectors are  $U_n^+$  and  $U_{n+1}^-$ . The emergent intensity vectors are  $U_n^-$  and  $U_{n+1}^+$ . The emergent radiation field will have the contributions from the internal sources, say,  $\Sigma^+(n+1, n)$  and  $\Sigma^-(n, n+1)$  corresponding to the output intensity vectors  $U_{n+1}^+$  and  $U_n^-$  respectively.

We assume certain linear operators which reflect and transmit the incident radiation e.g.,  $t(n, n+1)$ ,  $t(n+1, n)$ ,  $r(n, n+1)$  and  $r(n+1, n)$ . These operators are calculated based on the physics of the medium. Then we can write the output intensities in terms of the transmitted and reflected input intensities together with the internal sources as

$$U_{n+1}^+ = t(n+1, n)U_n^+ + r(n, n+1)U_{n+1}^- + \Sigma^+(n+1, n) \quad (3.1)$$

$$U_n^- = r(n+1, n)U_n^+ + t(n, n+1)U_{n+1}^- + \Sigma^-(n, n+1). \quad (3.2)$$

The relationship given by equation (3.1) and equation (3.2) is called the Interaction Principle. Equation (3.1) and equation (3.2) can be written concisely as

$$\begin{pmatrix} U_{n+1}^+ \\ U_n^- \end{pmatrix} = \mathbf{S}(n, n+1) \begin{pmatrix} U_n^+ \\ U_{n+1}^- \end{pmatrix} + \Sigma(n, n+1) \quad (3.3)$$

where

$$\mathbf{S}(n, n+1) = \begin{pmatrix} t(n+1, n) & r(n, n+1) \\ r(n+1, n) & t(n, n+1) \end{pmatrix} \quad (3.4)$$

### 3.2.2 Star Product

If there is another shell with boundaries  $(n+1, n+2)$  adjacent to  $(n, n+1)$ , interaction principle for this shell can be written as (Grant and Hunt 1969a)

$$\begin{pmatrix} U_{n+2}^+ \\ U_{n+1}^- \end{pmatrix} = \mathbf{S}(n+1, n+2) \begin{pmatrix} U_{n+1}^+ \\ U_{n+2}^- \end{pmatrix} + \Sigma(n+1, n+2) \quad (3.5)$$

where  $\mathbf{S}(n+1, n+2)$  is similarly defined as in equation (3.4). If we combine the two shells  $(n, n+1)$  and  $(n+1, n+2)$  then the interaction principle for the combined shell is written as (for the thickness is arbitrarily defined):

$$\begin{pmatrix} U_{n+2}^+ \\ U_n^- \end{pmatrix} = \mathbf{S}(n, n+2) \begin{pmatrix} U_n^+ \\ U_{n+2}^- \end{pmatrix} + \Sigma(n, n+2). \quad (3.6)$$

$\mathbf{S}(n, n+2)$  is called the star product of the two S-matrices  $\mathbf{S}(n, n+1)$  and  $\mathbf{S}(n+1, n+2)$ ; and  $\mathbf{S}(n, n+2)$  can be written as

$$\mathbf{S}(n, n+2) = \mathbf{S}(n, n+1) \star \mathbf{S}(n+1, n+2). \quad (3.7)$$

Equation (3.6) is obtained by eliminating  $U_{n+1}^+$  and  $U_{n+1}^-$  from equation (3.3) and equation (3.5). We can write  $r$  and  $t$  operators for the composite cell as

$$t(n+2, n) = t(n+2, n+1)[I - r(n+2, n+1)r(n, n+1)]^{-1}t(n+1, n), \quad (3.8)$$

$$t(n, n+2) = t(n, n+1)[I - r(n, n+1)r(n+2, n+1)]^{-1}t(n+1, n+2), \quad (3.9)$$

$$\begin{aligned} r(n+2, n) &= r(n+1, n) + t(n, n+1)[I - r(n+2, n+1)r(n, n+1)]^{-1} \times \\ &\quad r(n+2, n+1), \end{aligned} \quad (3.10)$$



$$\begin{aligned} r(n, n+2) &= r(n+1, n+2) + t(n+2, n+1)[I - r(n, n+1)r(n+2, n+1)]^{-1} \times \\ &\quad r(n, n+1) \end{aligned} \quad (3.11)$$

and

$$\Sigma(n, n+2) = \Lambda(n, n+1; n+2)\Sigma(n, n+1) + \Lambda'(n; n+1, n+2)\Sigma(n+1, n+2) \quad (3.12)$$

where  $I$  is the identity matrix and

$$\begin{aligned} \Lambda(n, n+1; n+2) &= \begin{pmatrix} t(n+2, n+1)[I - r(n+2, n+1)r(n, n+1)]^{-1} & 0 \\ t(n, n+1)r(n+2, n+1)[I - r(n+2, n+1)r(n, n+1)]^{-1} & I \end{pmatrix} \\ \Lambda'(n; n+1, n+2) &= \begin{pmatrix} I & t(n+2, n+1)r(n, n+1)[I - r(n, n+1)r(n+2, n+1)]^{-1} \\ 0 & r(n, n+1)[I - r(n, n+1)r(n+2, n+1)]^{-1} \end{pmatrix} \end{aligned}$$

and

$$\Sigma(n, n+1) = \begin{pmatrix} \Sigma^+(n+1, n+2) \\ \Sigma^-(n, n+1) \end{pmatrix}.$$

Similarly,  $\Sigma(n+1, n+2)$  is defined.

In order to obtain physical interpretation of the equations (3.8) - (3.11) we expand the operator inverse in a power series. For example,

$$t(n+2, n) = \sum_{k=0}^{\infty} t_k(n+2, n),$$

$$t_k(n+2, n) = t(n+2, n+1)[r(n, n+1)r(n+2, n+1)]^k t(n+1, n).$$

This operator acts on intensities to the right and gives the contribution to  $U_{n+2}^+$  from  $U_n^+$ . The term  $t_k(n+2, n)$  may be recognized as diffuse transmission from  $n$  to  $n+1$ , diffuse reflection from the layer  $(n, n+1)$ ,  $k$  times in succession and finally diffuse transmission through  $(n+1, n+2)$ . Thus  $t(n+2, n)$  is the sum of contributions involving scattering of all orders  $k = 0, 1, 2, \dots, \infty$ . A similar interpretation can be given for other operators.

If we write  $S(\alpha)$  ( $\alpha$  to designate the cell) then

$$S(\alpha \star \beta) = S(\alpha) \star S(\beta) \quad (3.13)$$

where  $\alpha \star \beta$  denotes the region obtained by putting the two cells  $\alpha$  and  $\beta$  together. If the cells are homogeneous and plane parallel then

$$\alpha \star \beta = \beta \star \alpha. \quad (3.14)$$

In general star multiplication is non-commutative. However, star multiplication is associative. If we have to add several layers  $\alpha, \beta, \gamma, \dots$  then,

$$[(\alpha \star (\beta \star \gamma) \star \dots)] = S[(\alpha \star \beta) \star \gamma \star \dots]. \quad (3.15)$$

If the medium is homogeneous and very thick then we can use what is known as ‘doubling method’. For example,

$$S(2^P d) = S(2^{P-1} d) \star S(2^{P-1} d), (P = 1, 2, 3, \dots) \quad (3.16)$$

which means that we can generate the S-matrix for a layer of thickness  $2^P d$  in  $P$  cycles starting with  $S(d)$  rather than in  $2^P$  cycles of adding the  $S(d)$ s one by one. For example if  $P = 10$ , then only a fraction  $10/2^{10} \simeq 10^{-2}$  of the computational work is needed to add  $2^{10}$  layers of thickness  $d$ .

### 3.2.3 Calculation of radiation field at internal points

We expect the reflection and the transmission operators to be non-negative on the physical grounds that intensities are always non-negative. This condition will be satisfied only when the optical thickness of the shell is less than certain value called the ‘critical size’ or  $\tau_{crit}$ . If the optical thickness  $\tau$  of the shell in question is larger than  $\tau_{crit}$  then we can divide the shell into several subshells whose thickness  $\tau$  is less than  $\tau_{crit}$  and then use star algorithm to calculate combined response from the subshells whose total thickness is  $T$ . If, for example, we need the radiation field at internal points in the atmosphere, we shall have to divide the entire medium into as many shells as we need and calculate the radiation field at the  $N$  points in the medium. One can write down the interaction principle for each shell and solve the whole system of equations.

Figure 3.2 shows the atmosphere in which the internal radiation field is calculated. The atmosphere is divided into  $N$  shells (homogeneous or inhomogeneous) with  $A$  and  $B$  as the inner and outer radii.

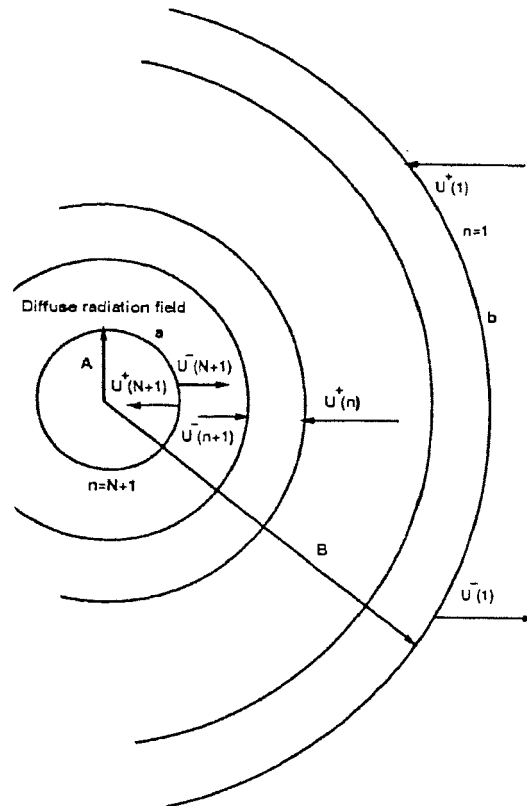


Figure 3.2: Schematic diagram showing the diffuse radiation.

The solution  $U_{n+1}^+$  and  $U_N^-$  (for any shell between shell 1 (at  $b$ ) and shell  $N$  (at  $a$ )) are obtained from the relations

$$U_{n+1}^+ = r(1, n+1)U_{n+1}^- + V_{n+1/2}^+ \quad (3.17)$$

and

$$U_n^- = t(n, n+1)U_{n+1}^- + V_{n+1/2}^- \quad (3.18)$$

with the boundary conditions  $U_{N+1}^- = U^-(a)$ .

The quantities  $r(1, n+1)$ ,  $V_{n+1}^+$  and  $V_{n+1}^-$  are calculated by employing the initial conditions  $r(1, 1) = 0$  and  $V_{1/2}^+ = U^+(b)$ . The computation is done by the following recursive relations :

$$\begin{aligned} r(1, n+1) &= r(n, n+1) + t(n+1, n)r(1, n)[I - r(n+1, n)r(1, n)]^{-1}t(n, n+1), \\ V_{n+1/2}^+ &= t(n+1, n)V_{n-1/2}^+ + \Sigma^+(n+1, n) + R_{n+1/2}\Sigma^-(n, n+1), \\ V_{n+1/2}^- &= r(n+1, n)V_{n-1/2}^+ + T_{n+1/2}\Sigma^-(n, n+1), \end{aligned} \quad (3.19)$$

where

$$\begin{aligned} t(n+1, n) &= t(n+1, n)[I - r(1, n)r(n+1, n)]^{-1}, \\ r(n+1, n) &= r(n+1, n)[I - r(1, n)r(n+1, n)]^{-1}, \\ R_{n+1/2} &= t(n+1, n)r(1, n), \\ T_{n+1/2} &= [I - r(n+1, n)r(1, n)]^{-1}, \\ t(n, n+1) &= T_{n+1/2}t(n, n+1). \end{aligned} \quad (3.20)$$

To calculate the radiation field at the internal points we proceed as follows :

- (1) Divide the medium into a number of shells (say  $N$ ) with  $N+1$  boundaries as mentioned earlier.
- (2) Start calculating the two pairs of reflection and transmission operators  $r(n+1, n)$ ,  $r(n, n+1)$ ,  $t(n+1, n)$  and  $t(n, n+1)$  in each shell. If the optical thickness of any shell is larger than  $\tau_{crit}$  then apply star algorithm to use doubling procedure if the medium is homogeneous.
- (3) With the boundary condition that  $r(1, 1) = 0$  and  $V_{1/2}^+ = U^+(b)$  and the  $r$  and  $t$  operators mentioned in (2) compute recursively  $r(1, n+1)$ ,  $V_{1/2}^+$  and  $t(n, n+1)$  given in equation (3.18) to equation (3.20) from shell 1 to shell  $N$  i.e., from  $b$  to  $a$  in Figure 3.2.
- (4) Next sweep back from  $a$  to  $b$  calculating the radiation field given in equation (3.17) with the boundary condition  $U_{n+1}^- = U^-(a)$ .

### 3.3 Application of Discrete Space Theory

Since all the equations in spherically symmetric case reduce to the special case of plane parallel medium when the curvature term is taken to be zero and the boundary conditions remain the same for both the geometries. we describe, for the sake of convenience and brevity, the application of discrete space theory for solving the transfer equations of polarized radiation in comoving frame for spherically symmetric atmospheres only.

#### 3.3.1 Boundary conditions

In the present work, two types of media have been considered. (1)  $\epsilon = \beta = 0$ , which corresponds to a purely scattering medium. (2)  $\epsilon \neq 0, \beta \neq 0$ , which corresponds to a partially scattering medium with both line and continuum emission. We solve the problem subject to two kinds of boundary conditions : (1) the radiation incident on either side of the atmosphere and (2) the frequency derivative  $\partial U/\partial x$  appearing in the comoving term. Accordingly the boundary conditions adopted are

$$\begin{bmatrix} \mathbf{U}_{N+1}^-(x_i, \tau = T, \mu_j) = 0.5 \\ \mathbf{U}_1^+(x_i, \tau = 0, \mu_j) = 0 \end{bmatrix}; \epsilon = \beta = 0 \quad (3.21)$$

$$\begin{bmatrix} \mathbf{U}_{N+1}^-(x_i, \tau = T, \mu_j) = 0 \\ \mathbf{U}_1^+(x_i, \tau = 0, \mu_j) = 0 \end{bmatrix}; \epsilon, \beta > 0. \quad (3.22)$$

In the second case, we assume  $\partial \mathbf{U}/\partial x = 0$ .

With the above boundary conditions we solve the transfer equations by using discrete space theory described in the previous section.

#### 3.3.2 Method of solution for spherically symmetric medium

To start with, we discretize equation (2.42) and equation (2.43). For frequency discretization we choose discrete frequency points  $x_i$  and weights  $a_i$  so that

$$\int_{-\infty}^{\infty} \phi(x)f(x) \approx \sum_{i=-I}^{+I} a_i f(x_i), \sum_{i=-I}^{+I} a_i = 1,$$

and for angular discretization, we choose angular points  $\mu_j$  and weights  $c_j$  such that

$$\int_0^1 f(\mu) d\mu \approx \sum_{j=1}^m b_j f(\mu_j), \sum_{j=1}^m b_j = 1.$$

We integrate the equation over an interval  $[r_n, r_{n+1}] \times [\mu_{j-1/2}, \mu_{j+1/2}]$  defined on a two dimensional grid. By choosing the roots  $\mu_j$  and the weights  $c_j$  of Gauss-Legendre quadrature formula of order  $J$  over  $(0, 1)$  we calculate the sets  $\mu_{j+1/2}$  and  $\mu_{j-1/2}$  as given by

$$\mu_{j+1/2} = \sum_{k=1}^j c_k$$

and

$$\mu_{j-1/2} = \sum_{k=1}^{j-1} c_k; j = 1, 2, 3 \dots J$$

We define the boundary of the angular interval as  $\mu_{1/2} = 0$ .

Integrating equation (2.42) and equation (2.43) over the angular interval  $[\mu_{j-1/2}, \mu_{j+1/2}]$  and over the spatial cell  $[r_n, r_{n+1}]$  we obtain (Peraiah 1980b)

$$\begin{aligned} & \mathbf{M}[\mathbf{U}_{n+1}^+ - \mathbf{U}_n^+] + \rho_c[\mathbf{\Lambda}^+ \mathbf{U}_{n+1/2}^+ + \mathbf{\Lambda}^- \mathbf{U}_{n+1/2}^-] + \tau_{n+1/2} \mathbf{\Phi}_{n+1/2}^+ \mathbf{U}_{n+1/2}^+ = \\ & \tau_{n+1/2} \mathbf{S}_{n+1/2}^+ + \frac{1-\epsilon}{2} \tau_{n+1/2} [\mathbf{R}^{++} \mathbf{W}^{++} \mathbf{U}^+ + \mathbf{R}^{+-} \mathbf{W}^{+-} \mathbf{U}^-]_{n+1/2} + \mathbf{M}' d \mathbf{U}_{n+1/2}^+ \end{aligned} \quad (3.23)$$

$$\begin{aligned} & \mathbf{M}[\mathbf{U}_{n+1}^- - \mathbf{U}_n^-] - \rho_c[\mathbf{\Lambda}^+ \mathbf{U}_{n+1/2}^- + \mathbf{\Lambda}^- \mathbf{U}_{n+1/2}^+] + \tau_{n+1/2} \mathbf{\Phi}_{n+1/2}^- \mathbf{U}_{n+1/2}^- = \\ & \tau_{n+1/2} \mathbf{S}_{n+1/2}^- + \frac{1-\epsilon}{2} \tau_{n+1/2} [\mathbf{R}^{-+} \mathbf{W}^{-+} \mathbf{U}^+ + \mathbf{R}^{--} \mathbf{W}^{--} \mathbf{U}^-]_{n+1/2} + \mathbf{M}' d \mathbf{U}_{n+1/2}^- \end{aligned} \quad (3.24)$$

$$\mathbf{M} = [\mu \delta_{kk'}], \mathbf{U}_n^\pm = [U]_{k,n}^\pm, U_{k,n}^\pm = U(x_i, \pm \mu_j; r_n; p)$$

where  $k = j + (i - 1)J + (p - 1)IJ; 1 \leq k \leq pIJ, p =$  number of polarization states (in our case  $p = 2$ ).

$$\Phi_{n+1/2}^{\pm} = (\beta + \phi_k^{\pm})_{n+1/2} \delta_{kk'}; \phi_{k,n+1/2}^{\pm} = \phi(x_i, \pm\mu_j, r_{n+1/2}; p),$$

$S_{n+1/2}^{\pm} = [\rho\beta + \epsilon\phi_k^{\pm}]_{n+1/2} B_{n+1/2} \delta_{kk'}, \rho$  being an unspecified parameter.

$W_{n+1/2}^{++}$  are the weight matrices defined as  $W_{n+1/2}^{++} = [W_{k,n+1/2}^{++} \delta_{kk'}]$  with  $\phi_{k,n+1/2}^{+} W_{k,n+1/2}^{++} = a_{i,n+1/2}^{++} c_j$ .

Here the subscripts  $n, n+1, n+1/2$  refer to quantities at  $r_n, r_{n+1}, r_{n+1/2}$  where  $n+1/2$  refers to a suitable average over the cell, i.e.,

$$\begin{aligned} r_{n+1/2} &= \frac{1}{2}(r_{n+1} + r_n), \Delta r_{n+1/2} = r_{n+1} - r_n, \\ \tau_{n+1/2} &= k_L(r_{n+1/2}) \Delta r_{n+1/2}, \\ U_{i,n+1/2}^{+} &= \frac{1}{2}(U_{i,n+1}^{+} + U_{i,n}^{+}), \\ U_{i,n+1/2}^{-} &= \frac{1}{2}(U_{i,n+1}^{-} + U_{i,n}^{-}). \end{aligned}$$

The renormalized weights of integration are defined by :

$$\begin{aligned} a_{i,n+1/2}^{++} &= \frac{a_i \phi_{k,n+1/2}}{\sum_{k=1}^{2IJ} a_i c_j \sum_{k'=1}^{2IJ} R_{k,k',n+1/2}^{++}}, \\ R_{i,j,i',n}^{++} &= R(x_i \mu_j; x'_i \mu'_j; r_n). \end{aligned}$$

The redistribution matrices

$$\mathbf{R}_{i,i',n}^{++}(z) = \begin{bmatrix} \mathbf{R}_{i,i',n}^{++}(1,1) & \mathbf{R}_{i,i',n}^{++}(1,2) \\ \mathbf{R}_{i,i',n}^{++}(2,1) & \mathbf{R}_{i,i',n}^{++}(2,2) \end{bmatrix}$$

where the block matrices corresponding to the components of the phase matrix are defined as

$$\mathbf{R}_{i,i',n}^{++}(\alpha, \beta) = \begin{bmatrix} R_{i,1,i',1,n}^{++}(\alpha, \beta) & \cdots & R_{i,1,i',J,n}^{++}(\alpha, \beta) \\ \vdots & & \\ R_{i,J,i',1,n}^{++}(\alpha, \beta) & \cdots & R_{i,J,i',J,n}^{++}(\alpha, \beta) \end{bmatrix}$$

$$R_{i,j,i',j',n}^{++} = R(x_i \mu_j; x_i' \mu_j'; r_n).$$

$\rho_c$  is the curvature factor given by  $\rho_c = \Delta r / r_{n+1/2}$ ,  $\Lambda^\pm$  is the curvature matrix given by :

$$\Lambda^\pm = \Lambda_{2J}^\pm = \begin{bmatrix} \Lambda_j^\pm & 0 \\ 0 & \Lambda_j^\pm \end{bmatrix}$$

where the  $(J \times J)$  matrices  $\Lambda_j^\pm$  are given by :

$$\begin{aligned} c_j \Lambda_{jk}^+ &= \frac{(1 - \mu_{j+1/2}^2)(\mu_{j+1/2} - \mu_j)}{(\mu_{j+1} - \mu_j)}, k = j+1, j = 1, 2, \dots, J-1 \\ &= \frac{(1 - \mu_{j+1/2}^2)(\mu_{j+1/2} - \mu_{j+1})}{(\mu_{j+1} - \mu_j)} - \frac{(1 - \mu_{j+1/2}^2)(\mu_{j-1/2} - \mu_{j-1})}{(\mu_j - \mu_{j-1})}, \\ &\quad k = j, j = 1, 2, \dots, J \\ &= -\frac{(1 - \mu_{j-1/2}^2)(\mu_j - \mu_{j-1/2})}{(\mu_j - \mu_{j-1})}, k = j-1, j = 2, 3, \dots, J \end{aligned}$$

and

$$c_j \Lambda_{jk}^- = -\frac{1}{2} \delta_{j,1} \delta_{k,1}.$$

The quantities  $\Lambda^+$  and  $\Lambda^-$  are called the curvature matrices. These matrices are the representation of curvature term given by

$$\frac{1}{r} \frac{\partial}{\partial \mu} \begin{pmatrix} U_l(r, \mu) \\ U_r(r, \mu) \end{pmatrix}.$$

For  $J=3$  we have

$$\Lambda^+ = \begin{pmatrix} 0.106 & 1.42 & 0 \\ -1.19 & -0.426 & 0.62 \\ 0 & -0.734 & -0.988 \end{pmatrix}$$

and

$$\Lambda^- = -1.8 \delta_{j,i} \delta_{k,1}.$$



The curvature matrices satisfy the relationship

$$\sum_{j=1}^J c_j (\Lambda_{jj'}^+ - \Lambda_{jj'}^-) = 0, j' = 1, 2, \dots, J$$

which is a necessary and sufficient condition for flux conservation in the spherically symmetric case.

The co-moving terms

$$\left[ (1 - \mu^2) \frac{V(r)}{r} + \mu^2 \frac{dV(r)}{dr} \right] \frac{\partial}{\partial x} \begin{bmatrix} U_l(x, \pm\mu, r) \\ U_r(x, \pm\mu, r) \end{bmatrix}$$

are discretized and put in the term  $\mathbf{M}'\mathbf{d}$ .

$$\mathbf{d} = \begin{bmatrix} \mathbf{d}' & \mathbf{0} \\ \mathbf{0} & \mathbf{d}' \end{bmatrix}$$

where the matrix  $\mathbf{d}'$  is determined from the condition of the flux conservation,  $d'_i = (\mathbf{x}_{i+1} - \mathbf{x}_{i-1})^{-1}$  for  $i = 1, 2, 3, \dots, I - 1$  and  $d'_1 = d'_I = 0$ .

$$\mathbf{M}' = \begin{bmatrix} \mathbf{M}^\circ & \mathbf{0} \\ \mathbf{0} & \mathbf{M}^\circ \end{bmatrix}$$

$$\mathbf{M}^\circ = [\mathbf{M}^1 \Delta V_{n+1/2} + \mathbf{M}^2 \rho_c V_{n+1/2}]$$

$\mathbf{M}^1$  and  $\mathbf{M}^2$  are two diagonal matrices whose nonzero elements are  $[M_m^1]$  and  $[M_m^2]$  where

$$M_m^1 = [\mu_j^2 \delta_{jl}], M_m^2 = [(1 - \mu_j^2) \delta_{jl}]; j, l = 1, 2, \dots, J.$$

$\Delta V_{n+1/2}$  is the radial velocity difference  $V_{n+1} - V_n$  where  $V_{n+1}$  and  $V_n$  represent the velocities at  $r_{n+1}$  and  $r_n$  respectively, while  $V_{n+1/2}$  is the average velocity over the cell bounded by the radii  $r_{n+1}$  and  $r_n$ . The normalization of the curvature matrices is given by :

$$\sum_{j=1}^J c_j (\Lambda_{jk}^+ - \Lambda_{jk}^-) = 0; k = 1, 2, \dots, J.$$

The average intensities  $U_{n+1/2}^{\pm}$  are approximated by the diagonal scheme given by :

$$(1 - \mathbf{X}_{n+1/2})\mathbf{U}_n^+ + \mathbf{X}_{n+1/2}\mathbf{U}_{n+1}^+ = \mathbf{U}_{n+1/2}^+, \quad (3.25)$$

$$(1 - \mathbf{X}_{n+1/2})\mathbf{U}_{n+1}^- + \mathbf{X}_{n+1/2}\mathbf{U}_n^- = \mathbf{U}_{n+1/2}^- \quad (3.26)$$

with

$$\mathbf{X}_{n+1/2} = \frac{1}{2} \begin{bmatrix} \mathbf{X} & \mathbf{0} \\ \mathbf{0} & \mathbf{X} \end{bmatrix}; \mathbf{X} = \frac{1}{2}\mathbf{1}; \mathbf{1} = \begin{bmatrix} 1 & 0 \\ 0 & 1 \end{bmatrix},$$

$\mathbf{1}$  being the unit matrix.

Introducing equation (3.25) and equation (3.26) into equation (3.23) and equation (3.24) we write the resulting equations in the form of interaction principle

$$\begin{bmatrix} \mathbf{M} + \frac{1}{2}\tau[\Phi^+ - \frac{\sigma}{2}\mathbf{R}^{++}\mathbf{W}^{++}] - \frac{1}{2}\mathbf{M}'\mathbf{d} + \frac{\ell\epsilon}{2}\mathbf{\Lambda}^+ & -\frac{\tau\sigma}{4}\mathbf{R}^{+-}\mathbf{W}^{+-} + \frac{\ell\epsilon}{2}\mathbf{\Lambda}^- \\ -\frac{\tau\sigma}{4}\mathbf{R}^{-+}\mathbf{W}^{-+} - \frac{\ell\epsilon}{2}\mathbf{\Lambda}^- & \mathbf{M} + \frac{\tau}{2}[\Phi^- - \frac{\sigma}{2}\mathbf{R}^{--}\mathbf{W}^{--}] - \frac{1}{2}\mathbf{M}'\mathbf{d} - \frac{\ell\epsilon}{2}\mathbf{\Lambda}^+ \end{bmatrix} \\ \times \begin{bmatrix} \mathbf{U}_{n+1}^+ \\ \mathbf{U}_n^- \end{bmatrix} =$$

$$\begin{bmatrix} \mathbf{M} - \frac{1}{2}\tau[\Phi^+ - \frac{\sigma}{2}\mathbf{R}^{++}\mathbf{W}^{++}] + \frac{1}{2}\mathbf{M}'\mathbf{d} - \frac{\ell\epsilon}{2}\mathbf{\Lambda}^+ & \frac{\tau\sigma}{4}\mathbf{R}^{+-}\mathbf{W}^{+-} - \frac{\ell\epsilon}{2}\mathbf{\Lambda}^- \\ \frac{\tau\sigma}{4}\mathbf{R}^{-+}\mathbf{W}^{-+} + \frac{\ell\epsilon}{2}\mathbf{\Lambda}^- & \mathbf{M} - \frac{\tau}{2}[\Phi^- - \frac{\sigma}{2}\mathbf{R}^{--}\mathbf{W}^{--}] + \frac{1}{2}\mathbf{M}'\mathbf{d} + \frac{\ell\epsilon}{2}\mathbf{\Lambda}^+ \end{bmatrix} \\ \times \begin{bmatrix} \mathbf{U}_n^+ \\ \mathbf{U}_{n+1}^- \end{bmatrix} + \tau \begin{bmatrix} \mathbf{S}^+ \\ \mathbf{S}^- \end{bmatrix}$$

where  $\sigma = (1 - \epsilon)$  and the subscript  $(n + 1/2)$  is left out for convenience.

Comparing that with the interaction principle we obtain the ‘cell’ reflection and transmission matrices and the source vectors.

The transmission and reflection matrices are

$$t(n+1, n) = \mathbf{G}^{+-}[\Delta^+ \mathbf{A} + \mathbf{g}^{+-} \mathbf{g}^{-+}]$$

$$t(n, n+1) = \mathbf{G}^{-+}[\Delta^- \mathbf{D} + \mathbf{g}^{-+} \mathbf{g}^{+-}]$$

$$r(n+1, n) = \mathbf{G}^{-+} \mathbf{g}^{-+} [\mathbf{I} - \Delta^+ \mathbf{A}]$$

$$r(n, n+1) = \mathbf{G}^{+-} \mathbf{g}^{+-} [\mathbf{I} - \Delta^- \mathbf{D}]$$

The source vectors are

$$\Sigma^+(n+1, n) = \mathbf{G}^{+-}[\Delta^+ \mathbf{S}^+ + \mathbf{g}^{+-} \Delta^- \mathbf{S}^-] \tau$$

$$\Sigma^-(n, n+1) = \mathbf{G}^{-+}[\Delta^- \mathbf{S}^- + \mathbf{g}^{-+} \Delta^+ \mathbf{S}^+] \tau$$

where

$$\mathbf{G}^{+-} = [\mathbf{I} - \mathbf{g}^{+-} \mathbf{g}^{-+}]^{-1}$$

$$\mathbf{G}^{-+} = [\mathbf{I} - \mathbf{g}^{-+} \mathbf{g}^{+-}]^{-1}$$

$$\mathbf{g}^{+-} = \frac{\tau}{2} \Delta^+ \mathbf{Y}_-$$

$$\mathbf{g}^{-+} = \frac{\tau}{2} \Delta^- \mathbf{Y}_+$$

$$\mathbf{D} = \mathbf{M} - \frac{\tau}{2}\mathbf{Z}_-$$

$$\mathbf{A} = \mathbf{M} - \frac{\tau}{2}\mathbf{Z}_+$$

$$\Delta^+ = [\mathbf{M} + \frac{\tau}{2}\mathbf{Z}_+]^{-1}$$

$$\Delta^- = [\mathbf{M} + \frac{\tau}{2}\mathbf{Z}_-]^{-1}$$

$$\mathbf{Z}_+ = \Phi^+ - \frac{\sigma}{2}\mathbf{R}^{++}\mathbf{W}^{++} - \frac{1}{2}\mathbf{M}'\mathbf{d} + \frac{\rho_c}{\tau}\Lambda^+$$

$$\mathbf{Z}_- = \Phi^- - \frac{\sigma}{2}\mathbf{R}^{--}\mathbf{W}^{--} - \frac{1}{2}\mathbf{M}'\mathbf{d} - \frac{\rho_c}{\tau}\Lambda^+$$

$$\mathbf{Y}_+ = \frac{\sigma}{2}\mathbf{R}^{-+}\mathbf{W}^{-+} + \frac{\rho_c}{\tau}\Lambda^-$$

$$\mathbf{Y}_- = \frac{\sigma}{2}\mathbf{R}^{+-}\mathbf{W}^{+-} - \frac{\rho_c}{\tau}\Lambda^-$$

### 3.4 Stability condition and correctness check

The method discussed in the previous sections can handle the problem arising out of the coupling of the co-moving points across the line profile and the local velocity gradients. The stability of the solution is achieved by controlling the step-size, which arises in the discretization in radial, angle and frequency integrations. For this purpose the optical and the geometrical depths in each shell should be chosen such that unique and non-negative solution is obtained. This can be achieved by obtaining non-negative  $\mathbf{r}$  and

t matrices. Therefore the diagonal elements  $(\Delta^\pm)^{-1}$  should be dominant and positive. This condition leads to the inequality

$$\tau_{k,k} < \left| \frac{2\mu_k \pm \rho_c \Lambda_{k,k}^+ - d_{k,k} \{ \mu_{k,k}^2 \Delta V_{n+1/2} + (1 - \mu_{k,k}^2) \rho_c V_{n+1/2} \}}{(\beta + \phi_k) - \frac{1}{2} \sigma(\phi \phi^T W)_{kk}} \right|$$

Further, the off-diagonal elements of  $[\Delta^\pm]^{-1}$  should be negative and consequently

$$\tau_{k,k+1} < \left| \frac{2\rho_c \Lambda_{k,k+1}^+ - 2d_{k,k+1} \{ \Delta V_{n+1/2} \mu_{k,k+1}^2 + \rho_c V_{n+1/2} (1 - \mu_{k,k+1}^2) \}}{\sigma(\phi \phi^T W)_{k,k+1}} \right|$$

for the upper diagonal elements and

$$\tau_{k+1,k} < \left| \frac{2\rho_c \Lambda_{k+1,k}^+ + 2d_{k+1,k} \{ \Delta V_{n+1/2} \mu_{k+1,k}^2 + \rho_c V_{n+1/2} (1 - \mu_{k+1,k}^2) \}}{\sigma(\phi \phi^T W)_{k+1,k}} \right|$$

for the lower diagonal elements.

Therefore, we have to select  $\tau_{crit}$  such that

$$\tau_{crit} = \min\{\tau_{k,k}, \tau_{k,k+1}, \tau_{k+1,k}\}$$

Hence the 'cell' optical depth  $\tau_{crit}$  depends on the number of cosines selected for the angle integration, the frequency differencing, the radial mesh, the differential velocity, the local velocity of the gas and the profile function.

It is worth mentioning that along with the step-size criteria, the normalization conditions on the polarized redistribution matrix, the profile function and the curvature matrix for spherical medium must be satisfied.

The inclusion of differential velocity gradient makes the control of critical step-size quite difficult as the optical depth changes significantly with the increase in velocity. However, we have obtained stable solutions for various situations upto 20 mean thermal unit of velocity of the atmosphere by taking  $\tau_{crit} \leq 0.1$ .

The correctness checking of the method has been performed in two different ways.

### 3.4.1 Global flux conservation

A convenient test of the efficacy of the numerical method is to study the case of conservative scattering. In a purely scattering medium, the physical system must neither

create nor destroy energy. For this purpose we apply unpolarized incident radiation at the boundary of the inner radius of the shell and no radiation is incident at the outer shell. For a conservatively scattering medium, the total flux that is introduced at the inner boundary should be the sum of the flux that comes out of the outer boundary and the backscattered flux at the inner boundary.

If  $F_I^-(A)$  is the incident total flux (*i.e.*,  $F_I^- + F_r^-$ ) at the innermost shell at point  $r = A$  (see Figure 3.2),  $F_I^-(B)$  is emerging flux at  $r = R$  and  $F_I^+(A)$  is the flux backscattered into the inner region at  $r = A$  with the additional condition that no incident flux is given at B, then we must have the identity for conservatively scattering medium as

$$F_I^-(A) = F_I^+(A) + F_I^-(B).$$

We have considered several optical depths, geometrical thickness and velocity gradients of the medium and calculated the global energy conservation. In a plane-parallel and homogeneous medium the numbers are satisfied to one part in  $10^{-14}$ . In spherically symmetric case the numbers are satisfied to one part in  $10^{-9}$ .

For an example, in a spherically symmetric atmosphere with inner radius  $10^{11}$  cm and outer radius  $3 \times 10^{11}$  cm, total optical depth  $T = 10^3$ , velocity at the innermost shell  $V_A = 0$  and that at the outermost shell  $V_B = 20$  mtu, incident intensity for each component ( $l$  and  $r$ ) at  $A$  equal to 0.5, we obtain

$$F_I^-(A) = 2.00$$

$$F_I^-(B) = 0.027992526$$

$$F_I^+(A) = 1.9720075$$

Hence,  $F_I^-(A) - F_I^-(B) - F_I^+(A) = 8.32 \times 10^{-10}$

In the above calculation a 3 point Gauss-Legendre quadrature formula and 17 points trapezoidal rule have been applied.

### 3.4.2 Specular reflection at the inner boundary

The second set of problems we have used to test the method are those in which the outer boundary is illuminated isotropically and specular reflection at the inner boundary. In such a case the positive and negatively directed fluxes at every interface must be equal (Peraiah 1973).

If the surface at  $a$  is reflecting, one can write

$$\begin{pmatrix} U_l^- \\ U_r^- \end{pmatrix}_{N+1} = \mathbf{r}_G \begin{pmatrix} U_l^+ \\ U_r^+ \end{pmatrix}_{N+1}$$

where  $\mathbf{r}_G$  is the reflection operator. For a totally reflecting surface

$$\mathbf{r}_G = \begin{pmatrix} 1 \\ 1 \end{pmatrix}.$$

Therefore, we have

$$\begin{pmatrix} U_l^+ \\ U_r^+ \end{pmatrix}_{N+1} = [\mathbf{I} - \mathbf{r}(1, N+1)\mathbf{r}_G]^{-1} \mathbf{V}_{N+1/2}^+$$

from which one can calculate  $\begin{pmatrix} U_l^- \\ U_r^- \end{pmatrix}_{N+1}$ . Rest of the calculations follow equation (3.17).

The results have been presented in Table 3.1, Table 3.2 and in Table 3.3. In the calculations we have taken the total optical depth  $T$  equal to  $10^3$ , the velocity at the innermost shell is set as  $V_A = 0$  and the velocity at the outermost shell is denoted by  $V_B$ . We have employed a linear velocity rule. In the plane parallel case the medium is considered to be homogeneous whereas in the spherically symmetric case the medium is considered to be inhomogeneous with the optical depth varies as the inverse square of the geometrical depth. The quantity  $B/A$  which denotes the ratio between the inner radius and the outer radius of the atmosphere is set to 3 for spherically symmetric medium whereas it is kept 1 for plane-parallel case. The input intensity at the outermost shell is taken to be 0.5 for each components. The equality of inward and outward net fluxes at each shell boundary confirms the correctness of the numerical method.

Table 3.1: Net fluxes  $(F_I^-)_n = (F_I^+)_n$  at nth shell interface with  $B/A = 1$  and  $V_B = 20$ .

n	$(F_I^-)_n = (F_I^+)_n$
100	5.000
90	5.038
80	5.033
70	5.030
50	5.028
30	5.039
20	5.049
15	5.053
10	5.056
5	5.057
1	6.000



Table 3.2: Net fluxes  $(F_I^-)_n = (F_I^+)_n$  at nth shell interface with  $B/A = 3$  and  $V_B = 0$ .

$n$	$(F_I^-)_n = (F_I^+)_n$
100	0.728
90	1.0424
80	1.409
70	1.826
60	2.292
50	2.805
40	3.36
30	3.959
20	4.6
15	4.933
10	5.275
5	5.63
1	6.000

Table 3.3: Net fluxes  $(F_I^-)_n = (F_I^+)_n$  at nth shell interface with  $B/A = 3$  and  $V_B = 20$ .

n	$(F_I^-)_n = (F_I^+)_n$
100	0.900
90	1.194
80	1.501
70	1.836
60	2.164
50	2.526
40	2.975
30	3.544
20	4.245
15	4.636
10	5.038
5	5.475
1	6.000

### 3.5 Calculation of the flux at the observer's frame

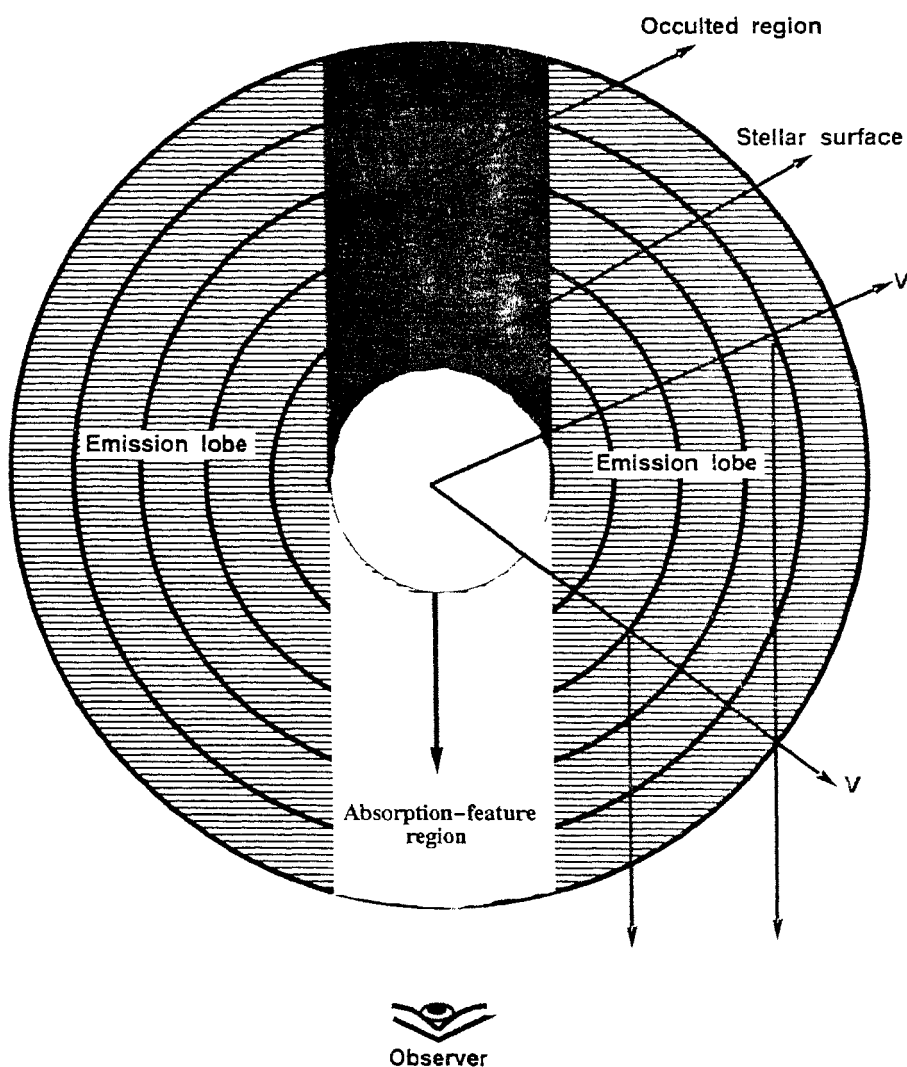


Figure 3.3: Diagram showing how fluxes are calculated at infinity.

The radiation field obtained in the comoving frame should be translated into either (i) the rest frame of the star which describes the solution of radiative transfer in spherical symmetry or (ii) onto the frame of reference of the observer at infinity. In the present work we have performed the latter type of calculations as these could be useful for direct comparison with observations. In Figure 3.3 we have described how the radiation field in

the comoving frame has been translated into the frame of reference of the observer at the earth. The procedure is briefly as follows (Mihalas 1978): we solve the transfer equations for polarized radiation in comoving frame by assuming a certain velocity distribution  $V(\mathbf{r})$  and density distribution  $\rho(\mathbf{r})$ . When the solution is obtained, one can calculate the  $l$  and the  $r$  components of the frequency-independent but angle dependent source functions  $S_l(\mathbf{r})$  and  $S_r(\mathbf{r})$  at every radial point along a certain angle by the relations (Peraiah 1980b):

$$(S_l)_n = \sum_{i=1}^I a_i \sum_{j=1}^J S_l(x_i, \tau_n) c_j \quad (3.27)$$

and

$$(S_r)_n = \sum_{i=1}^I a_i \sum_{j=1}^J S_r(x_i, \tau_n) c_j \quad (3.28)$$

The optical depth is calculated along the parallel rays as shown in Figure 3.3 and not along the radial direction in the atmosphere. With the help of equation (3.27) and equation (3.28) along with prescribed velocity and density distribution one can find out the  $l$  and the  $r$  components of the fluxes received at infinity and hence the degree of polarization.

## Chapter 4

# Resonance line polarization in expanding stellar atmosphere stratified into plane-parallel<sup>1</sup>

---

### 4.1 Introduction

Having described the numerical procedure to solve the transfer equation for polarized radiation in comoving frame we now present the detail results under various physical conditions. There are several processes which can be affected by the inclusion of a velocity field. In order to obtain a clear picture of how the polarized profile gets affected by the velocity field, we divide the discussions into two separate parts according to the geometry of the medium which depends on the size of the star and does not depend on the velocity field. For stars with comparatively small size, one can assume the geometry of the medium to be stratified into plane-parallel layers. Physically this type of situation is ideal for white dwarf and solar type stars. However, in the whole discussion we neglect the effect of any external magnetic field and therefore the axial symmetry of the

---

<sup>1</sup>Also see : Sengupta, S., MNRAS 265 (1993) 513.

radiation field is always restored. In the present discussion we consider a homogeneous and isothermal medium for simplicity as the basic aim of the investigation is to find out the effect of radial expansion of the atmosphere to line intensity and polarization.

One of the essential parameters of the two-level atom model is  $\epsilon$ , the probability that a photon is destroyed by collisional de-excitation during scattering which is also called the thermalization parameter. The range of variation of this probability factor is  $[0,1]$ . the case  $\epsilon = 1$  refers to the pure LTE case. Other values of  $\epsilon$  refer to the non-LTE situation. The extreme case of  $\epsilon = 0$  means the atmosphere is a purely scattering medium. As  $\epsilon$  increases starting from zero, the thermalization of photons also increases, i.e., the thermal coupling with continuum radiation field increases due to an increase in the number of collisions instead of scatterings. Therefore, one expects maximum polarization in the case  $\epsilon = 0$ , i.e., in a purely scattering medium. In the present investigation, we consider first a purely scattering medium and then a partially scattering medium with non-zero  $\epsilon$ .

In the calculations we have always taken a 13 frequency point Trapezoidal rule with equal spacing. Since with the inclusion of velocity, the profile becomes asymmetric with respect to the line center, we have presented the full frequency grid. For angle integration, we have taken a three point Gauss-Legendre quadrature formula with  $\mu_1 = 0.11$ ,  $\mu_2 = 0.5$ , and  $\mu_3 = 0.88$ . the radiation field has always been calculated along  $\mu_1 = 0.11$ . The results are presented graphically for the sake of convenience.

## 4.2 Model parameters

In order to make the geometry compatible with the expansion of the medium, we have taken the inner radius of the star equal to  $1 \times 10^{10}$  while the outer radius being equal to  $1.1 \times 10^{10}$  so that the geometrical depth is as small as  $10^9$ . However, we have always kept the ratio of the outer radius to the inner radius denoted by  $B/A$  as 1. Off course, while transforming all the physical quantities from the comoving frame to the observer's frame again the actual ratio, i.e., 1.1 has been restored. The purpose is to exclude the

curvature effect in calculating various physical quantities in comoving frame, specially the source functions. The total optical depth is considered as  $T = 50$  and the medium is divided into 50 homogeneous layers.

In all the earlier investigations (Rees & Saliba 1982, Faurobert 1987), it was found that the effect of complete frequency redistribution does not differ much compared to that of partial frequency redistribution at the line. This is because of the fact that in both the cases the redistribution probability is much higher at the line (maximum at the line center) compared to that at the wing or at the continuum. So the photons in the line retain a high degree of coherence in the scattering process (Rees & Saliba 1982). Mihalas et al. (1976) found that both in the static and the moving atmospheres, the profile obtained using complete redistribution function and partial redistribution function are virtually identical. Hence, we always consider complete frequency redistribution which is easier to handle in the numerical calculation.

Regarding the thermalization parameter we consider two situations, (i)  $\epsilon = \beta = 0$ , i.e., a purely scattering medium with unpolarized radiation at the innermost layer and no emission in the medium; (ii)  $\epsilon = \beta = 10^{-5}$ , i.e., a partially scattering medium with no incident radiation at the boundaries but constant emission of radiation in the medium. For both the cases we have provided the amount of radiant energy emitted at each layer as  $B = 0.5$  in the unit of Planck function for each component. For the plane-parallel case we have assumed a Doppler profile given as:

$$\phi(x) = \frac{e^{-x^2}}{\sqrt{\pi}}.$$

In the calculation of the total flux as well as the degree of polarization along the line of sight of an observer at infinity, an inverse square law for the matter density distribution has been adopted with the damping parameter set to be  $10^{-3}$ .

Finally, we have to select a velocity distribution law. For the isotropic case, Mihalas and co-workers (Mihalas, Kunasz & Hummer 1975, Mihalas, Shine, Kunasz & Hummer 1976, Mihalas, Kunasz & Hummer 1976) considered a linear as well as a tangential velocity rules whereas Peraiah (1980a, 1980b, 1991) considered a linear velocity rule as

well as a velocity rule prescribed by Lucy (1971) and Castor & Lamers (1979). Peraiah & Varghees (1993) presented the relevant mass-momentum equations and calculated the expected velocity profile in the context of stellar winds in O and B type stars. Since, in the isotropic case it is found that the velocity rule plays an important role in determining the radiation field, we therefore would like to investigate the effect of velocity field by considering more than one velocity rule. For this purpose, we adopt the velocity rule given by Lucy (1971) and Castor & Lamers (1979) which can be written as

$$V(r) = V_B \left[ 1 - (1 - \alpha) \left( \frac{R}{r} \right) - \alpha \left( \frac{R}{r} \right)^2 \right]^{1/2} \quad (4.1)$$

where  $V(r)$  is the velocity at the radial point  $r$ ,  $V_B$  is the velocity at the outermost boundary,  $R$  is the photospheric radius or the inner radius of the star and  $\alpha$  is an arbitrary constant whose value is set as +0.9 and -1.0. It is worth mentioning at this point that for a plane-parallel atmosphere the velocity distribution  $V(r)$  does not play any role in determining various physical quantities in comoving frame as can be seen from equations (2.36). Rather it is the quantity  $\Delta V / \Delta z = (V_B - V_A) / z$  that is used in the calculations. However, when we calculate the flux and the degree of polarization in the observer's frame,  $V(r)$  plays important role. In the present work we have taken the velocity at the outermost layer to be 5, 10 and 20 mean thermal units in order to investigate the effect of small, medium and large velocity gradient. The velocity at the innermost layer  $V_A$  is always kept 0. The results have been compared with that of the static case by taking  $V_B = 0$  as well.

### 4.3 Results and discussions

As mentioned earlier, in a purely scattering medium one usually expects maximum polarization and so we first discuss this situation. In Figure 4.1 we show how the intensity of a photon with the line-center frequency  $X = 0$  changes from the innermost to the outermost layer. In the absence of a velocity field the emergent intensity of a photon remains the same throughout the atmosphere as depicted in Figure 4.1. This implies that



the photon essentially does not lose its energy while traversing through the atmosphere. Since  $\epsilon = 0$ , there is no collisional de-excitation and the photon is not destroyed but merely changes its direction after scattering. The intensity of the backscattered photon also remains constant throughout the atmosphere as can be seen from Figure 4.2. This clearly indicates that in a purely scattering, homogeneous and plane-parallel atmosphere, the amount of emergent and backscattered intensities of the radiation field is the same at each point along the geometrical depth, i.e., there is no loss in photon energy at any layer of the atmosphere. However the intensity of the backscattered radiation is much smaller than that of the emergent radiation at each layer. Because of the low optical depth the backscattered radiation is small and most of the radiation is capable of emerging out from the boundary of each layer.

This situation is altered significantly with the inclusion of a non-zero velocity field. With the inclusion of a velocity field as small as 5 mtu at the outermost layer, the intensity of the emergent radiation falls slowly from the innermost layer to the outermost layer. As the velocity gradient increases, the fall in the intensity towards the outer region is more rapid. On the other hand, the intensity of the backscattered radiation remains almost the same upto the middle of the atmosphere and then it starts decreasing rapidly. This result indicates that with the inclusion of velocity field, the matter in the atmosphere is driven outwards creating a blockade to the emergent radiation. Since the number of scatterer increases in the outward direction the line photon cannot escape to the outer layer and hence the intensity falls. From Figure 4.2 it is clear that the photon after scattering moves in different direction and not in exactly the opposite direction as the intensity of the backscattered radiation also drops outwards. Owing to the adopted boundary conditions given as:

$$\left[ \begin{array}{l} I_{N+1}^-(x_i, \tau = T, \mu_j) = 0.5 \\ I_1^+(x_i, \tau = 0, \mu_j) = 0 \end{array} \right]; \epsilon = \beta = 0 \quad (4.2)$$

the emergent intensity at the innermost layer is the same for all the velocity gradient while the backscattered intensity is the same at the outermost layer.

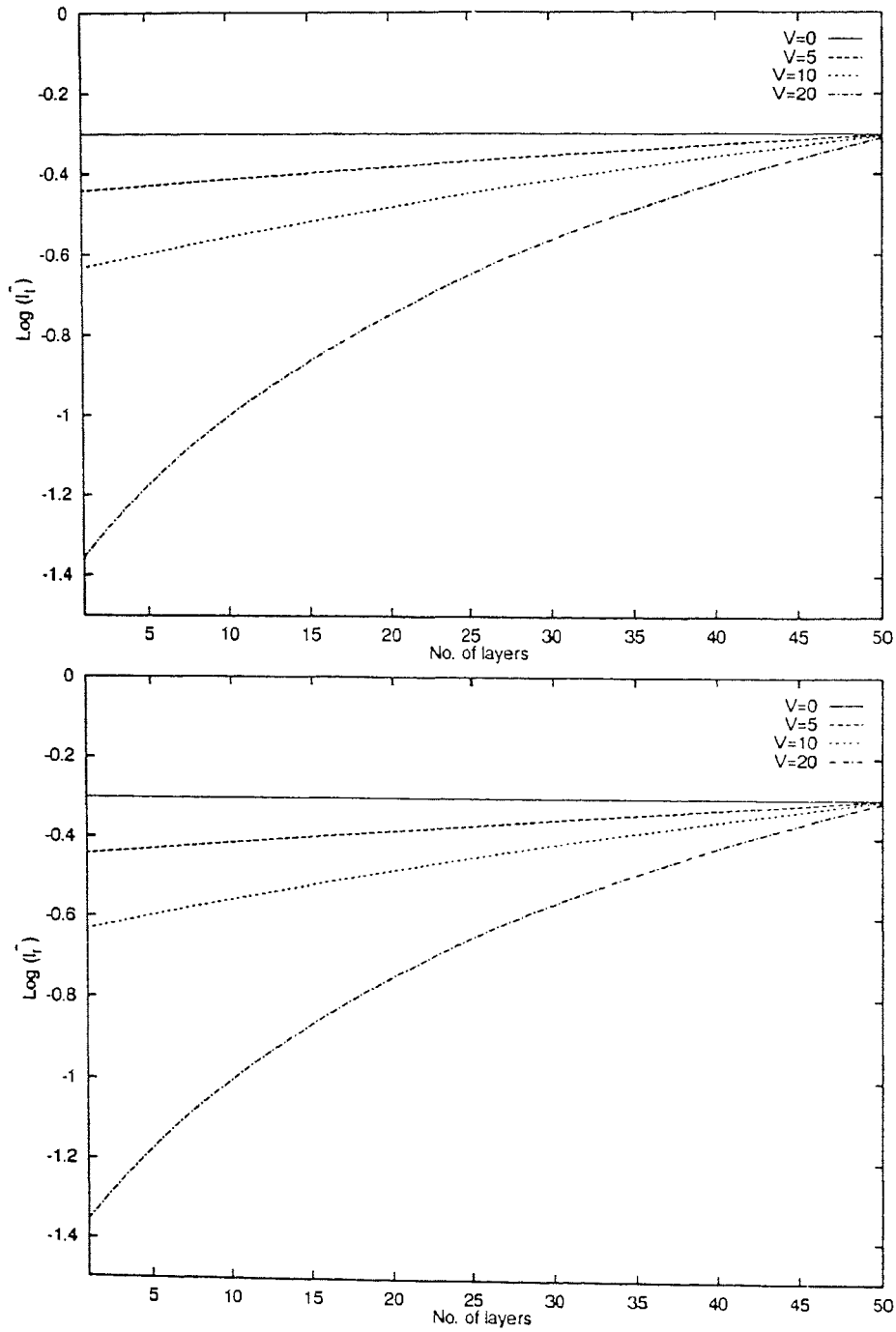


Figure 4.1:  $l$  and  $r$  components of the emergent intensity along the direction  $\mu = 0.11$  in comoving frame with frequency  $X = 0$ .  $\epsilon = \beta = 0$ ,  $B/A = 1$  and total optical depth  $T = 50$ . In all figures  $V$  represents the velocity at the outermost layer, i.e.,  $V$  in the figure means  $V_B$  in the text.

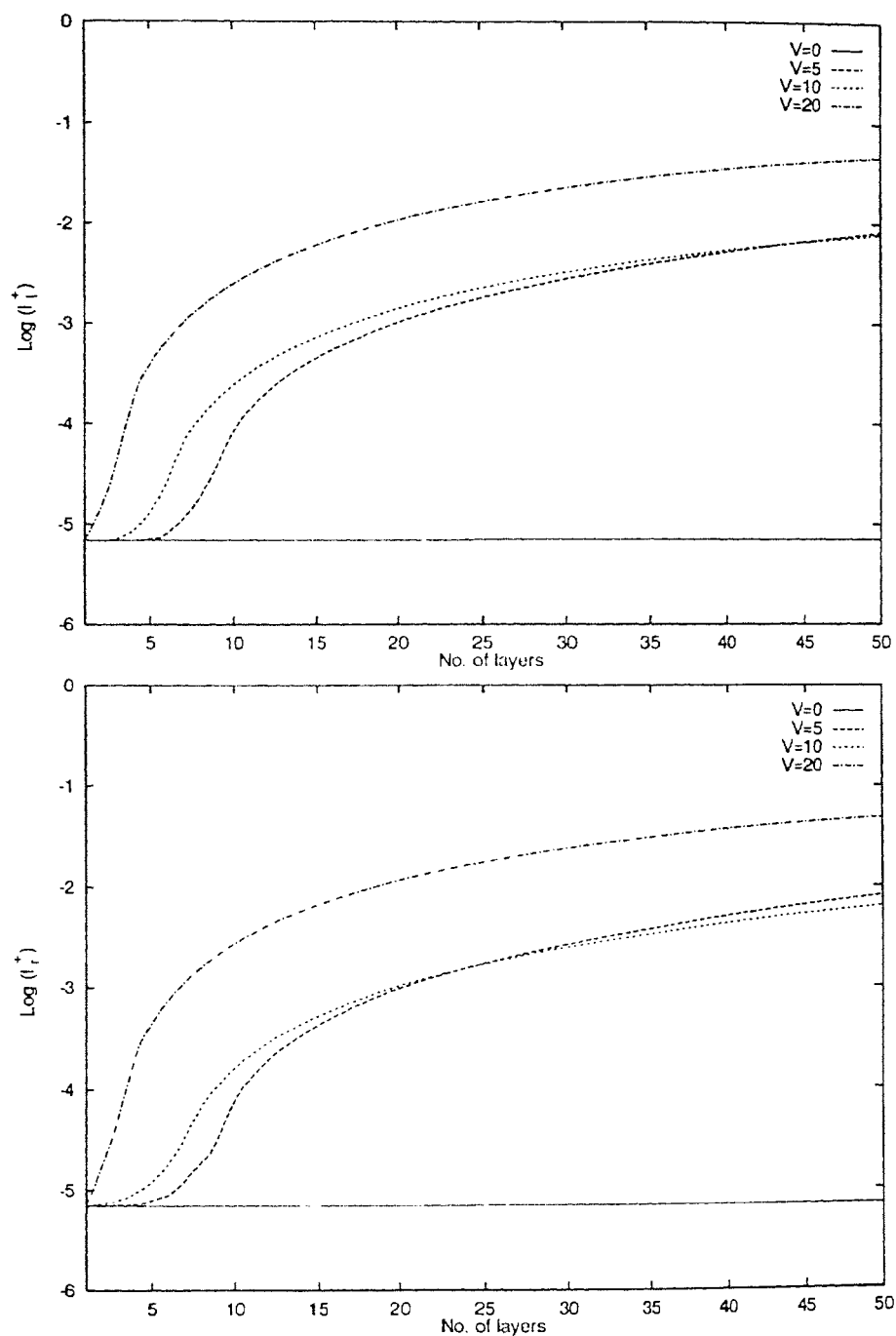


Figure 4.2:  $l$  and  $r$  components of the backscattered intensity along the direction  $\mu = 0.11$  in comoving frame with frequency  $X = 0$ .  $\epsilon = \beta = 0$ ,  $B/A = 1$  and total optical depth  $T = 50$ .

The small difference in the numerical values of the  $l$  and the  $r$  components of the emergent and the backscattered intensity cannot be resolved graphically but a small difference between them gives rise to non-zero polarization. It is found that this difference increases as the photon traverses outwards. This means the degree of polarization is essentially zero at the innermost layer and it increases with the increase in geometrical depth.

Figure 4.3 presents the total emergent intensity and the degree of polarization in the comoving frame along the direction  $\mu = 0.11$ . Since the medium under consideration is purely scattering, absorption profile at the line is formed. Although the total intensity decreases as the velocity increases, the profile remains symmetric at the line. But at the wing, there are significant asymmetry in the intensity profile when velocity field is taken into consideration. This asymmetry increases as the velocity gradient increases from 5 mtu to 20 mtu. The total emergent intensity for all the cases becomes zero at the continuum due to the adopted boundary condition.

The polarized profile in comoving frame is almost symmetric for all the cases. There is slight asymmetry observed at the wing. The degree of polarization is maximum at the line center and decreases towards the wing. At the continuum the degree of polarization is zero due to the boundary condition.

From Figure 4.3 it can be seen that except for large velocity gradient the degree of polarization in comoving frame remains almost the same for any velocity gradient. With large velocity gradient, it is larger than that without any velocity field. Therefore, in comoving frame the basic feature of the polarized profile remains the same.

Figure 4.4 shows the  $l$  and the  $r$  components of the frequency independent source function along the direction  $\mu = 0.11$ . From Figure 4.4 we observe that the source function for a static medium remains constant through out the atmosphere which reflects the adopted homogeneous and isothermal conditions in a purely scattering plane-parallel medium. With the inclusion of velocity field this behaviour of the source function gets altered dramatically. For a small velocity gradient both the  $l$  and the  $r$  components of the

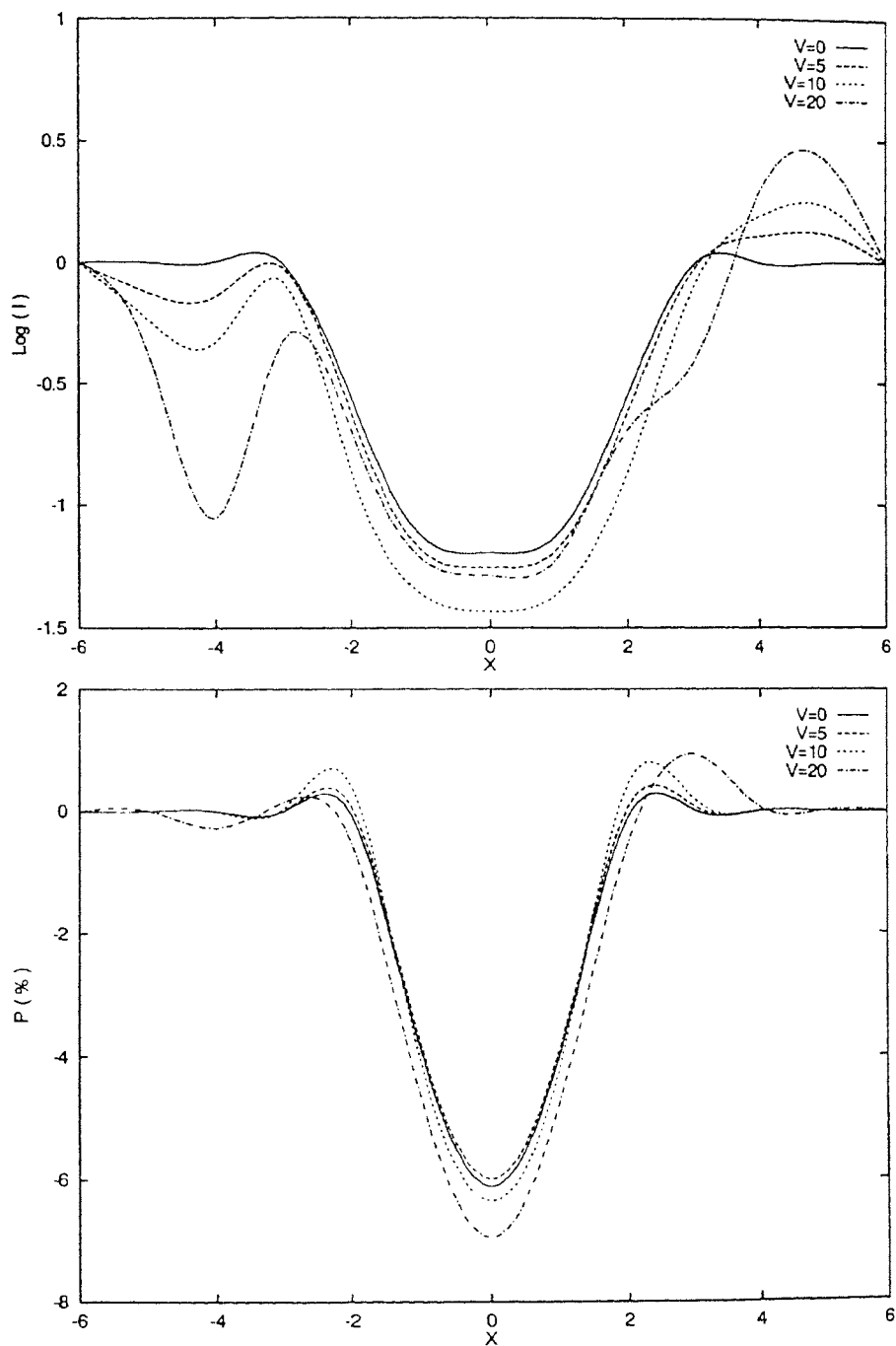


Figure 4.3: Emergent intensity and polarization profiles along the direction  $\mu = 0.11$  in comoving frame.  $\epsilon = \beta = 0$ ,  $B/A = 1$  and total optical depth  $T = 50$ .

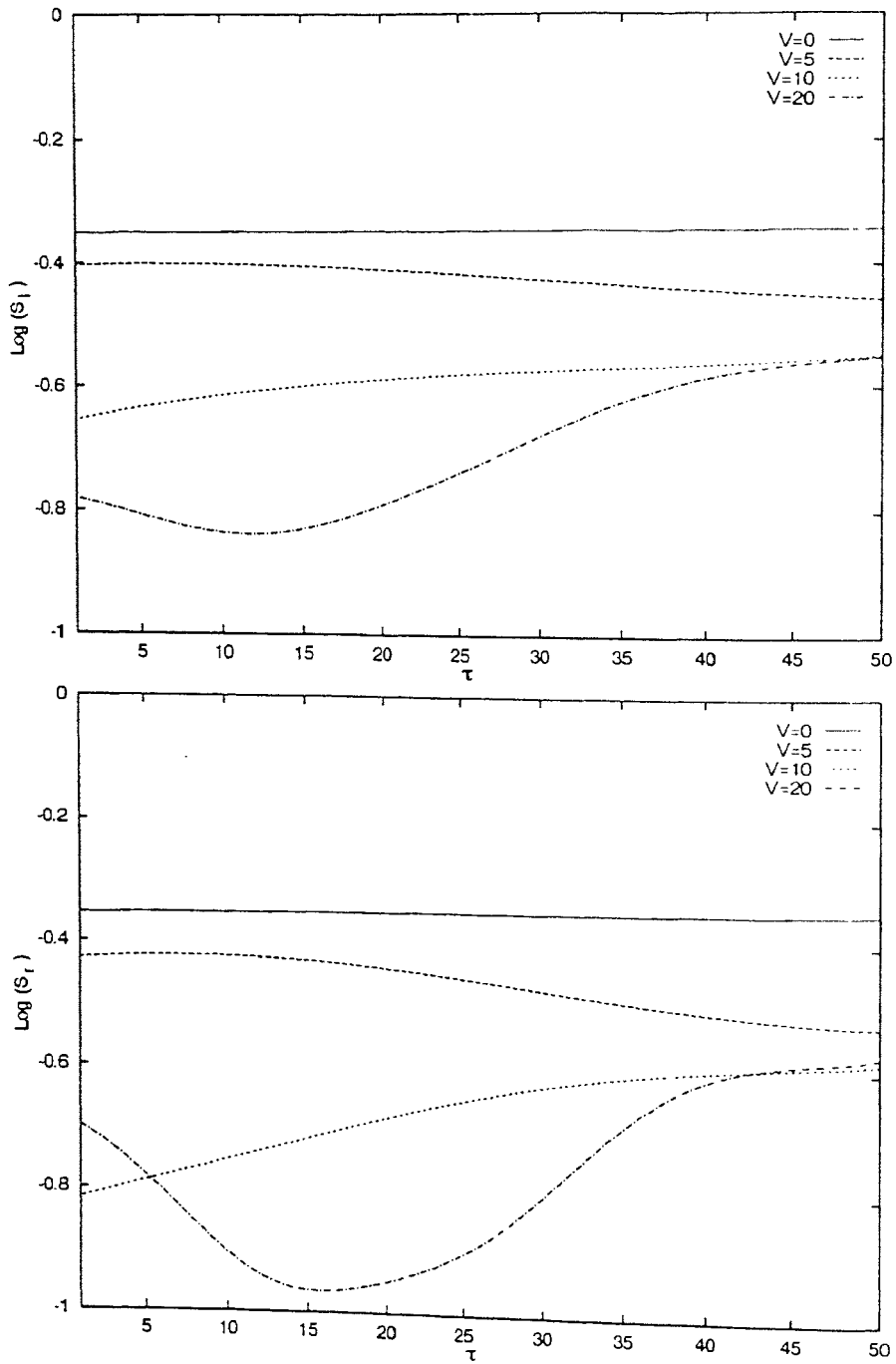


Figure 4.4:  $l$  and  $r$  components of the frequency independent source function along the direction  $\mu = 0.11$  in comoving frame.  $\epsilon = \beta = 0$ ,  $B/A = 1$  and total optical depth  $T = 50$ .

source function increases slowly with the decrease in optical depth while for a medium velocity gradient e.g., 10 mtu the source function increases with the increase in optical depth. For a large velocity gradient, the source function first decreases in the outward direction upto three fourth of the atmospheric height and then again increases. This behaviour of the source function can be attributed to the mass motion of the atmosphere. The value of the source function is maximum for the static case and minimum when the velocity gradient is maximum. This is because of the fact that with the increase in velocity the escape probability of the line photons enhances significantly which in the absence of velocity field would have remained trapped. From Figure 4.4 it can be seen that the significant change in the source function occurs when a velocity gradient of 10 mtu or more is taken into consideration. Since, the  $l$  and the  $r$  components of the source function are used to calculate the total flux and the degree of polarization along the line of sight of an observer at infinity, the difference in the magnitude of the  $l$  and the  $r$  components of the source function determines the amount of polarization along the line of sight. For the static case, Figure 4.4 shows insignificant difference between the two components of the source function and hence there must be less polarization in this case as depicted in Figure 4.5 and Figure 4.6.

As mentioned earlier, in the calculation of the physical quantities in comoving frame for plane-parallel medium the velocity law does not play any role. But, while transforming the quantities from the comoving frame to the observer's frame the form of the velocity rule carries an important role. Therefore, we have used the same source function in calculating the flux and the degree of polarization along the line of sight of an observer at infinity with two different velocity rules. Figure 4.5 shows the flux and the degree of polarization in the observer's frame by using the velocity laws given by equation (4.1) with  $\alpha = +0.9$  and Figure 4.6 shows that with  $\alpha = -1.0$ . In order to include all the results in a single figure we have taken the ratio of frequency to the maximum frequency. The total flux is presented in the unit of the flux at the continuum. The significant role played by the form of the velocity rule can be visualized from the polarized profile while the nature of the flux profile remains almost the same. From Figure 4.5 and Figure

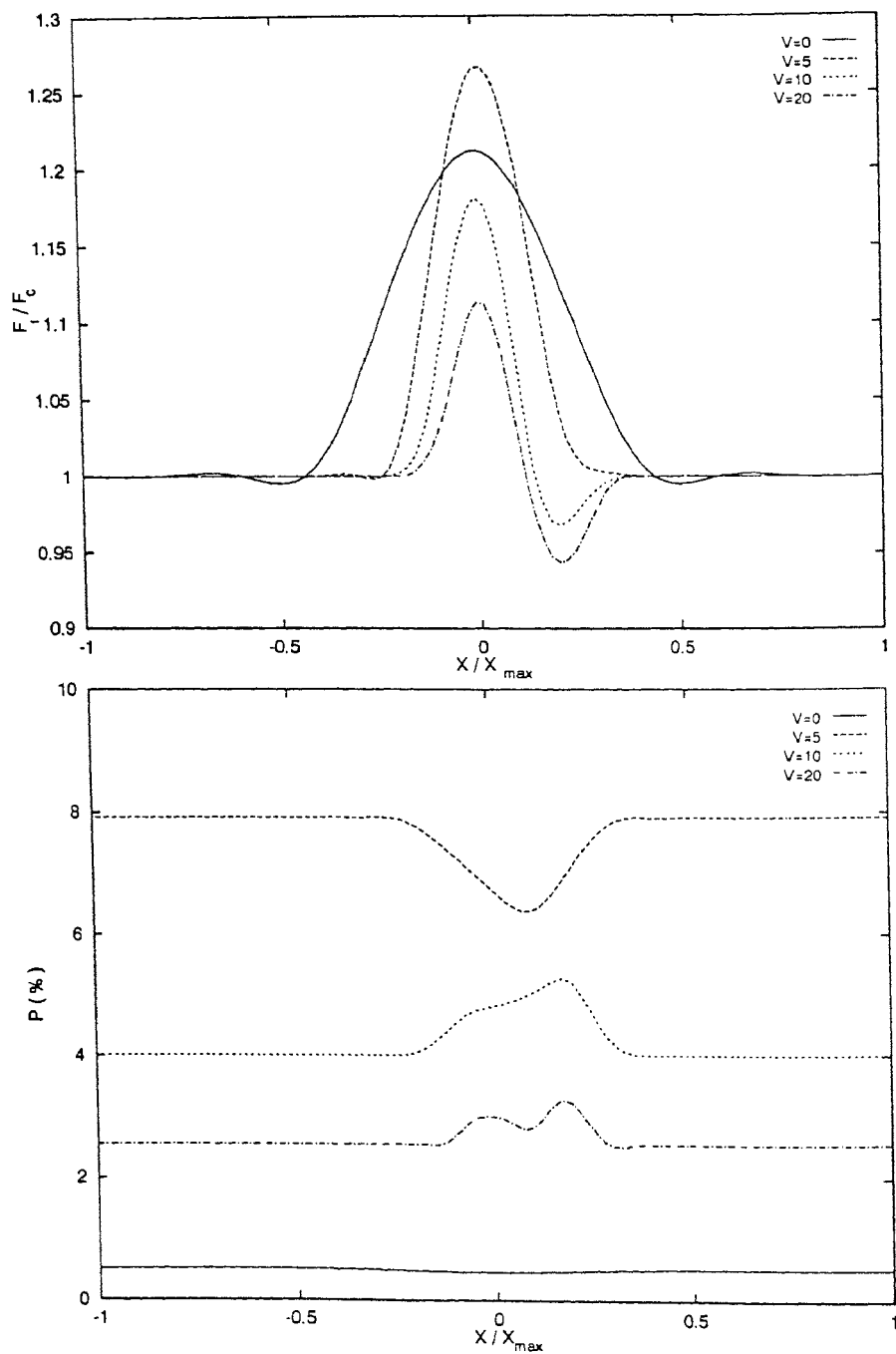


Figure 4.5: Total flux and the polarization profile in the observer's frame.  $\alpha = +0.9$  and the other parameters are the same as given in Figure 4.4.



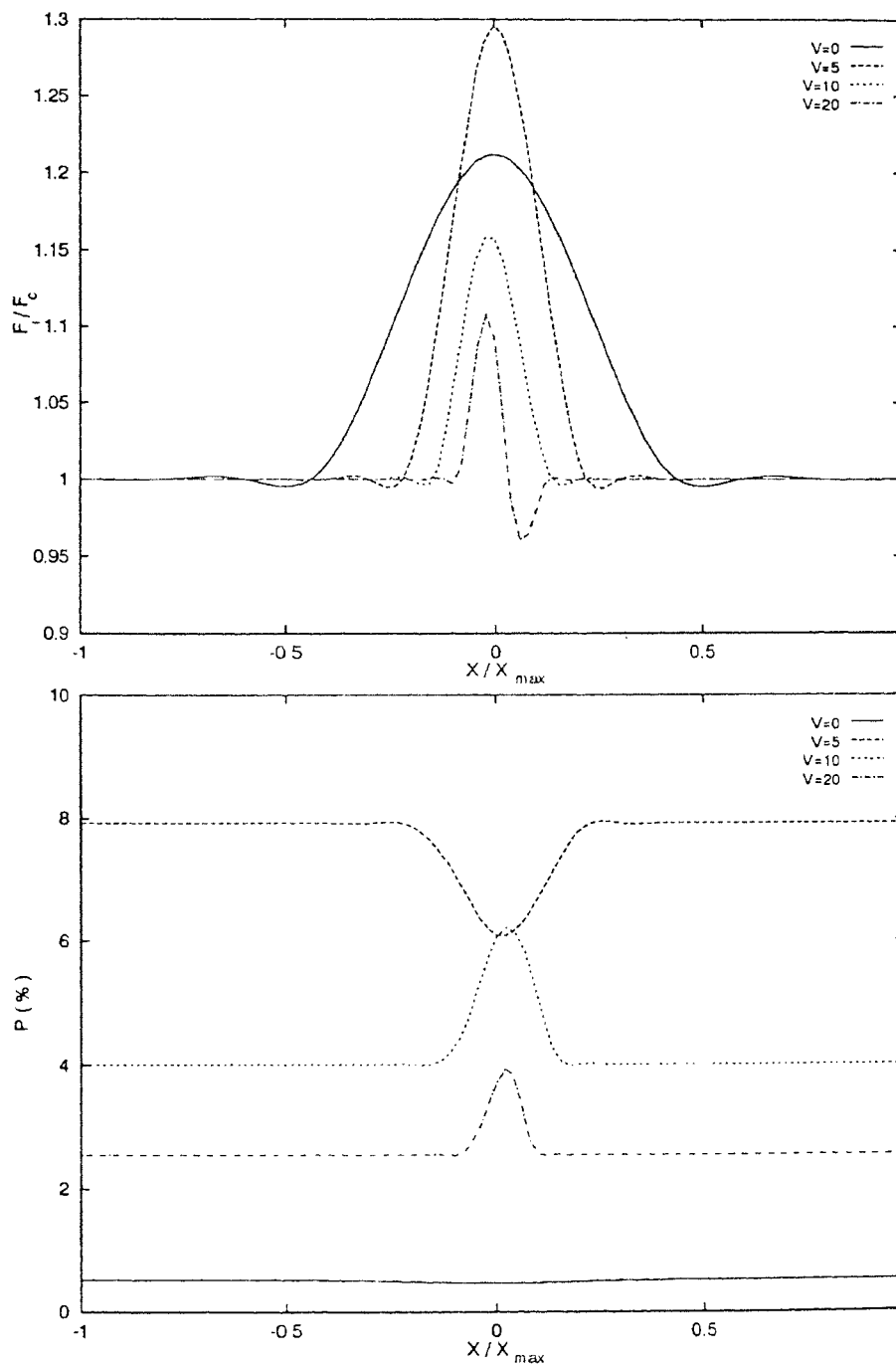


Figure 4.6: Total flux and the polarization profile in the observer's frame.  $\alpha = -1.0$  and the other parameters are the same as given in Figure 4.4.

4.6 it can be seen that the flux profile remains symmetric upto 5 mtu velocity of the medium. With the inclusion of higher velocity gradient the profile becomes more and more asymmetric with absorption feature. With small velocity gradient the amount of flux is higher than that of the static case, whereas it decreases with the increase in the velocity gradient.

For the static case, the degree of polarization is independent of frequency. But for the non-static case the degree of polarization is independent of frequency at the wing only and it increases towards the line center except for the case of small velocity gradient wherein it decreases towards the line center. For both the velocity rules, the degree of polarization is maximum for small velocity gradient and decreases with the increase in velocity. However, the degree of polarization is always larger than that for the static case, i.e., the effect of a velocity field is to enhance the anisotropy of the medium. With the increase in the velocity gradient the matter in the atmosphere is driven outwards decreasing the number of scattering in most of the atmosphere and hence the more is the velocity gradient the less is the degree of polarization.

Now we shall discuss how the results are affected if we consider non-zero thermalization parameter with continuum background. As mentioned earlier, due to the inclusion of non-zero thermalization parameter the photons suffer not only scattering but also collisional de-excitation which must help the medium to be less anisotropic than that of a purely scattering medium. In this case we consider small values of  $\epsilon$  and  $\beta$  in order to obtain sufficient amount of polarization. No radiation is incident at the boundaries but each layer is illuminated by a constant thermal source. The other parameters remaining the same as considered for the purely scattering case.

Unlike the case for a purely scattering medium, in a partially scattering medium the emergent intensity first increases rapidly in the deep interior due to the boundary condition and then remains almost constant upto the outer region where the continuum is formed. Since  $\beta$  is non-zero there is a sudden increase in the intensity at the outer region. The overall nature of the intensity profile in the comoving frame remains the

same with any velocity gradient, although there is slight decrease in the magnitude of the intensity with the increase in the velocity gradient. This variation takes place from the middle of the atmosphere. The result is presented in Figure 4.7. Figure 4.8 shows the backscattered intensity which is the same at the outermost layer irrespective of the velocity gradient, remains constant for the static case but decreases towards the deeper region when velocity field is included. With small and medium velocity gradient, the intensity of the backscattered radiation falls slowly towards the inner region whereas it falls rapidly when larger velocity gradient is considered. This shows that the number of backscattering increases as the photon traverses towards the outer region. This result can be attributed to the mass motion of the atmosphere towards the outer region due to the velocity field and hence the accumulation of more matter in the outer region.

Figure 4.9 shows the intensity and the polarized profile in the comoving frame. In a partially scattering medium the intensity and the polarized profile in comoving frame are unaffected by the inclusion of velocity field as seen in Figure 4.9. The degree of polarization is substantially less in this case compared to that in the purely scattering medium. This reveals the fact that a non-zero thermalization parameter decreases the anisotropy of the atmosphere.

Figure 4.10 presents the  $l$  and the  $r$  components of the frequency independent source function along the direction  $\mu = 0.11$  in the comoving frame. The inclusion of non-zero thermalization parameter increases the source function substantially compared to that in a purely scattering medium. For a static medium the source function slowly decreases towards the deep of the atmosphere while for an expanding medium with small velocity gradient it increases slowly. As the velocity gradient increases, the behaviour of the source function no longer remains smooth. For medium velocity gradient it is maximum at the middle of the atmosphere but for large velocity gradient the source function first increases towards the inner region, then decreases and achieves its minimum value at the middle of the atmosphere and then again increases with the increase in optical depth. However, unlike the case for a purely scattering medium, the numerical values of

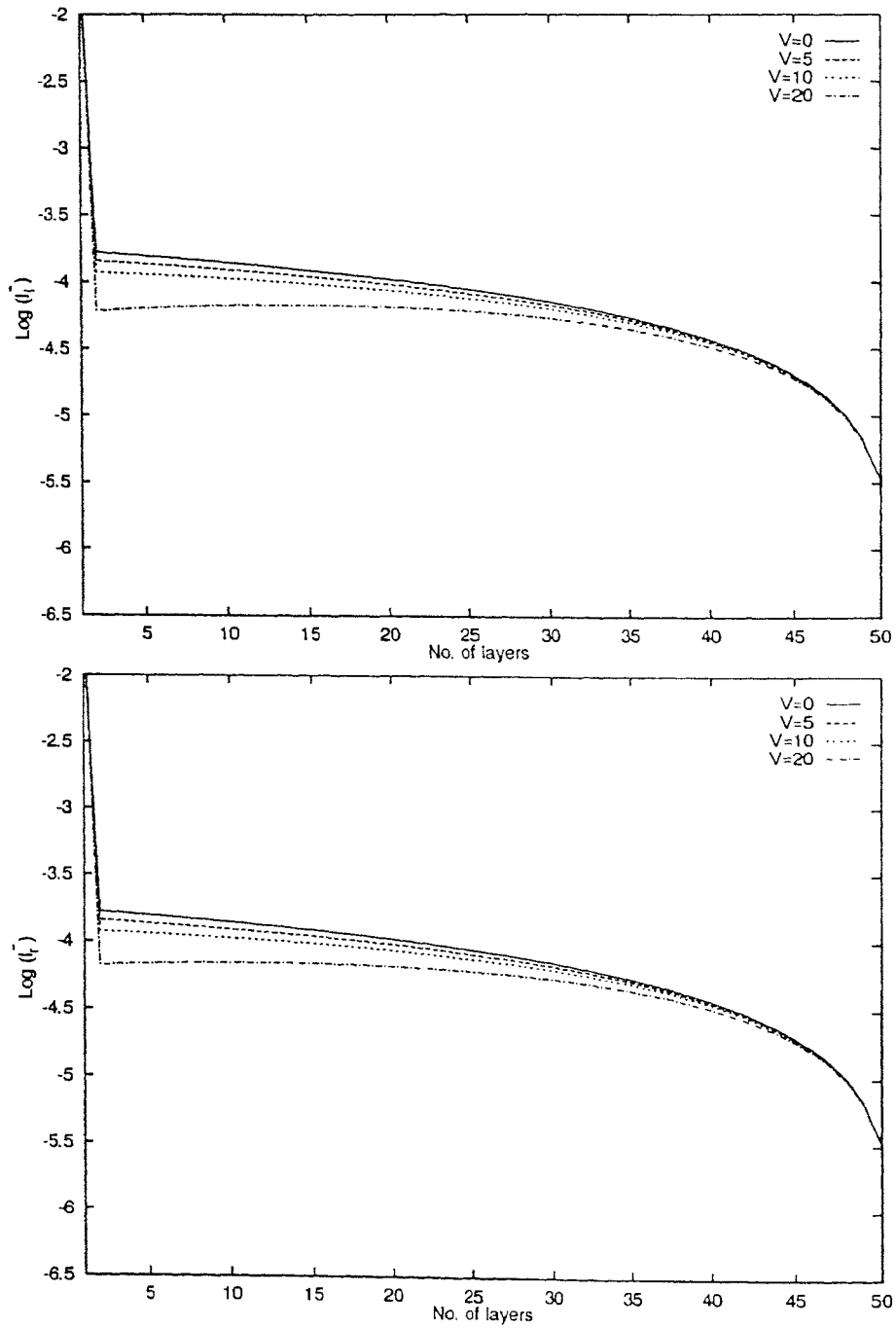


Figure 4.7:  $l$  and  $r$  components of the emergent intensity along the direction  $\mu = 0.11$  in comoving frame with frequency  $X = 0$ .  $\epsilon = \beta = 10^{-5}$ ,  $B/A = 1$  and total optical depth  $T = 50$ .

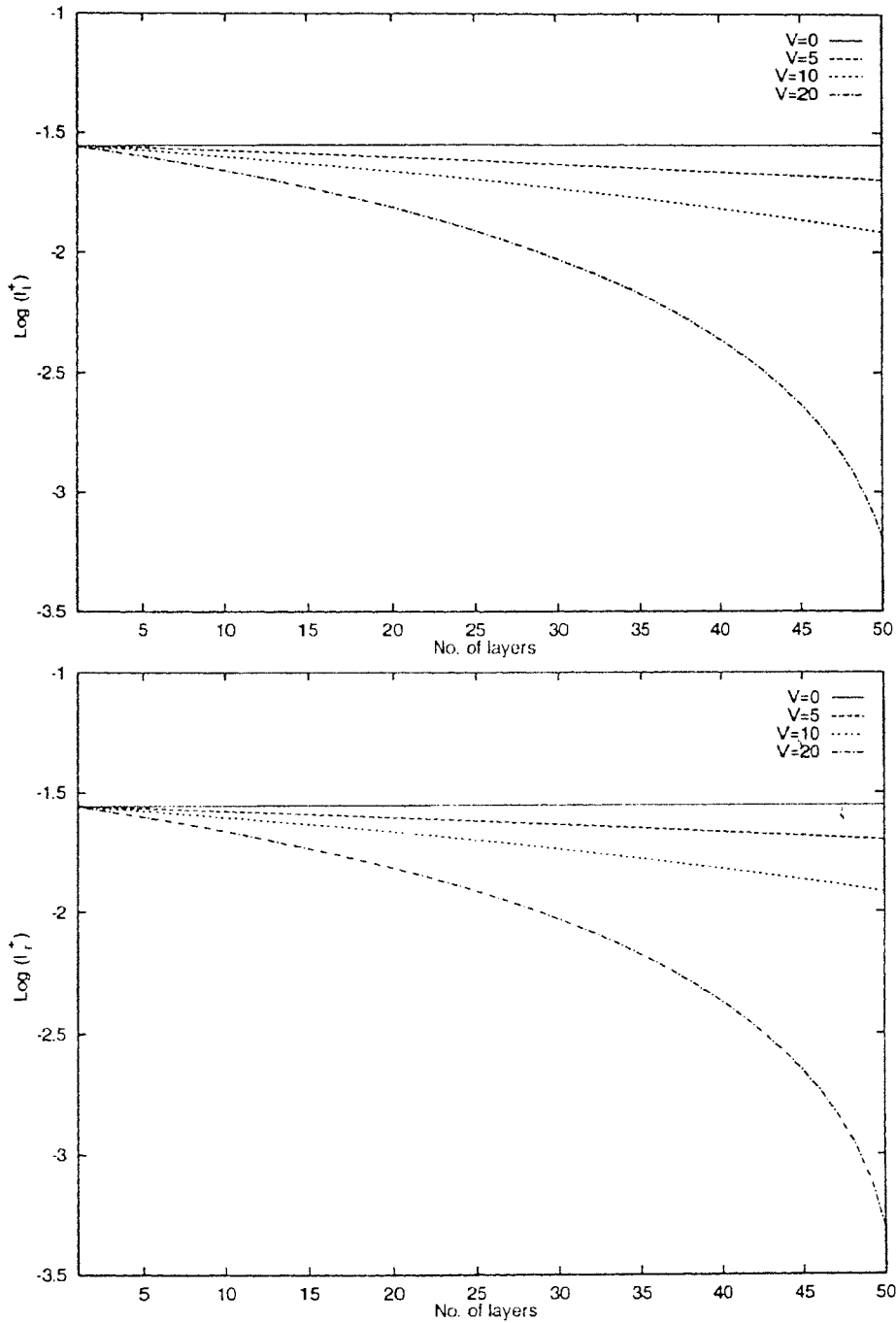


Figure 4.8:  $l$  and  $r$  components of the backscattered intensity along the direction  $\mu = 0.11$  in comoving frame with frequency  $X = 0$ .  $\epsilon = \beta = 10^{-5}$ ,  $B/A = 1$  and total optical depth  $T = 50$ .

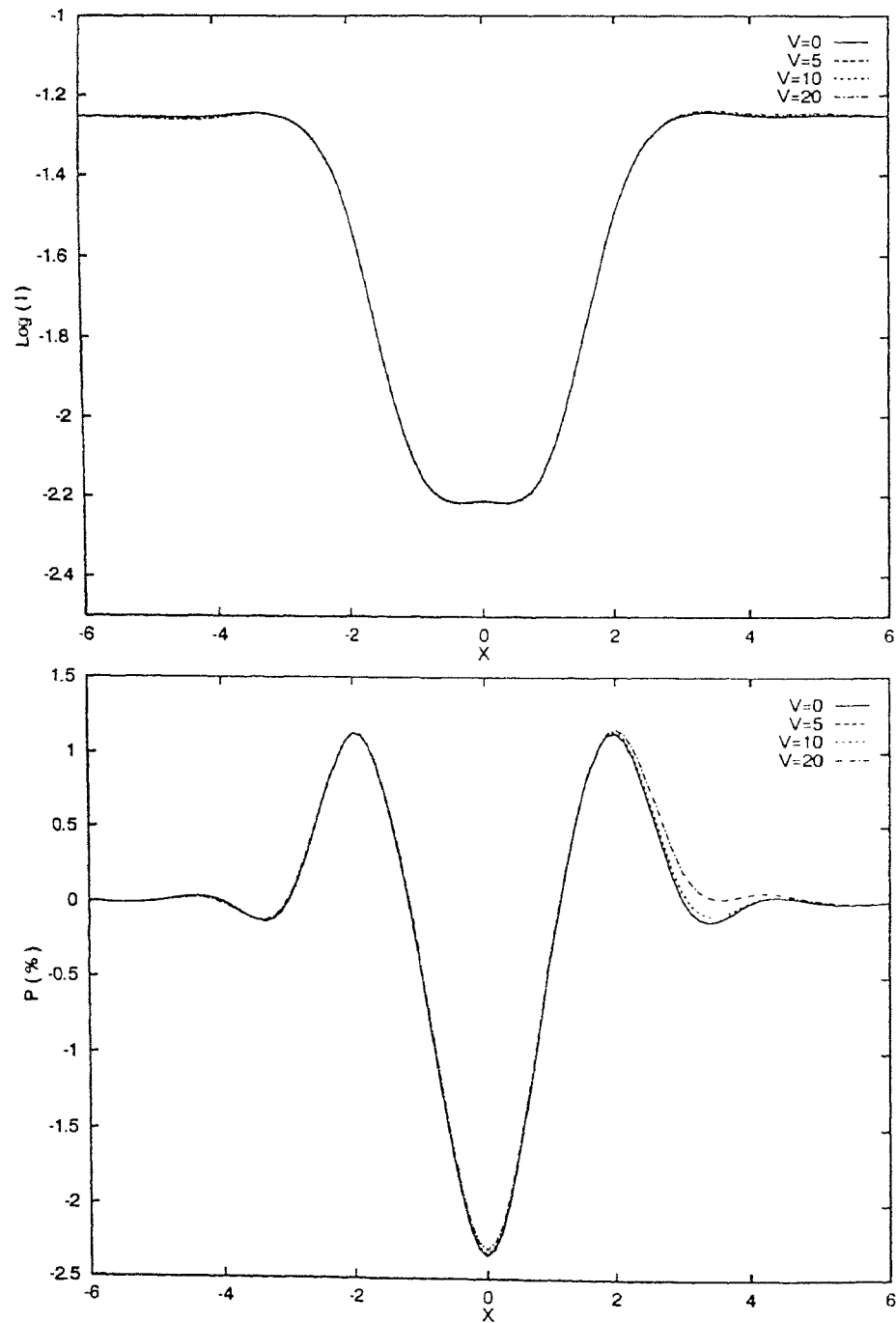


Figure 4.9: Emergent intensity and polarization profiles along the direction  $\mu = 0.11$  in comoving frame.  $\epsilon = \beta = 10^{-5}$ ,  $B/A = 1$  and total optical depth  $T = 50$ .

the source function for partially scattering medium differs only a few percent with the inclusion of any velocity gradient, i.e., the effect of velocity gradient is almost diluted by the inclusion of the thermalization parameter in the determination of the source function.

Finally Figure 4.11 and Figure 4.12 present the flux and the polarized profile along the line of sight of an observer at infinity with  $\alpha = +0.9$  and  $\alpha = -1.0$  respectively. Unlike the case for a purely scattering medium, here we obtain symmetric flux profile even with the inclusion of large velocity gradient. This implies that the inclusion of thermalization parameter suppresses the role of Doppler shift of the photon frequency. In other words, the gain in energy by the line photons at each layer dilutes the change in energy of the emerging photons due to the Doppler shift caused by the velocity field. The total flux decreases as the velocity gradient increases.

In a partially scattering medium, the degree of polarization in the observer's frame is almost frequency independent for any velocity gradient. Also it decreases substantially compared to that in purely scattering medium. This clearly indicates that the thermalization parameter plays an important role in decreasing the anisotropy of the atmosphere. Although we have considered  $\epsilon = \beta = 10^{-5}$ , significant amount of polarization has not been obtained. Therefore further increase in the thermalization parameter would make the medium completely isotropic. However, it can be seen from the polarized profile presented in Figure 4.11 and 4.12 that the degree of polarization is positive for the static case whereas it becomes negative with the inclusion of velocity field.

## 4.4 Summary

We summarize the main features of the results as follows: In a purely scattering medium the total flux profile becomes more and more asymmetric as the velocity gradient increases. The degree of polarization in this case is maximum with small velocity gradient and it decreases with the increase in velocity gradient. The degree of polarization is

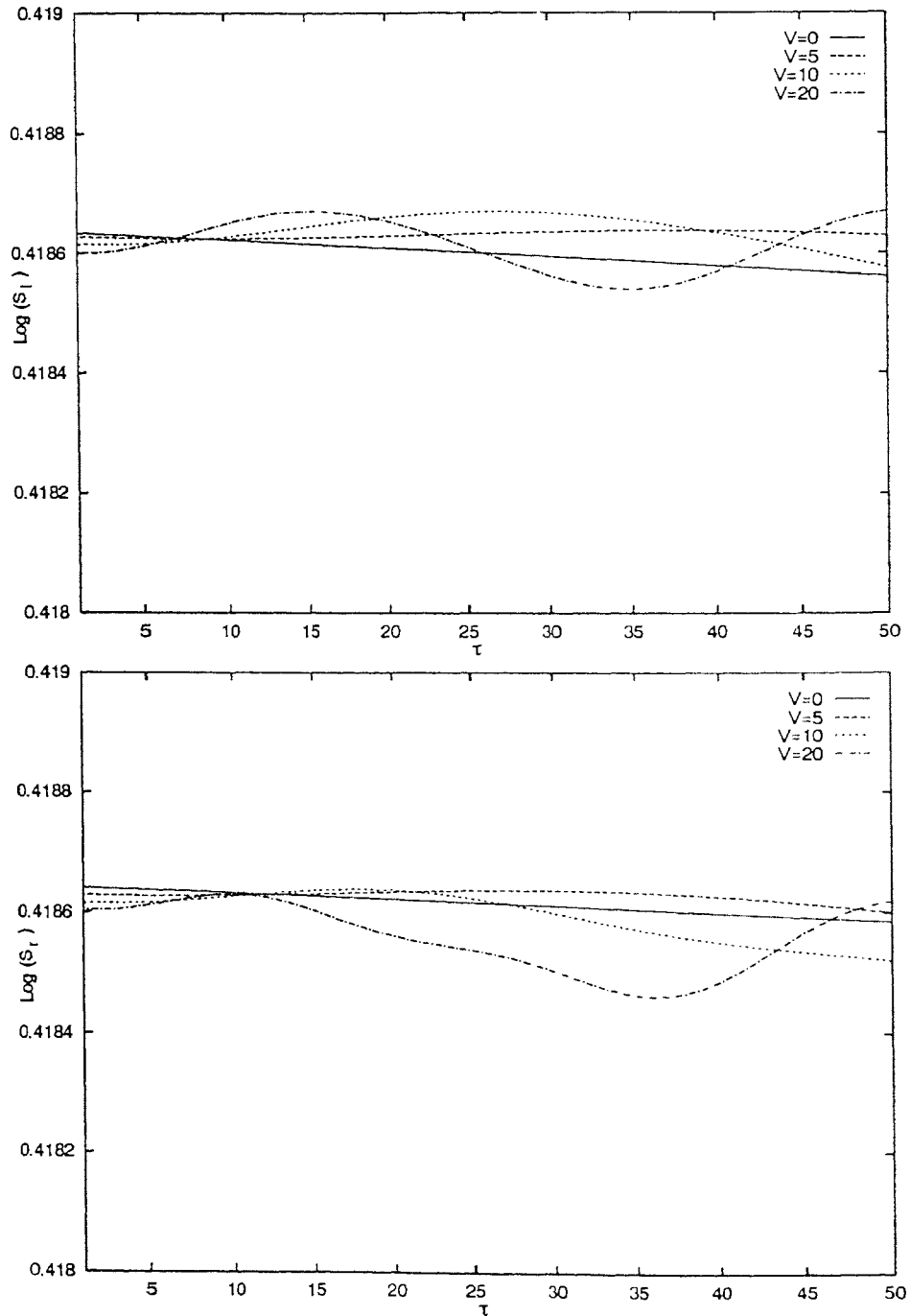


Figure 4.10:  $l$  and  $r$  components of the frequency independent source function along the direction  $\mu = 0.11$  in comoving frame.  $\epsilon = \beta = 10^{-5}$ ,  $B/A = 1$  and total optical depth  $T = 50$ .



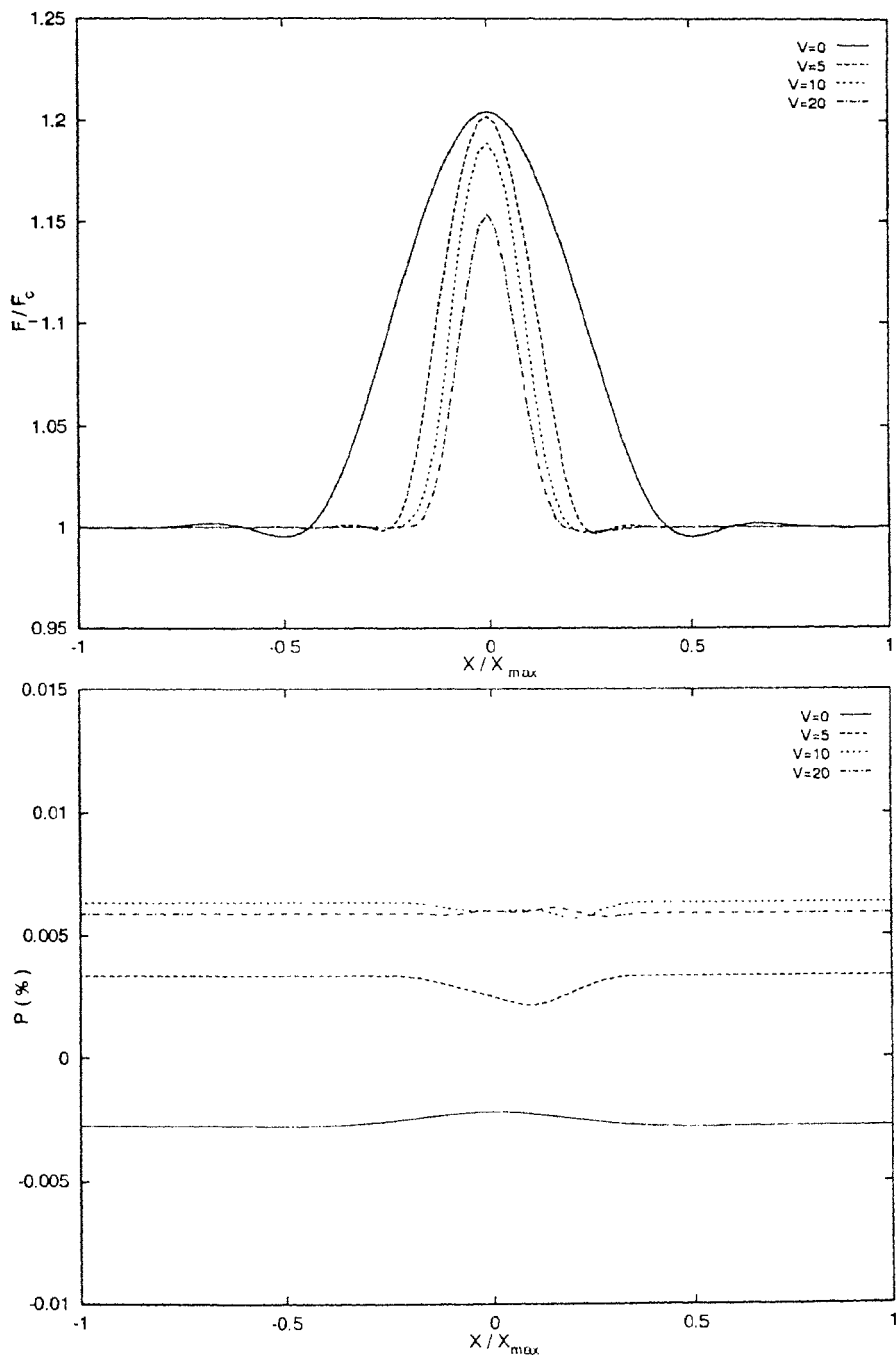


Figure 4.11: Total flux and the polarization profile in the observer's frame.  $\alpha = +0.9$  and the other parameters are the same as given in Figure 4.10.

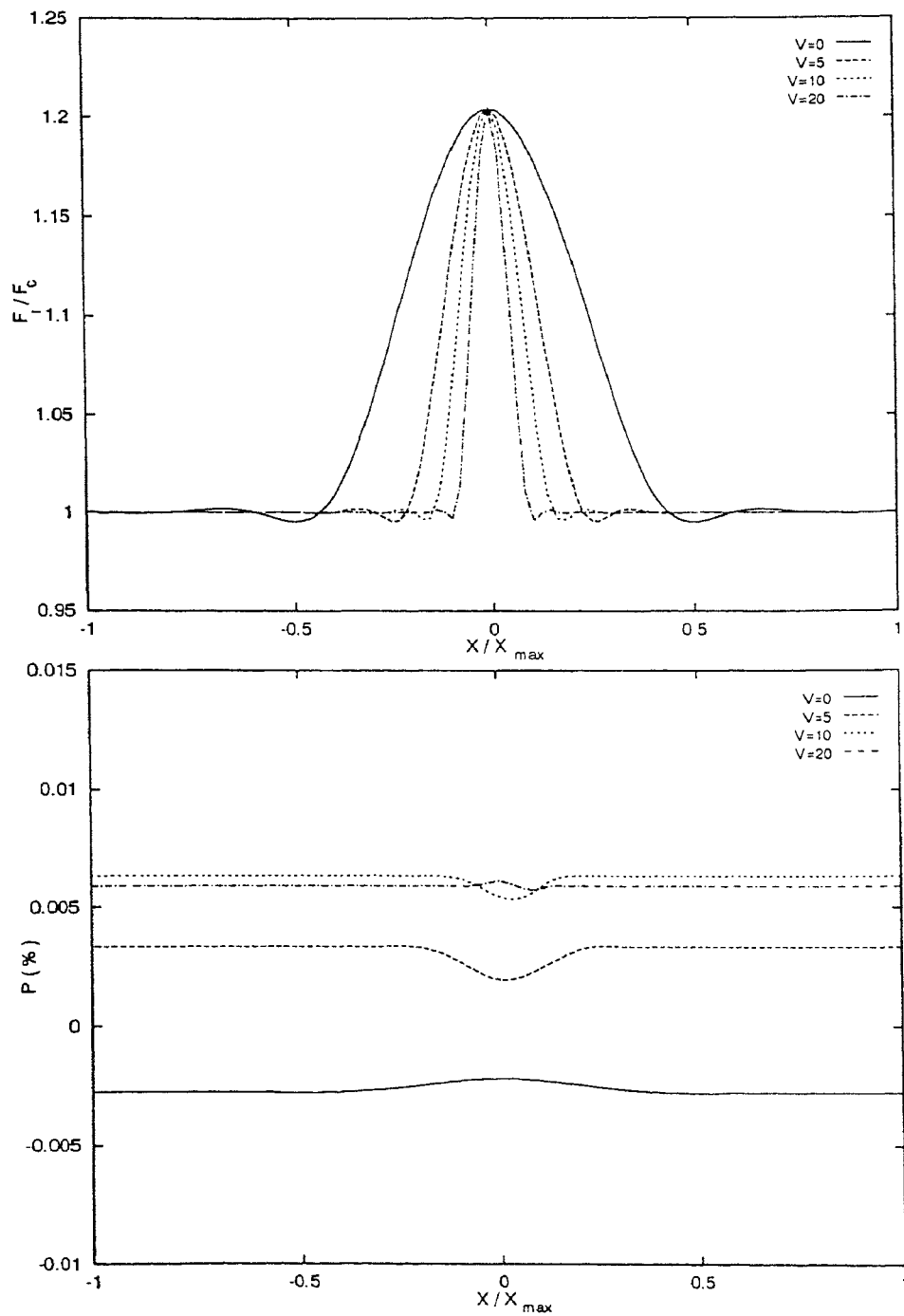


Figure 4.12: Total flux and the polarization profile in the observer's frame.  $\alpha = -1.0$  and the other parameters are the same as given in Figure 4.10.

---

minimum for the static case. The role of thermalization parameter is to decrease the anisotropy of the atmosphere substantially and hence decreases the degree of polarization. Also it suppresses the effect of Doppler shift of the frequency of photons caused by the velocity field. In a partially scattering medium the degree of polarization is almost frequency independent and the sign of the polarization changes with the inclusion of velocity field. Although the models employed in the present work are highly simplified, they can provide reasonably good insight on how the expansion of a stellar atmosphere stratified into plane-parallel affects the anisotropy of the medium.

## Chapter 5

# Resonance line polarization in extended and expanding spherical stellar atmosphere<sup>2</sup>

---

### 5.1 Introduction

In the previous chapter we have discussed the effect of differential radial expansion to line polarization by considering stellar atmosphere in plane parallel geometry. But early type stars, giant and supergiant stars, late type hot stars wherein the expansion of the atmosphere is a crucial physical phenomenon, contain atmospheres whose radii are several times larger than their photospheric radii.

As the stellar radius increases, the effect of sphericity plays a dominant role and hence a spherically symmetric geometry becomes more relevant. On the other hand the effects of sphericity are not manifested in full unless the opacity decreases outwards in the atmosphere. Therefore one has to consider an inhomogeneous medium.

In the previous chapter we have discussed the role of a non-zero thermalization para-

---

<sup>2</sup>Also see : Sengupta, S., MNRAS 269 (1994) 265.

meter and have shown how it helps in reducing the anisotropy of the atmosphere. In the case of a spherically symmetric stellar atmosphere, we therefore consider a fixed value of  $\epsilon$  and  $\beta$  in all models and present the discussions on the effect of differential radial expansion to line polarization under different optical depth as well as sphericity of the medium.

## 5.2 Model parameters

Since we would like to consider the effect of different velocity rules to the emergent intensity and polarization profiles, in the present investigation we adopt the same velocity rule as considered for the plane-parallel case, i.e.,

$$V(r) = V_B \left[ 1 - (1 - \alpha) \left( \frac{R}{r} \right) - \alpha \left( \frac{R}{r} \right)^2 \right]^{1/2},$$

where  $R$  is the inner radius of the star,  $V_B$  is the velocity at the outermost layer and  $\alpha$  is a constant. The value of  $\alpha$  is set at +0.9 and -1.0. The velocity profiles for two different values of  $\alpha$  are shown in Figure 5.1. The velocity profile for a linear velocity law given

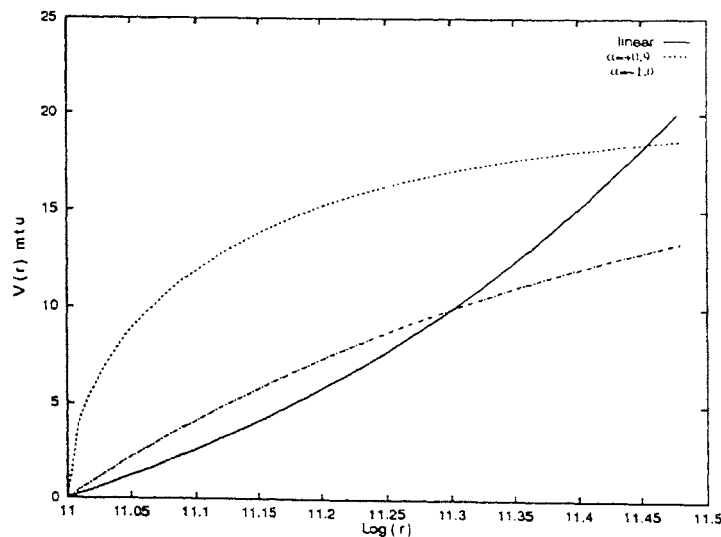


Figure 5.1: The velocity profiles for different velocity laws.

by (Peraiah 1980a)

$$V(r) = V_A + \frac{V_B - V_A}{B - A}(r - A),$$

where  $V_A$  is the velocity at the innermost region which is always kept zero,  $B$  is the outer radius and  $A$  is the inner radius of the star, is also provided for comparison. Unlike the case for a plane-parallel medium, the form of the velocity rule is crucial in determining the line intensity and polarization profile as well as the source function in comoving frame for a spherically symmetric atmosphere.

For the variation in the optical depth with the geometrical depth, we concentrate on the case where the opacity varies as  $r^{-1}$ . Figure 5.2 shows the variation of the optical depth with respect to  $r$ . The total optical depth is taken to be  $T = 10^3$  and  $T = 10^5$  with the aim to obtain the effect under different opacity that plays significant role in the formation of polarization profile.

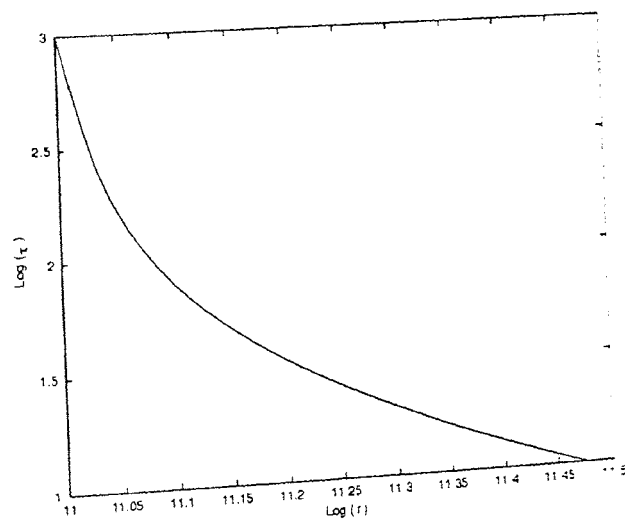


Figure 5.2: The variation of the optical depth with the radial points  $r$ .

In order to consider sufficient extension of the atmosphere, we take the inner radius equal to  $1 \times 10^{11}$  whereas the outer radius is considered to be  $3 \times 10^{12}$  and  $5 \times 10^{12}$  so that the effect of curvature can be visualized. The sphericity is determined by the ratio

of the outer radius to the inner radius and denoted by  $B/A$  in each figure.

In all the models the thermalization parameters are taken as  $\epsilon = \beta = 10^{-3}$  which makes the medium partially scattering with continuum background. In all cases, no incident radiation is provided at the boundaries but constant emission of radiation in term of the Planck function  $B(r) = 0.5$  for each component is considered.

For the frequency redistribution, a Voigt profile with constant damping parameter  $a = 10^{-3}$  is taken for all models. The small value of the parameter  $a$  is considered because of the fact that with the inclusion of velocity field, Doppler broadening dominates over collisional broadening.

We consider complete frequency redistribution function in all the calculations. The justification of adopting complete frequency redistribution function has been discussed in the previous section.

All the physical quantities in comoving frame are calculated along the direction  $\mu = 0.11$ . A few results corresponding to  $\mu = 0.88$  have also investigated. In order to present the asymmetry in the profiles caused by the velocity field, the profiles are graphically presented along full frequency grid. The emergent flux along the line of sight is presented in term of the flux at the continuum.

### 5.3 Results and discussions

Since the optical depth in the present case varies as  $\frac{1}{r}$  (see Figure 5.2), therefore the medium becomes more and more opaque towards the interior of the atmosphere. As a consequence, the intensity of radiation increases as it moves outwards. Figure 5.3 and Figure 5.4 show the  $l$  and the  $r$  components of the emergent intensity of a photon with line center frequency for  $\alpha = +0.9$  and  $\alpha = -1.0$  respectively. Firstly, we observe that the basic feature of the intensity remains the same in comoving frame with different velocity rules with a slight difference at the innermost region where the optical depth is maximum. The lines are formed in this region. The intensity of the photon for any

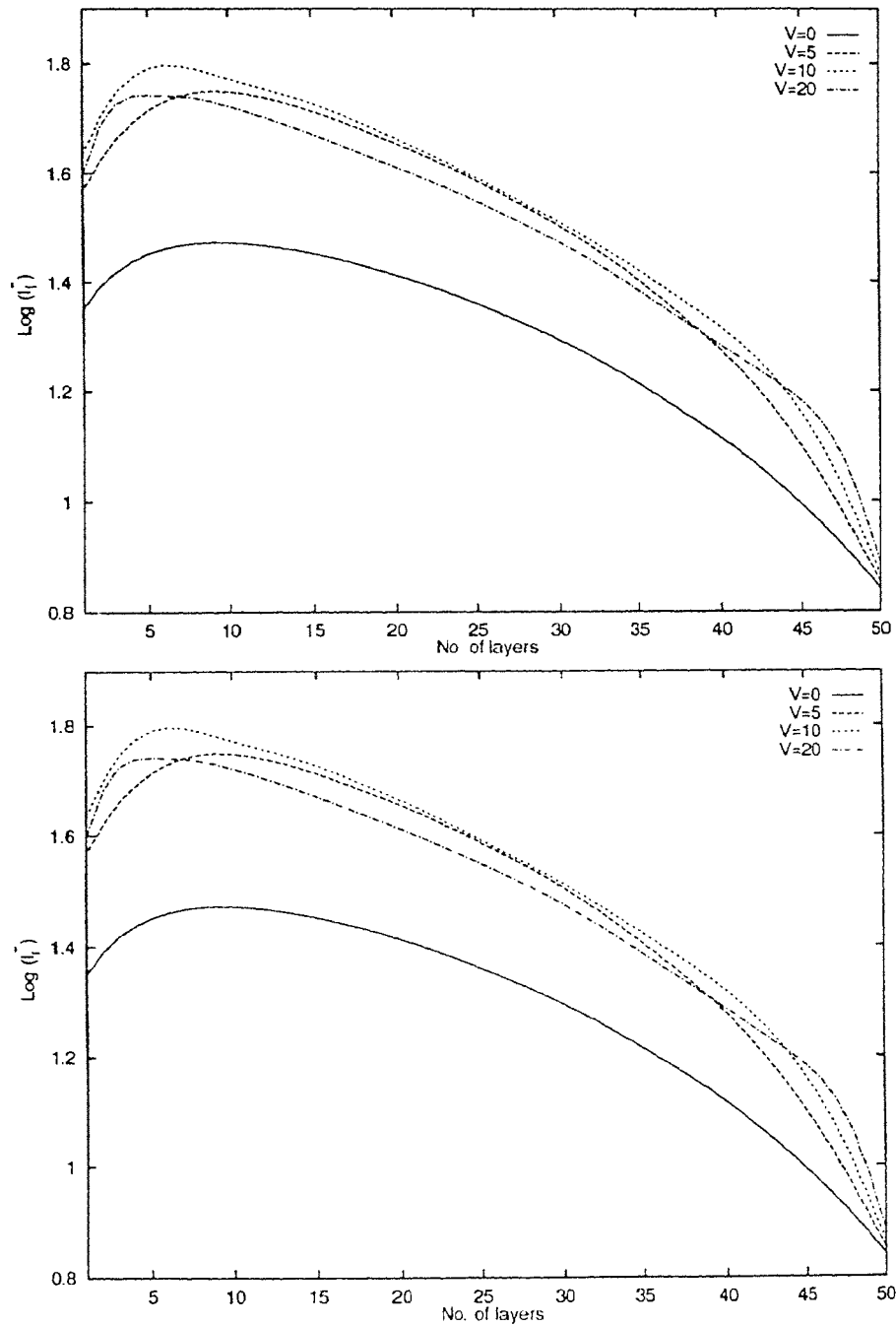


Figure 5.3:  $l$  and  $r$  components of the emergent intensity of radiation with the line center frequency at each shell along the direction  $\mu = 0.11$  in the comoving frame.  $\epsilon = \beta = 10^{-3}$ ,  $T = 10^3$ ,  $B/A = 3$  and  $\alpha = +0.9$ . In all figures  $V$  represents the velocity at the outermost shell, i.e.,  $V$  in figures means  $V_B$  in the text.



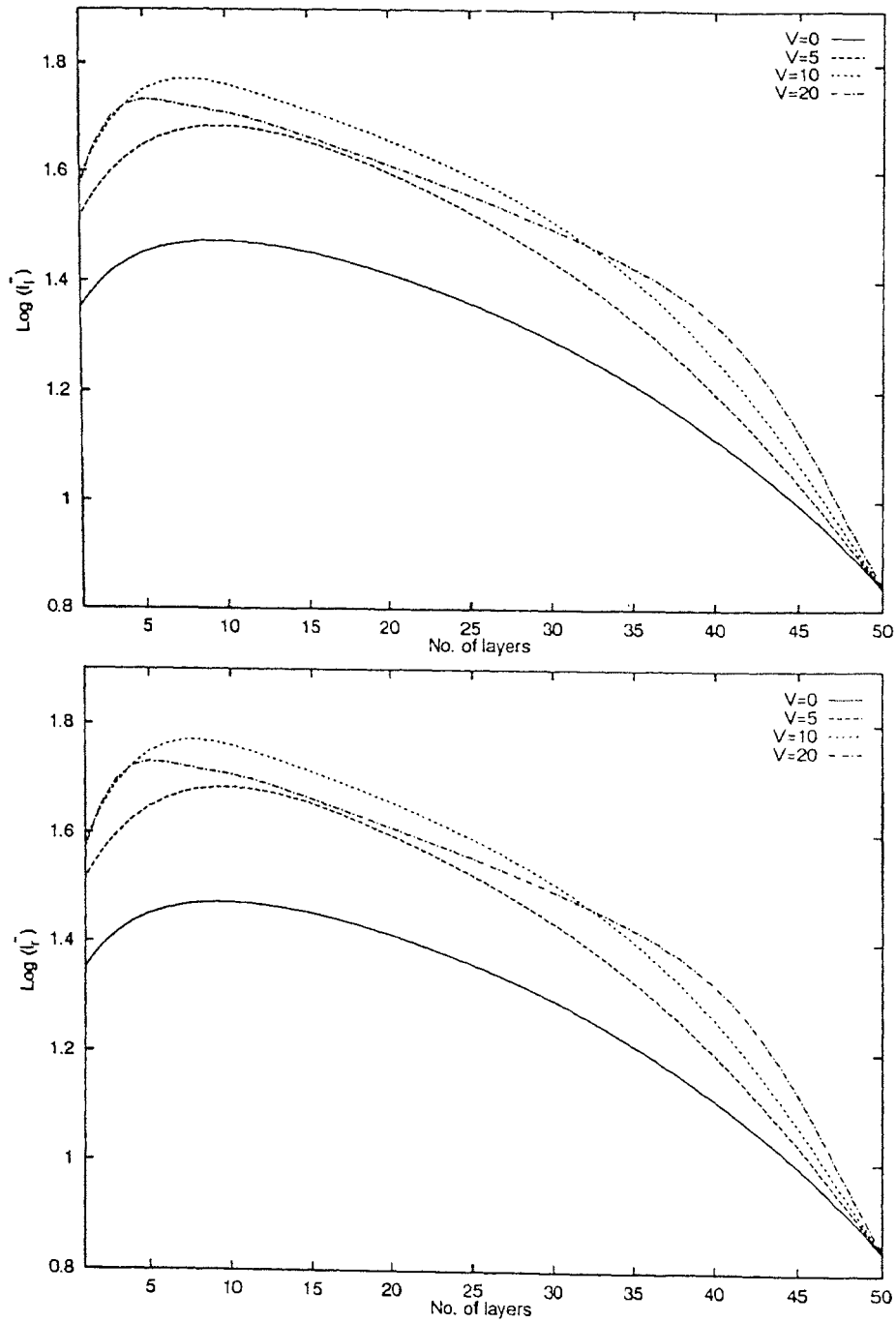


Figure 5.4:  $l$  and  $r$  components of the emergent intensity of radiation with the line center frequency at each shell along the direction  $\mu = 0.11$  in the comoving frame.  $\epsilon = \beta = 10^{-3}$ ,  $T = 10^3$ ,  $B/A = 3$  and  $\alpha = -1.0$ .

velocity gradient increases in the outward direction but it drops at the outermost region where the continuum is formed. The emergent intensity increases significantly with the inclusion of velocity field. However at the innermost region the emergent intensity remains the same for all velocity gradients due to the adopted boundary condition. With large velocity gradient the emergent intensity in the comoving frame of the photon with  $X = 0$  increases rapidly at the deeper region wherein its value is maximum. It should be noted from Figure 5.3 and Figure 5.4 that the change in the emergent intensity in comoving frame is maximum when a small velocity gradient is included.

Figure 5.5 and Figure 5.6 present the  $l$  and the  $r$  components of the backscattered intensity of a photon with line center frequency in the comoving frame for  $\alpha = +0.9$  and  $\alpha = -1.0$  respectively. Here we observe that the intensity of the backscattered radiation increases slowly to the outward direction but at the outer region it falls rapidly. This is just the opposite way of the variation of the emergent intensity. This means more energy is backscattered within the outer region. The backscattered intensity increases with the increase in velocity gradient. This picture is quite consistent with the behaviour of the emergent intensity. As the velocity increases more matter is driven outwards rising the backscattering phenomenon.

Figure 5.7 and Figure 5.8 show the emergent intensity and polarization profiles in the comoving frame along the direction  $\mu = 0.11$  for  $\alpha = +0.9$  and  $\alpha = -1.0$  respectively. The emergent intensity profile in the comoving frame for both the velocity rules remains almost symmetric at the line but significant asymmetry in the profile is found at the wing. The asymmetry increases as the velocity gradient increases. Multi-emission and absorption features are found with the inclusion of velocity field. For  $\alpha = -1.0$  the absorption is more at the near wing when large velocity gradient is considered. At the far wing emission peak is formed which rises with the increase in velocity field. The asymmetric nature of the profile at the wing is the manifestation of complete frequency redistribution.

The polarization profile in comoving frame also becomes asymmetric at the wing.

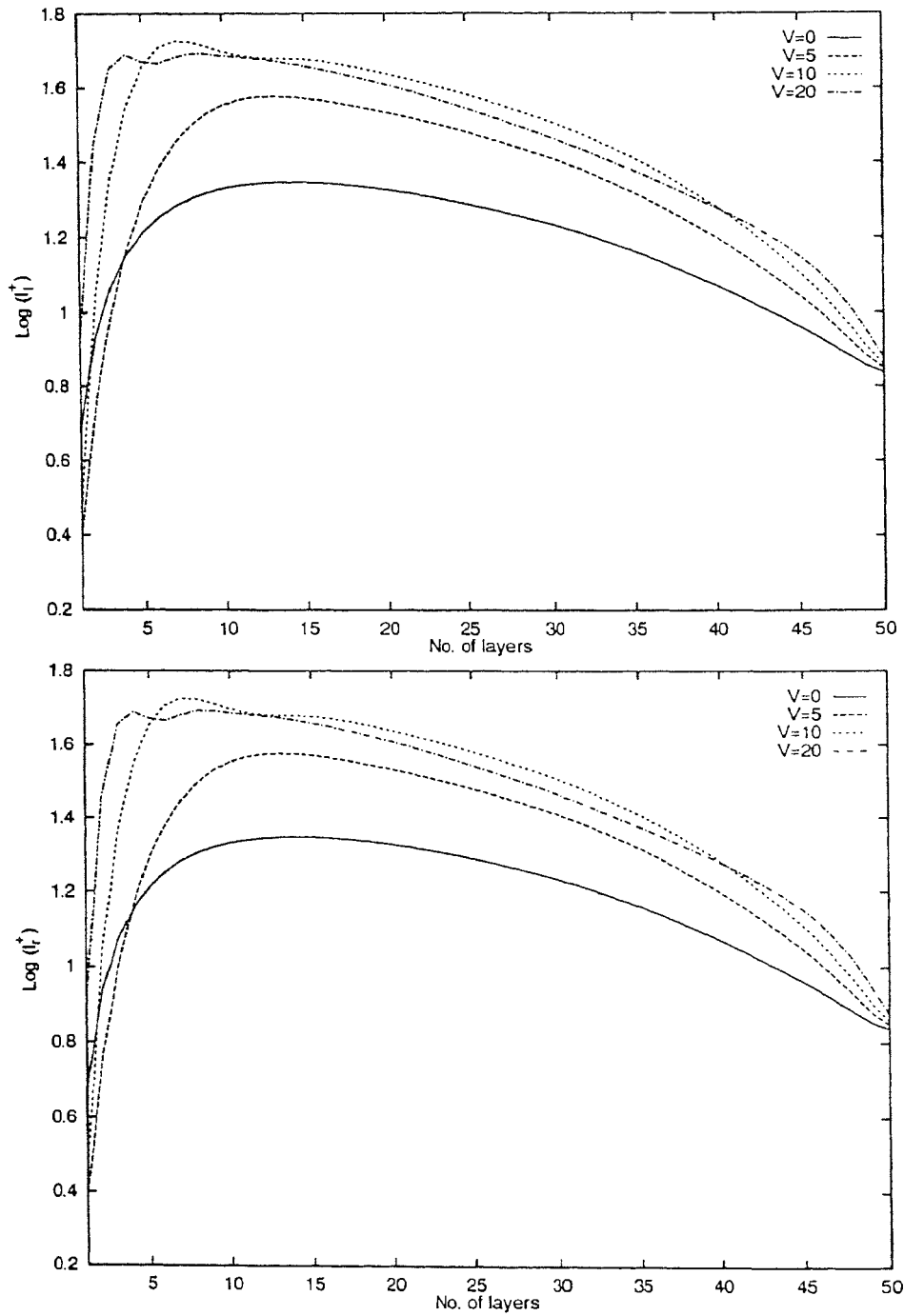


Figure 5.5:  $l$  and  $r$  components of the backscattered intensity of radiation with the line center frequency at each shell along the direction  $\mu = 0.11$  in the comoving frame.  $\epsilon = \beta = 10^{-3}$ ,  $T = 10^3$ ,  $B/A = 3$  and  $\alpha = +0.9$ .

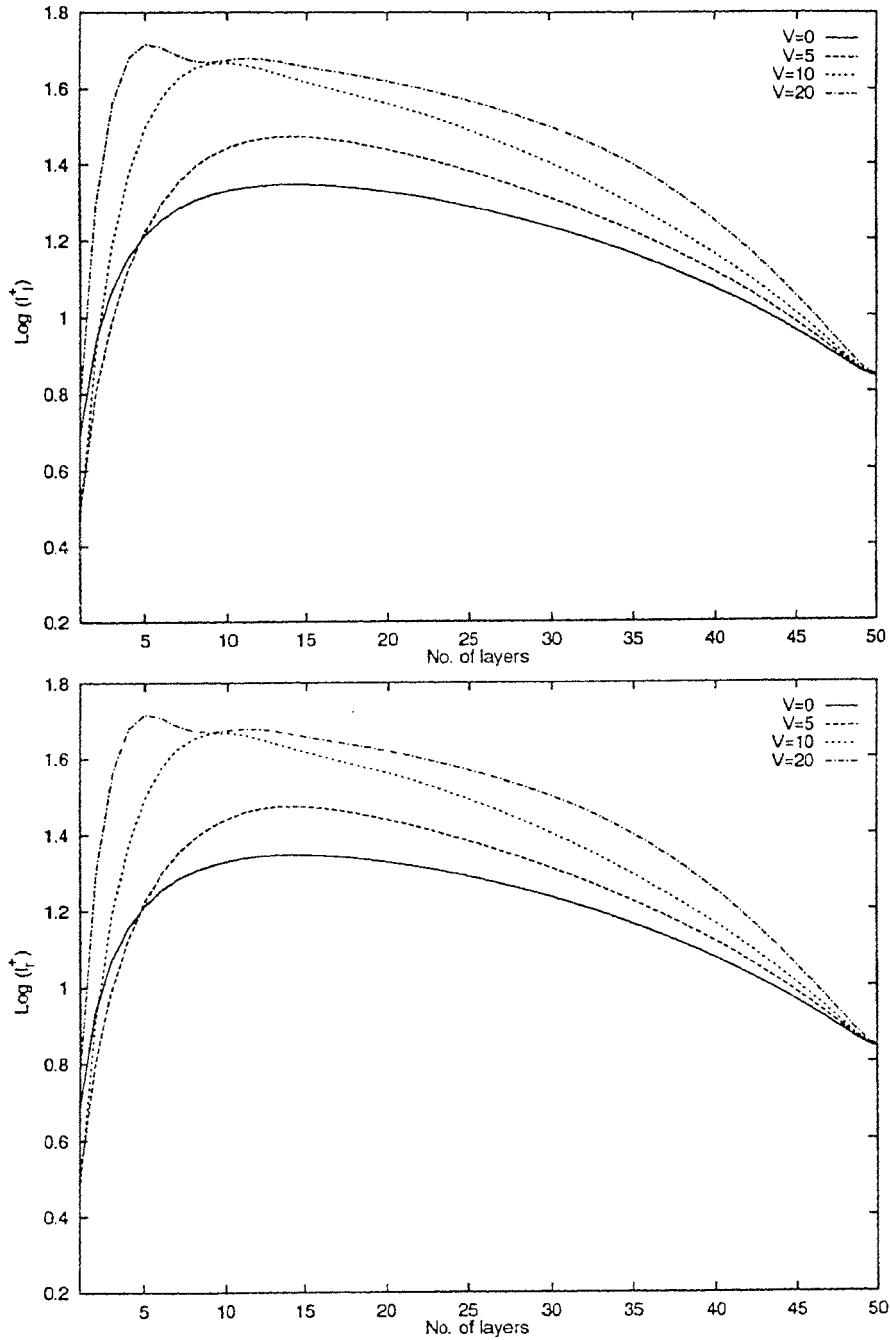


Figure 5.6:  $l$  and  $r$  components of the backscattered intensity of radiation with the line center frequency at each shell along the direction  $\mu = 0.11$  in the comoving frame.  $\epsilon = \beta = 10^{-3}$ ,  $T = 10^3$ ,  $B/A = 3$  and  $\alpha = -1.0$ .

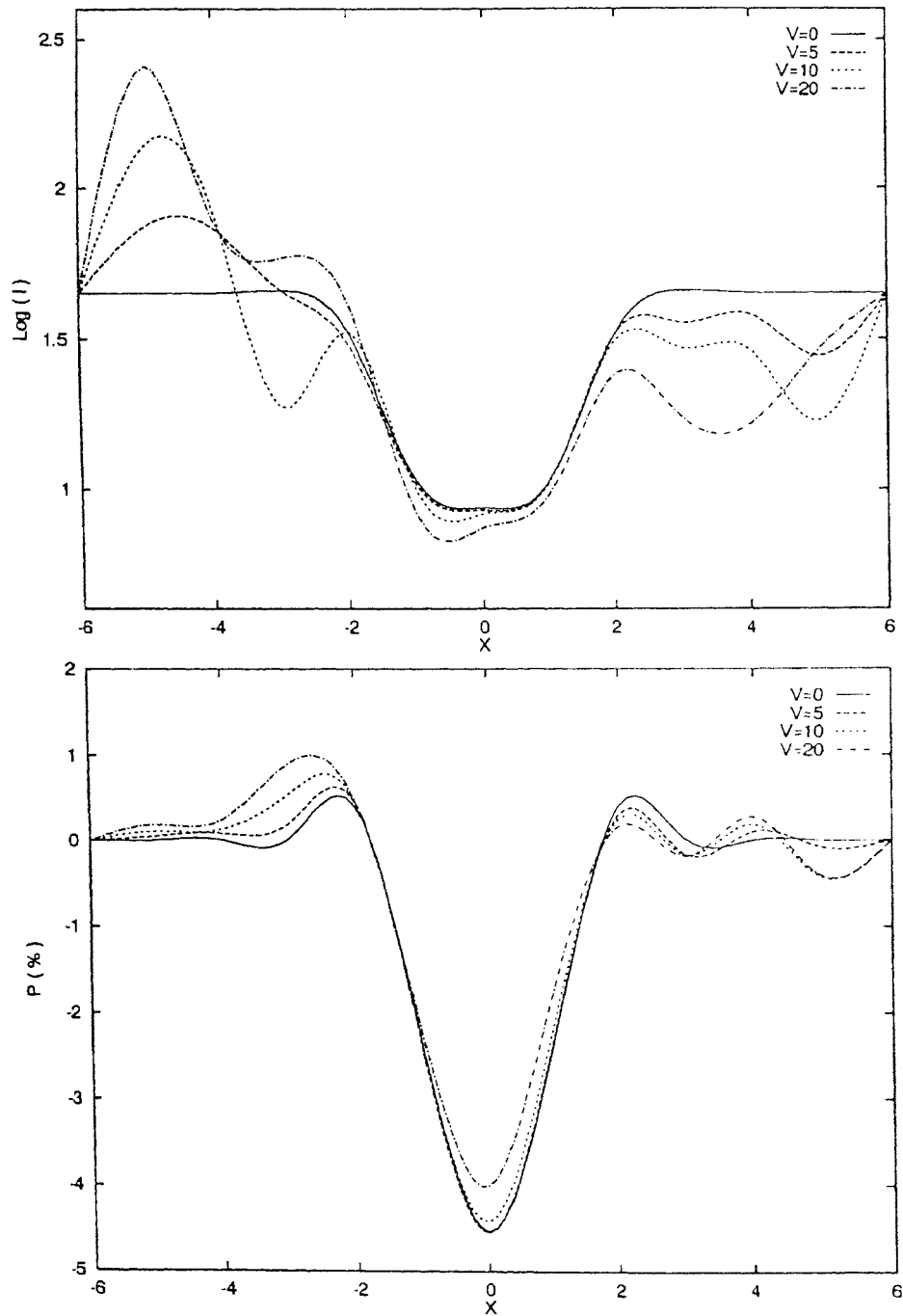


Figure 5.7: Emergent intensity and polarization profile along the direction  $\mu = 0.11$  in the comoving frame.  $\epsilon = \beta = 10^{-3}$ ,  $T = 10^3$ ,  $B/A = 3$  and  $\alpha = +0.9$ .

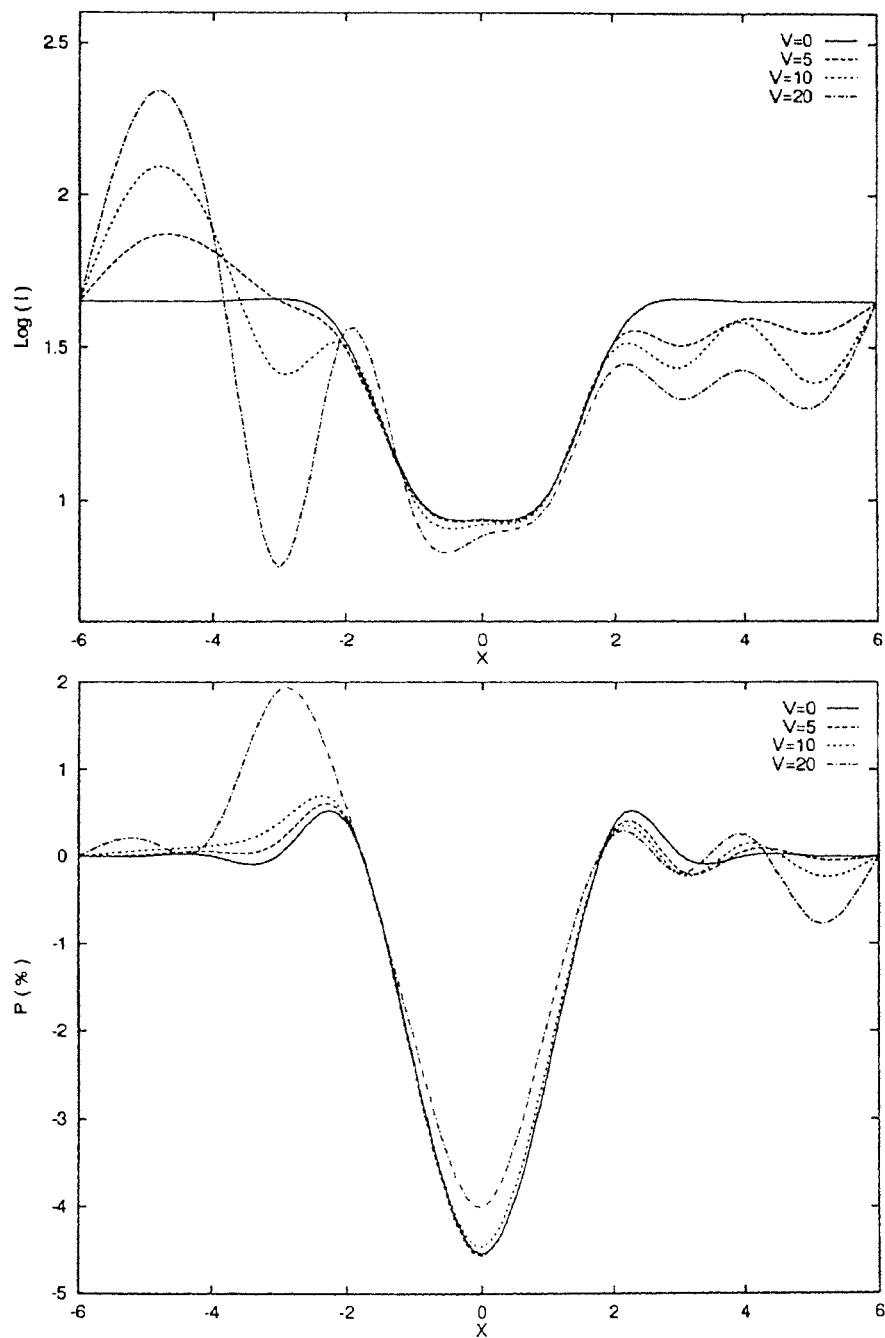


Figure 5.8: Emergent intensity and polarization profile along the direction  $\mu = 0.11$  in the comoving frame.  $\epsilon = \beta = 10^{-3}$ ,  $T = 10^3$ ,  $B/A = 3$  and  $\alpha = -1.0$ .

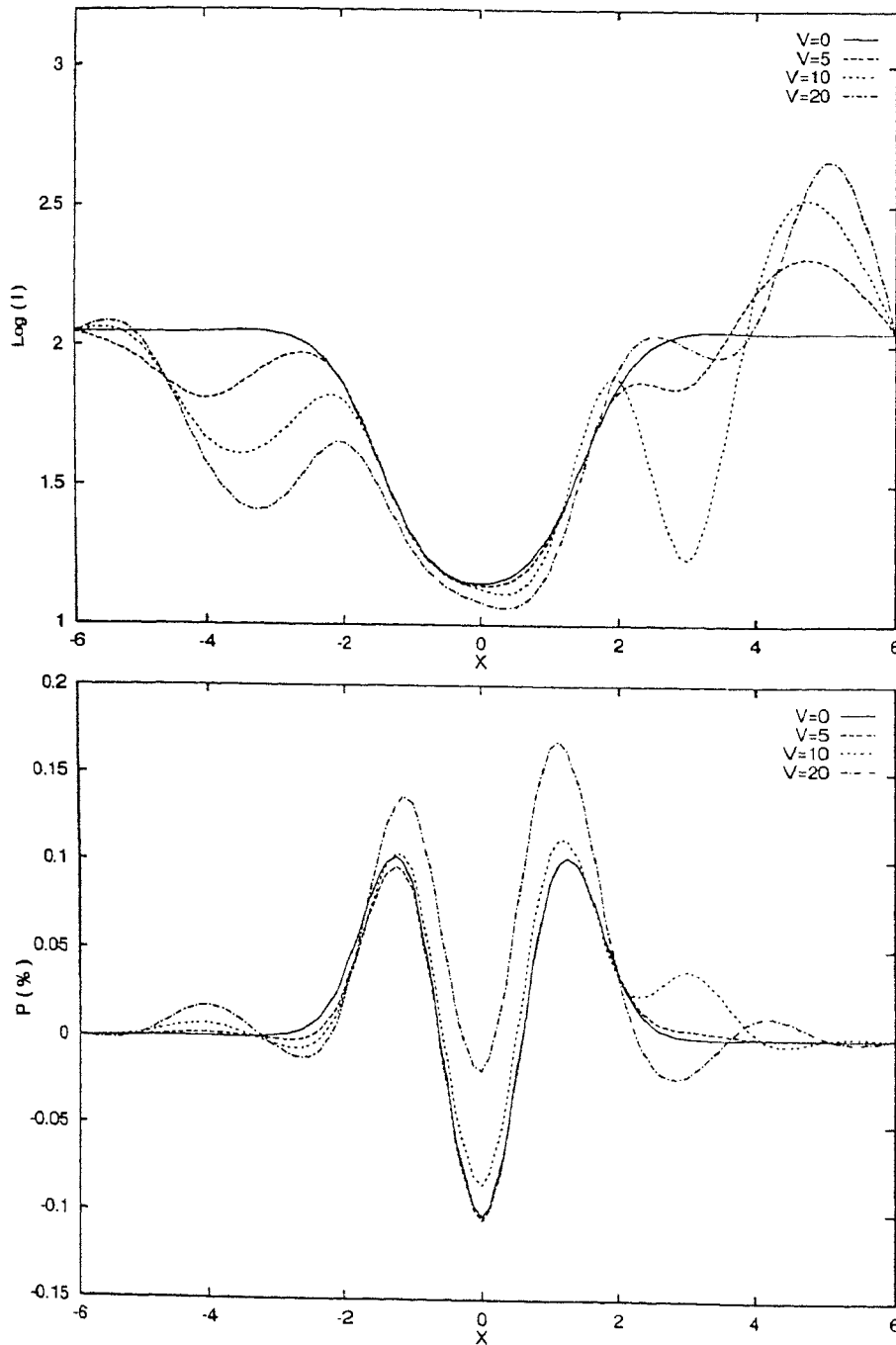


Figure 5.9: Emergent intensity and polarization profile along the direction  $\mu = 0.88$  in the comoving frame.  $\epsilon = \beta = 10^{-3}$ ,  $T = 10^3$ ,  $B/A = 3$  and  $\alpha = +0.9$ .

The degree of polarization in comoving frame decreases with the increase in velocity gradient. However, at the far wing the unpolarized continuum radiation makes the degree of polarization negligible. On the other hand, the degree of polarization at the near wing increases with the change in its sign when large velocity gradient is taken into consideration.

Figure 5.9 shows the emergent intensity and polarization profiles in the comoving frame along the direction  $\mu = 0.88$  for the velocity law with  $\alpha = +0.9$ . A comparison of the intensity profile presented in Figure 5.7 shows an almost mirror image of the profile when one considers  $\mu = 0.88$ . Here we see emission peak at the right wing for all velocity gradients. When the velocity gradient is the maximum, an absorption feature is also found at the right wing. At the left wing absorption features are observed when the velocity field is included. As the velocity increases, the amount of absorption increases. However, at the line center, the intensity are the same for all velocity gradients.

Significant change in the polarization profile (in comoving frame) occurs when the angular direction is altered. The important point is to be noted that with the increase in the value of  $\mu$ , the degree of polarization reduces substantially. It is found that at the near wings the degree of polarization is positive whereas at the line center it is negative for all the velocity gradients including the static case. This behaviour is produced by an enhancement of the parallel component of the radiation field with optical thickness and has been reported earlier by Faurobert (1987). The degree of polarization is maximum in absolute value at line center whereas it becomes zero at the far wing due to the dominance of the unpolarized continuum.

Figure 5.10 and Figure 5.11 present the variation of the  $l$  and the  $r$  components of the frequency independent source function along the direction  $\mu = 0.11$  in the comoving frame with the variation of the optical depth for  $\alpha = +0.9$  and  $-1.0$  respectively. The exact role played by the form of the velocity rule cannot be visualized properly. However, the difference in the value of the source functions with different velocity gradient becomes clearer as the optical depth decreases. At high optical depth the difference is negligible.



This is because of the fact that at deep interior the line photons are trapped and cannot escape the region whereas with the decrease in optical depth the line photons are able to escape due to the velocity field. Figure 5.12 presents the  $l$  and the  $r$  components of the frequency independent source function along the direction  $\mu = 0.88$  in the comoving frame for  $\alpha = +0.9$ . With the change in the value of  $\mu$ , any effect in the behaviour of the source function is not noticed. For all the cases the source function increases towards the inner region since more photons are trapped in the region with high optical depth but it falls rapidly at the innermost shell due to the adopted boundary condition. It should be worth mentioning that unlike the case for isotropic radiation field, here the source function is angle dependent. Although the  $l$  and the  $r$  components of the source function look similar in the figure but an unresolvable difference gives rise to non-zero polarization measured along the line of sight.

Figure 5.13, Figure 5.14 and Figure 5.15 show the total flux profile in the unit of continuum flux as well as the polarization profile along the line of sight corresponding to Figure 5.10, Figure 5.11 and Figure 5.12 respectively. For the static case a double emission feature is found with absorption at the center, i.e., absorption occurs at the line and emission at the near wing. The profile is symmetric. With the inclusion of velocity field the flux profile becomes highly asymmetric with the greatest change in the profile when small velocity gradient is considered. As the velocity gradient increases, the amount of emergent flux decreases at the line. This is because of the fact that the line is formed at the deep of the atmosphere and as the velocity increases the escape probability of the trapped photon increases causing a decrease in the amount of flux at the line. Multi-emission feature at the line is observed with the inclusion of large velocity gradient for  $\alpha = +0.9$ . But for  $\alpha = -1.0$  this feature is absent. This implies that the mass motion of the atmosphere which is governed by the velocity field affect the flux profile significantly. With  $\alpha = -1.0$ , the increase in the amount of flux is much greater for large velocity gradient than that when  $\alpha = +0.9$ . For both the values of  $\alpha$  the amount of flux is the same at the far wing irrespective of the velocity gradient.

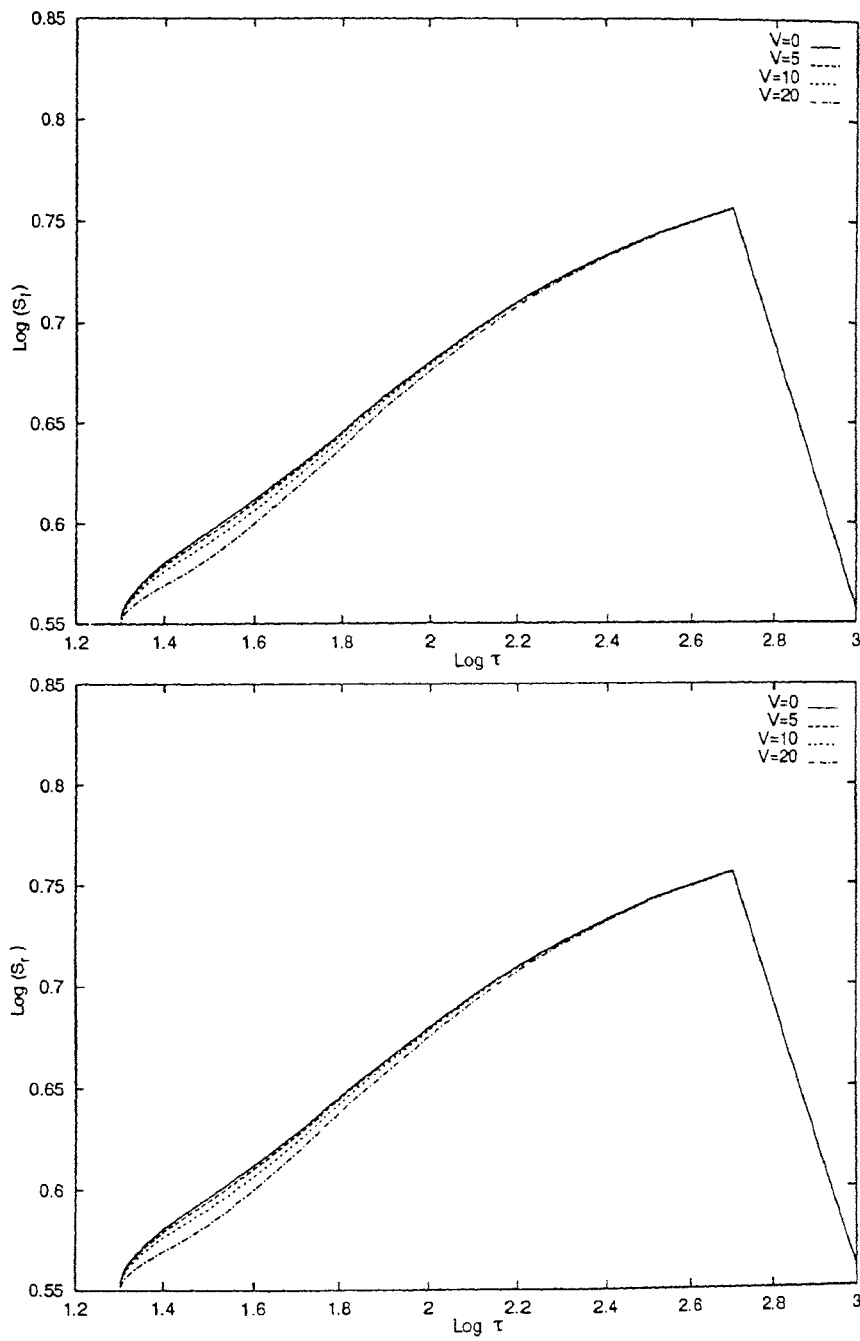


Figure 5.10:  $l$  and  $r$  components of the frequency independent source function along the direction  $\mu = 0.11$  in the comoving frame.  $\epsilon = \beta = 10^{-3}$ ,  $T = 10^3$ ,  $B/A = 3$  and  $\alpha = +0.9$ .

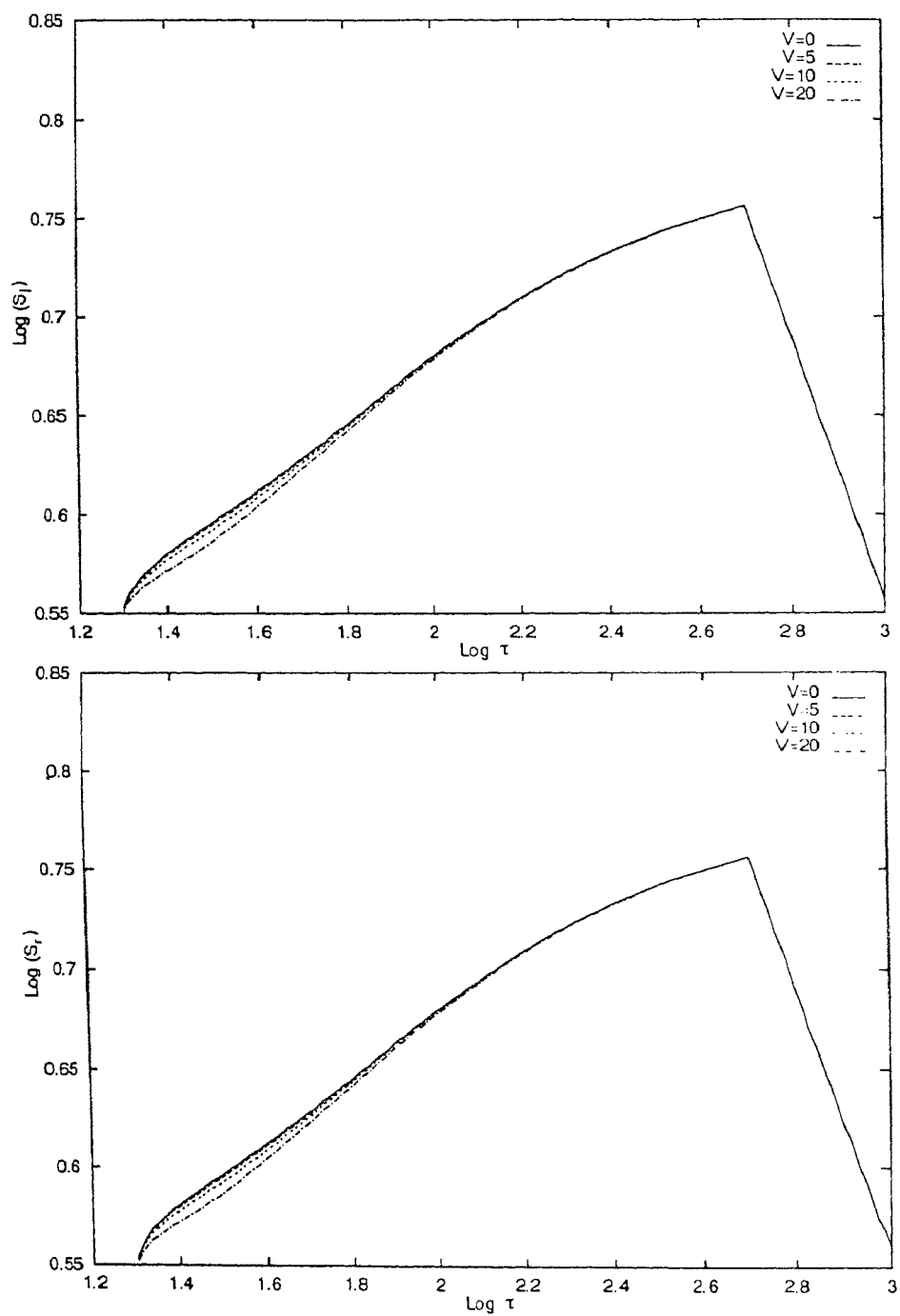


Figure 5.11:  $l$  and  $r$  components of the frequency independent source function along the direction  $\mu = 0.11$  in the comoving frame.  $\epsilon = \beta = 10^{-3}$ ,  $T = 10^3$ ,  $B/A = 3$  and  $\alpha = -1.0$ .

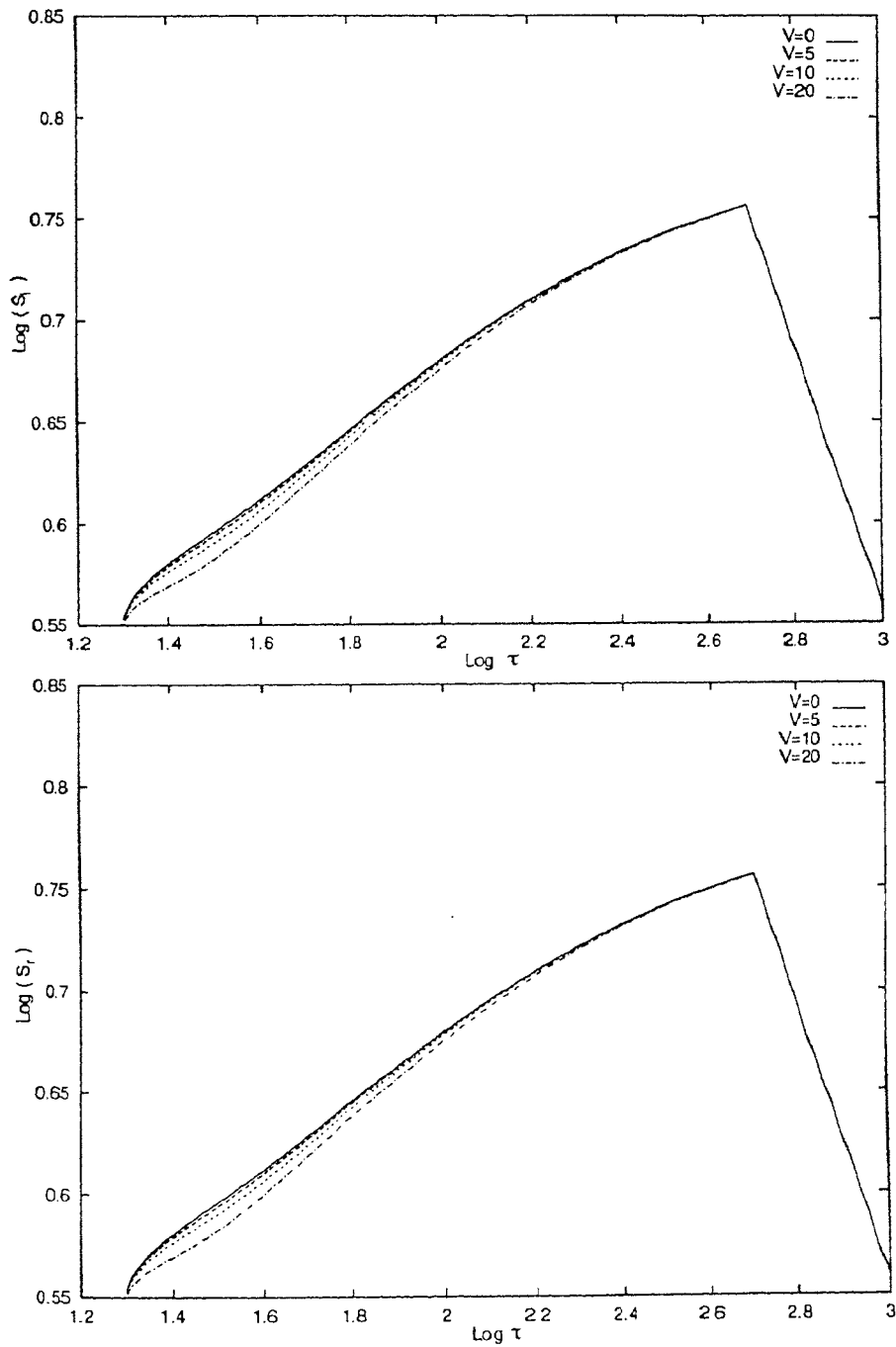


Figure 5.12:  $l$  and  $r$  components of the frequency independent source function along the direction  $\mu = 0.88$  in the comoving frame.  $\epsilon = \beta = 10^{-3}$ ,  $T = 10^3$ ,  $B/A = 3$  and  $\alpha = +0.9$ .

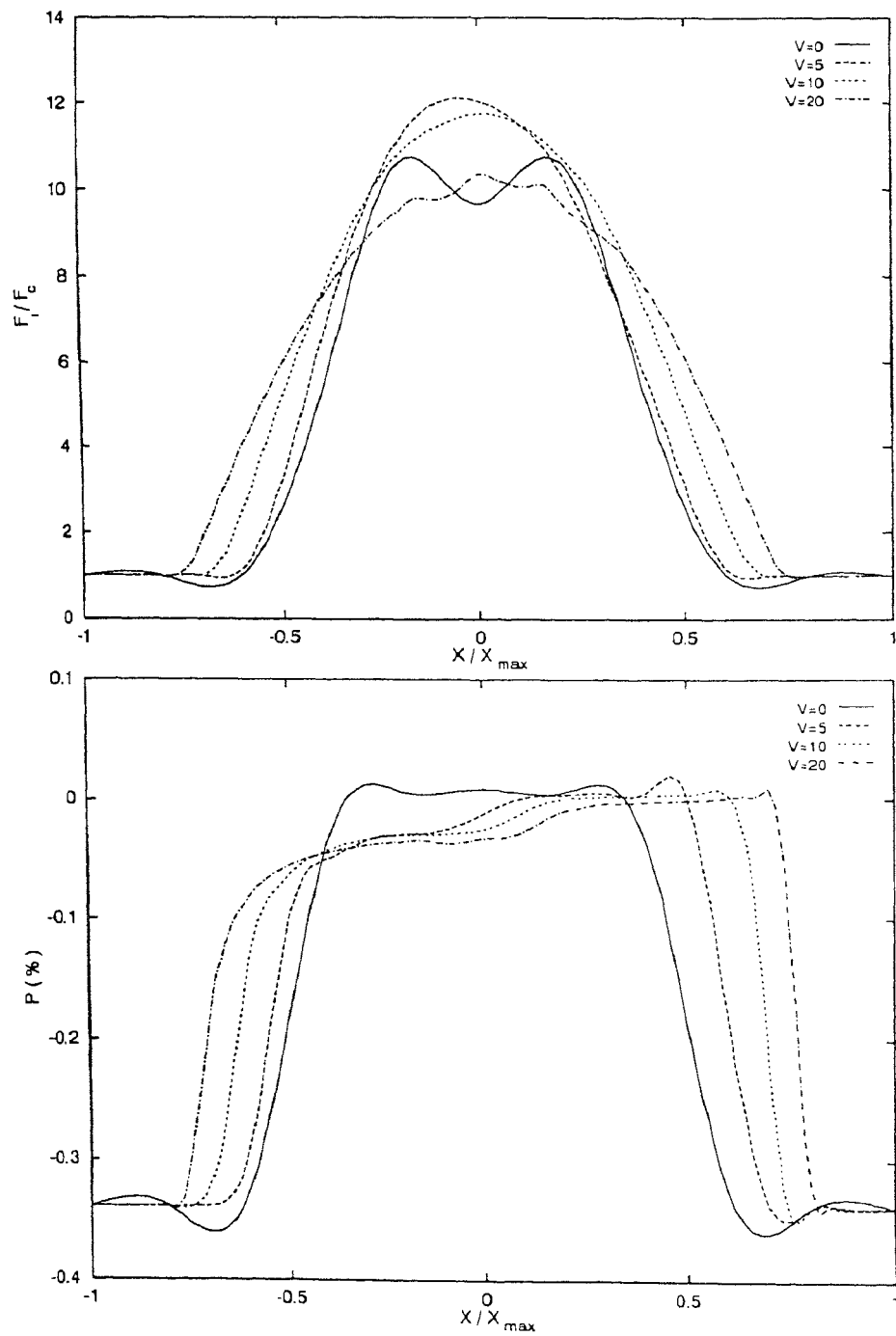


Figure 5.13: Emergent total flux and the polarization profile along the line of sight corresponding to Figure 5.10

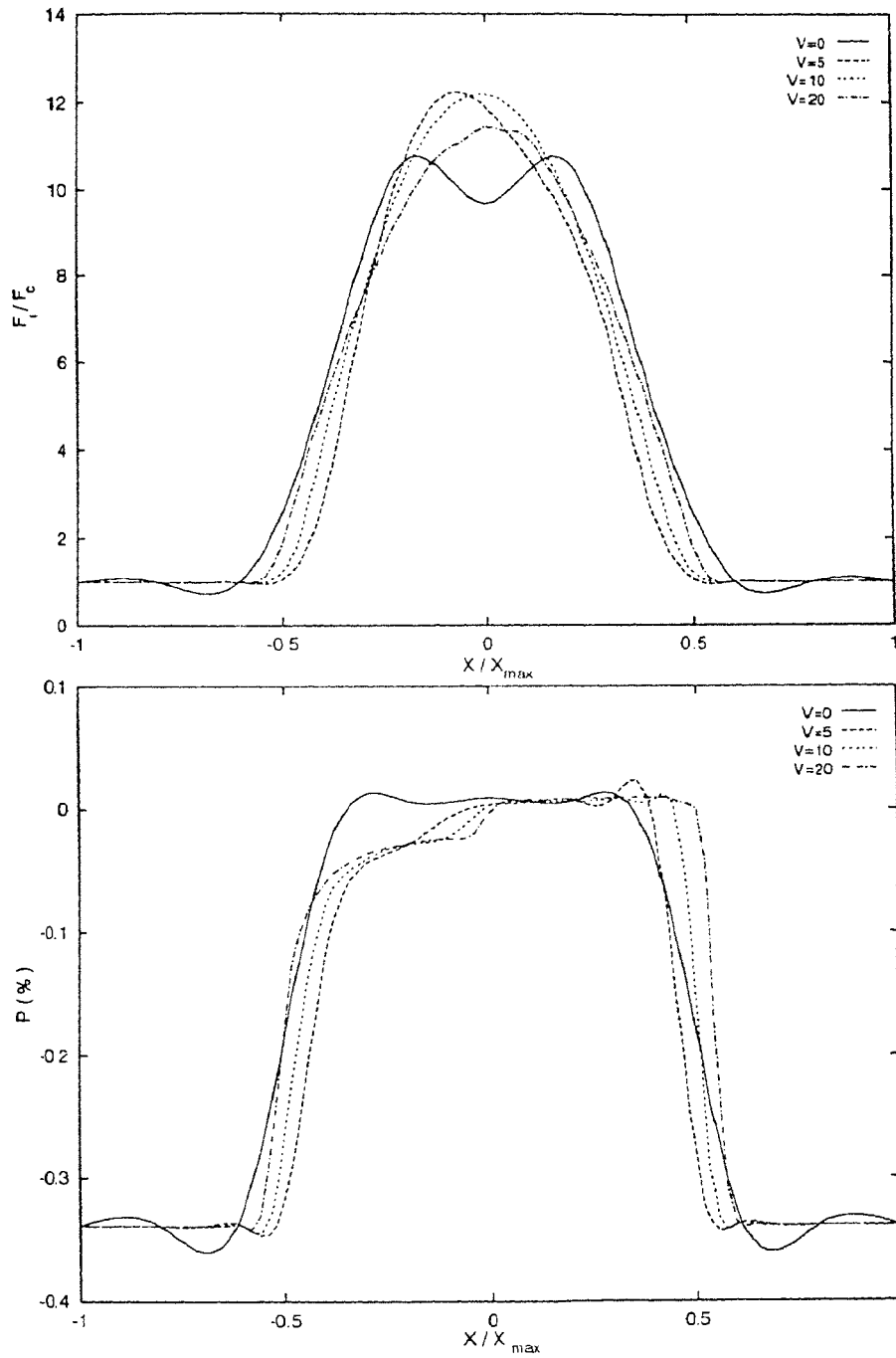


Figure 5.14: Emergent total flux and the polarization profile along the line of sight corresponding to Figure 5.11

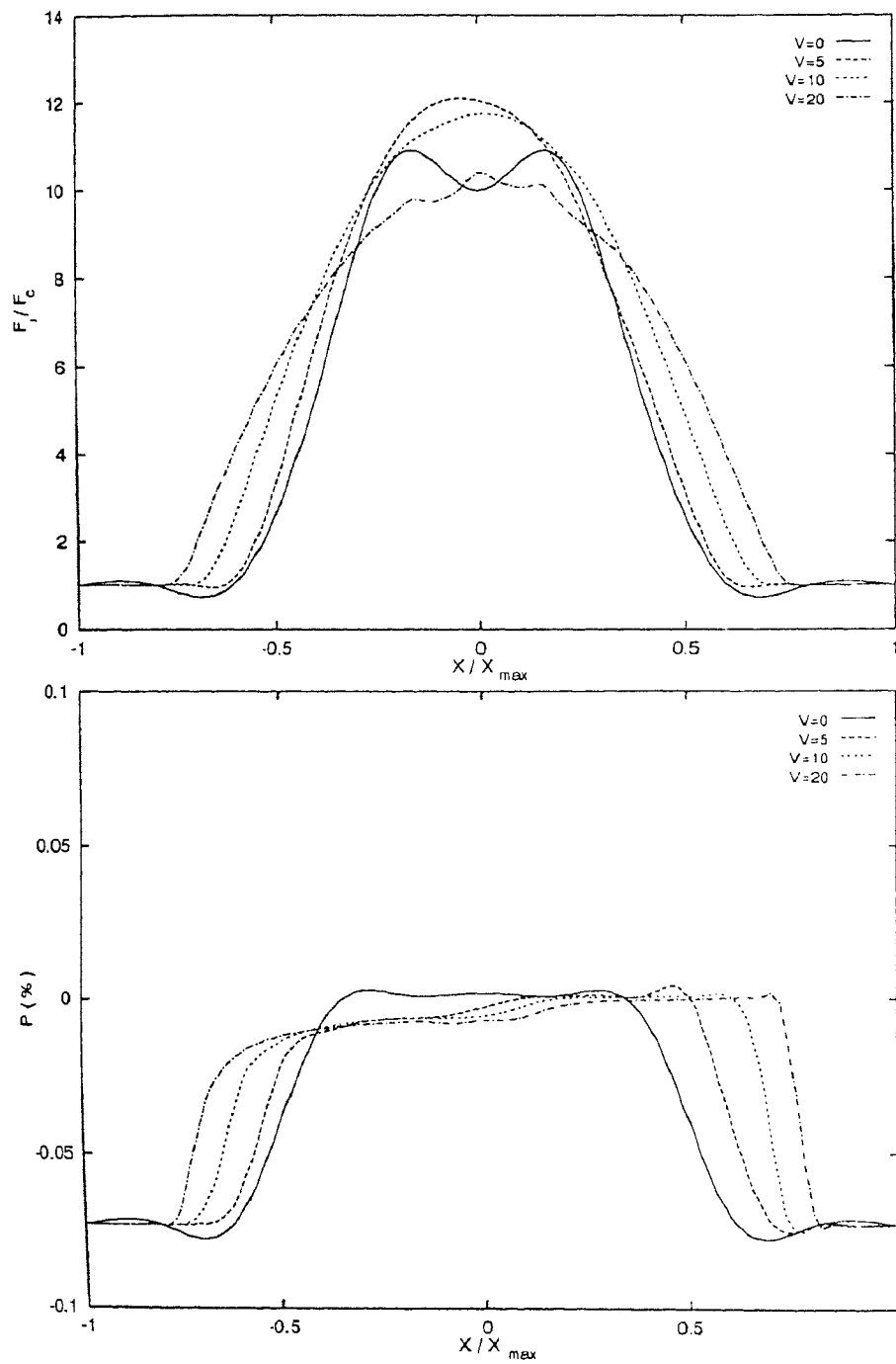


Figure 5.15: Emergent total flux and the polarization profile along the line of sight corresponding to Figure 5.12

The basic nature of the polarization profile in the observer's frame remains the same irrespective of the inclusion of velocity field, however, asymmetry in the profile caused by the velocity field is significant even with the introduction of small velocity gradient. The degree of polarization is negligible at the line but it increases rapidly towards the wings and takes a constant value at the continuum for any velocity gradient. The difference in degree of polarization is almost negligible at the line where the degree of polarization is almost zero for any velocity gradient but the difference increases at the wing when  $\alpha = +0.9$  and decreases when  $\alpha = -1.0$ . Therefore, the effect of different velocity rules is more important than the velocity gradient in the formation of the polarization profile along the line of sight.

From Figure 5.15 we notice that the total flux profile remains unaltered with the change in the value of  $\mu$ . However, the degree of polarization along the line of sight reduces substantially with the increase in the value of  $\mu$ . The other features of the polarization profile remains almost the same.

Figure 5.16 to Figure 5.20 show how the above results are altered when the total optical depth is increased. In this case, we consider the total optical depth to be 100 times larger than that considered in the previous model. Since the effect of velocity rule would remain the same, we investigate the effect of optical depth by considering just one velocity rule, e.g., that with  $\alpha = +0.9$ . All the other parameters remain the same as given in Figure 5.3 so that the effect of optical depth can be understood clearly.

In the models with  $T = 10^3$  it has been found that the amount of emergent intensity at each shell remain almost the same to the amount of backscattered intensity for a given velocity gradient. But the variation in the amount of both the emergent and the backscattered intensities differs significantly with the inclusion of different velocity gradient. With the increase in optical depth this difference reduces significantly from the outer region to the inner region making the emergent and the backscattered intensities almost independent of the velocity field as can be seen from Figure 5.16 and Figure 5.17. This implies that with the increase in optical depth the line photons are trapped and



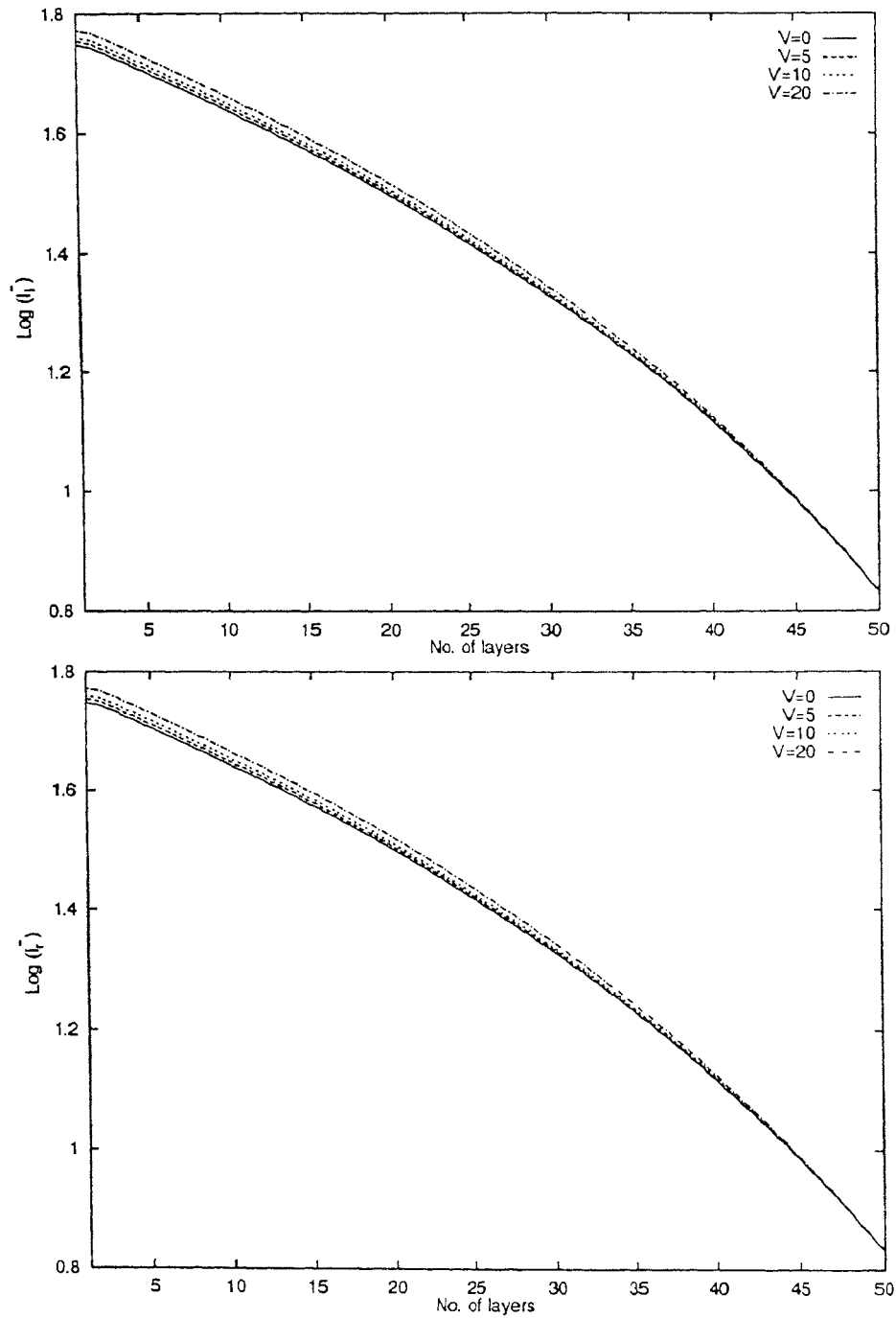


Figure 5.16:  $l$  and  $r$  components of the emergent intensity of radiation with the line center frequency at each shell along the direction  $\mu = 0.11$  in the comoving frame.  $\epsilon = \beta = 10^{-3}$ ,  $T = 10^5$ ,  $B/A = 3$  and  $\alpha = +0.9$ .

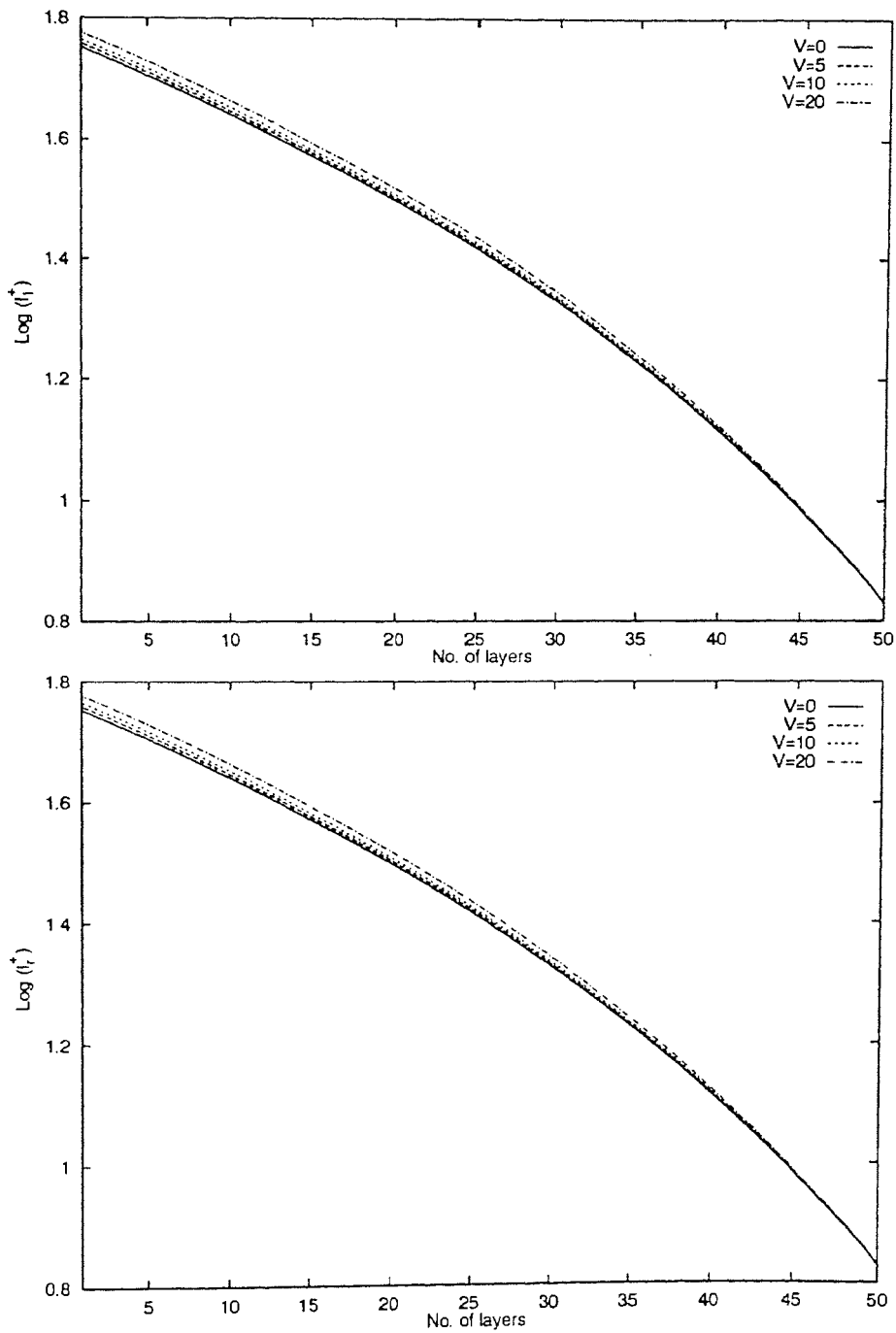


Figure 5.17:  $l$  and  $r$  components of the backscattered intensity of radiation with the line center frequency at each shell along the direction  $\mu = 0.11$  in the comoving frame.  $\epsilon = \beta = 10^{-3}$ ,  $T = 10^5$ ,  $B/A = 3$  and  $\alpha = +0.9$ .

unable to escape even with the help of large velocity field. As the optical depth decreases the escape probability of the photons become higher. The larger is the velocity gradient the higher is the escape probability and hence increase in the intensity with the increase in velocity gradient towards the outer region. With the increase in the optical depth, the amount of emergent intensity at each shell becomes equal to the amount of backscatter intensity. Further, a comparison with the results presented in Figure 5.3 and Figure 5.5 shows that both the emergent and the backscattered intensities in the comoving frame increase more rapidly towards the outer region with the increase in the total optical depth.

Figure 5.18 presents the emergent total intensity and the polarization profiles in comoving frame with  $T = 10^5$ . Significant changes in both the profiles are observed when the total optical depth is increased. With  $T = 10^5$  the emergent total intensity and the degree of polarization in comoving frame are not at all affected by the inclusion of velocity field.

Figure 5.19 shows the  $l$  and the  $r$  components of the frequency independent source function which too remains the same for any velocity gradient. This implies that the increase in total optical depth reduces the effect of velocity field in great extent. As the optical depth increases towards the interior of the medium the source function increases and it falls rapidly at the innermost region due to the adopted boundary condition. A comparison of the results with  $T = 10^3$  shows that at the outer region the source function becomes higher when the total optical depth is increased.

Finally from Figure 5.20 we can conclude that the emergent total flux and the degree of polarization along the line of sight are not affected significantly with the increase in total optical depth.

Now we discuss how a change in the sphericity or the curvature affects the whole scenario. For this purpose the outer radius of the atmosphere is increased to  $5 \times 10^{11}$  so that the ratio of the inner radius to the outer radius which determines the curvature becomes 5. the other parameters are kept the same as given in Figure 5.3.

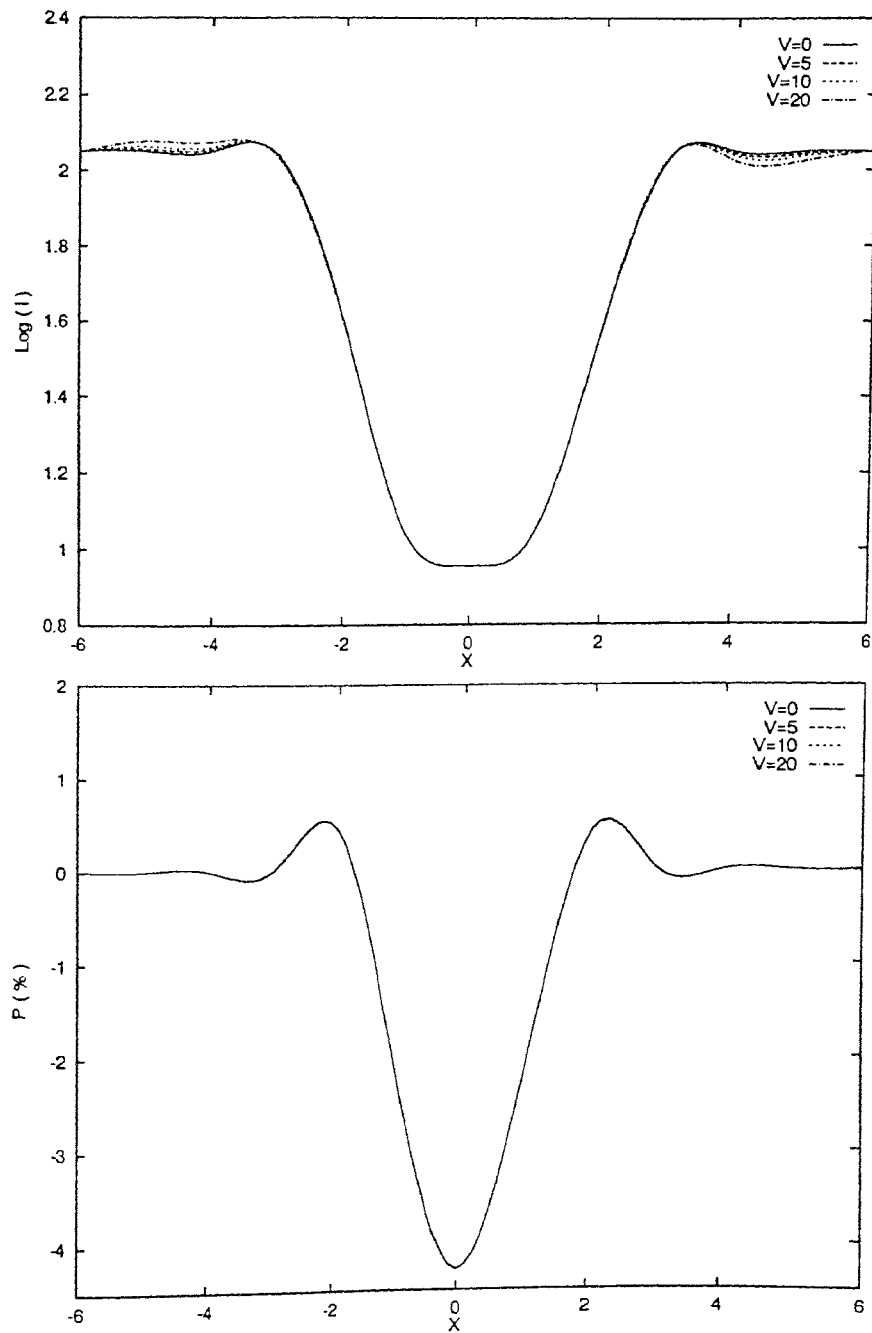


Figure 5.18: Emergent intensity and polarization profile along the direction  $\mu = 0.11$  in the comoving frame.  $\epsilon = \beta = 10^{-3}$ ,  $T = 10^5$ ,  $B/A = 3$  and  $\alpha = +0.9$ .

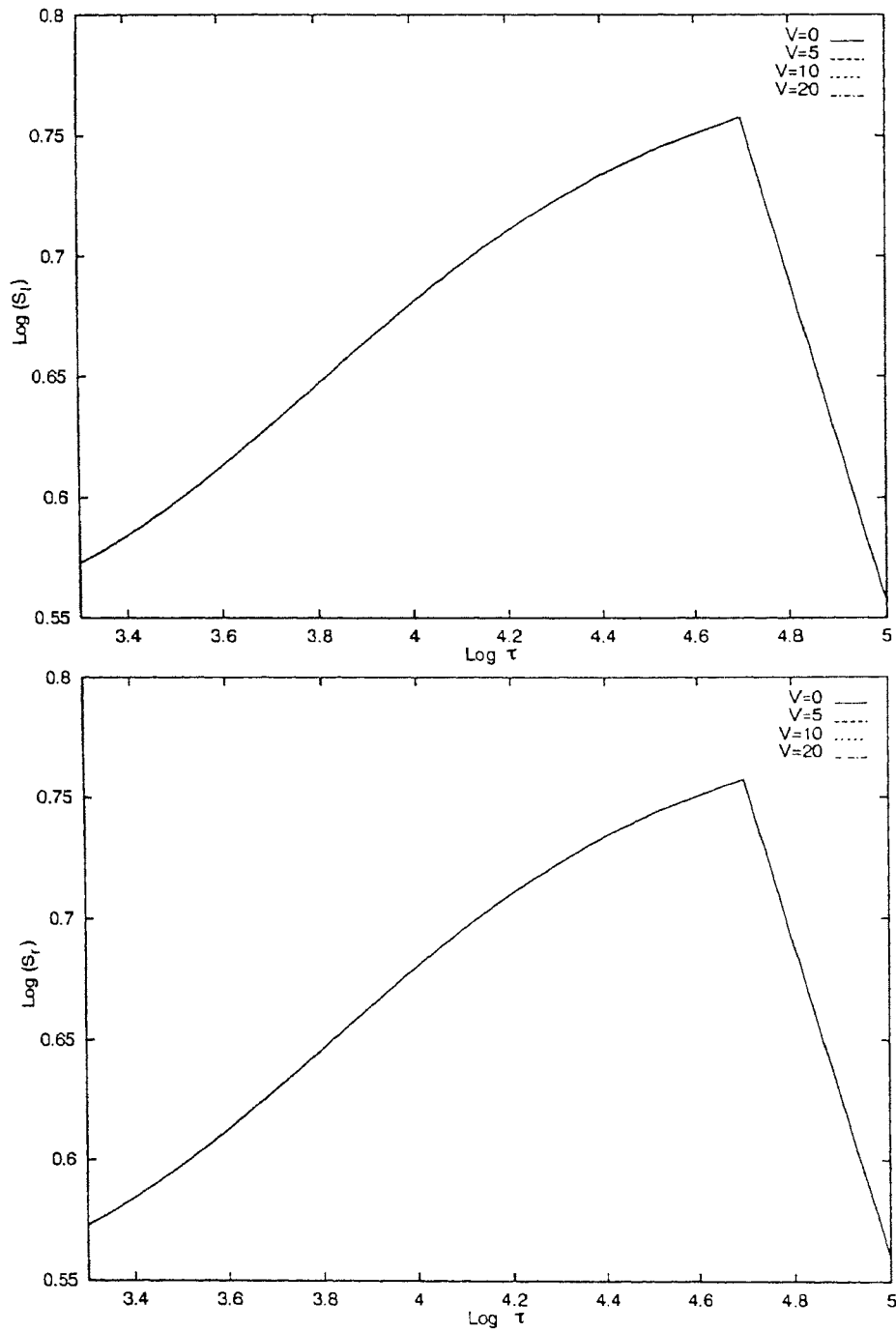


Figure 5.19:  $l$  and  $r$  components of the frequency independent source function along the direction  $\mu = 0.11$  in the comoving frame.  $\epsilon = \beta = 10^{-3}$ ,  $T = 10^5$ ,  $B/A = 3$  and  $\alpha = +0.9$ .

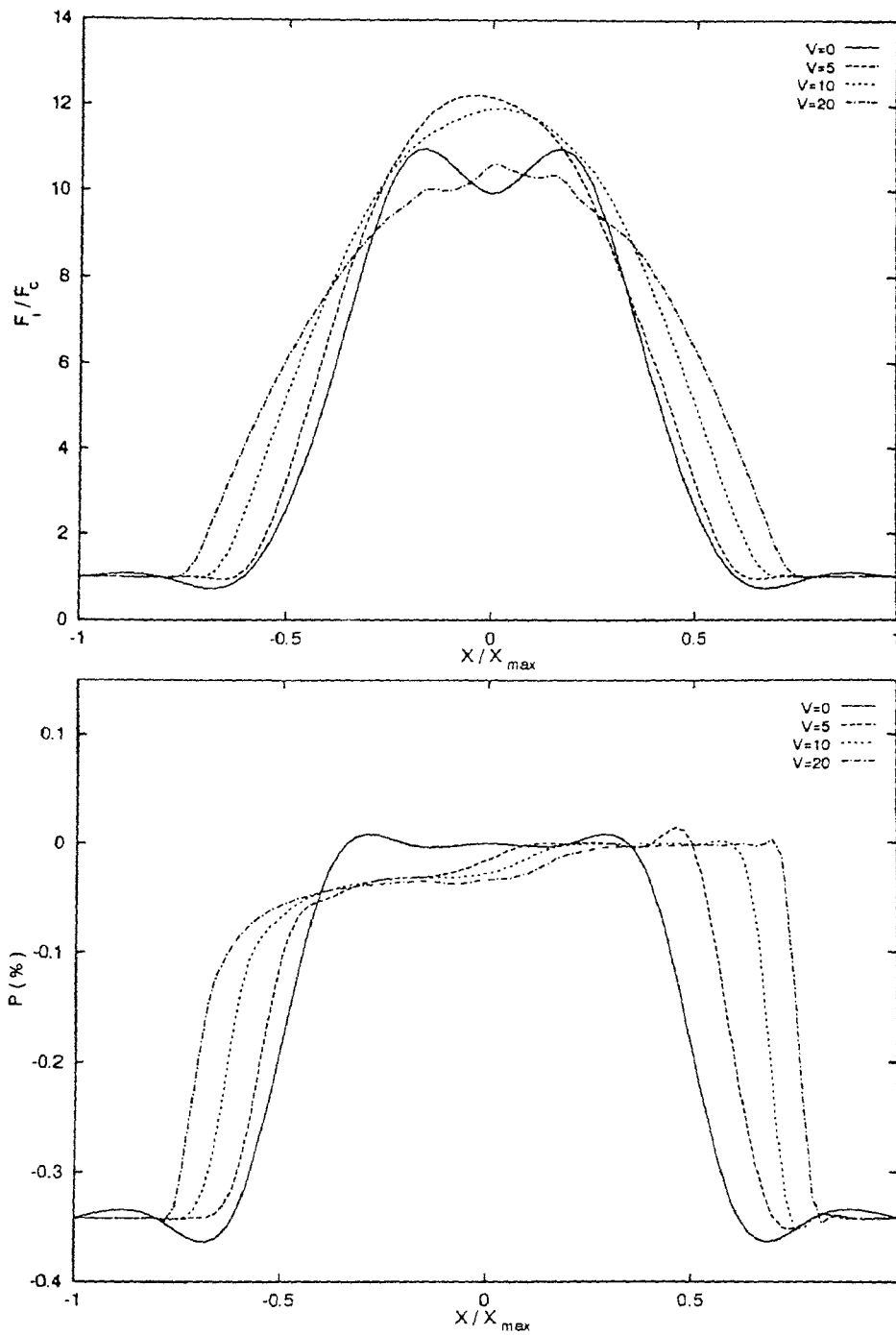


Figure 5.20: Emergent total flux and the polarization profile along the line of sight corresponding to Figure 5.19

Figure 5.21 shows the  $l$  and the  $r$  components of the emergent intensity of radiation with line center frequency at each shell. A comparison with Figure 5.3 indicates that for all the cases the emergent intensity increases significantly towards the outer region as  $B/A$ , the sphericity increases. This is because of the fact that with the increase in sphericity the medium gets diluted in great extent. Since we have considered the variation of the optical depth as  $\frac{1}{r}$ , therefore with the increase in the extension of the medium the optical depth decreases in larger extent with the increase in geometrical depth. Hence more energy is transferred as the photon traverses outwards. However the difference in the emergent intensity at each shell with different velocity gradient remains the same with the increase in sphericity. Therefore, the role of velocity field is unaltered with the increase in curvature.

Figure 5.22 shows the  $l$  and the  $r$  components of the backscattered radiation in comoving frame with  $B/A = 5$ . Just like the situation for emergent intensity, the backscattered intensity also increases for all velocity gradients with the increase in sphericity, making a balance between the emergent and backscattered intensity in comoving frame at each layer. The role of velocity field remains unaltered with the increase in  $B/A$ .

Figure 5.23 presents the emergent total intensity and the polarization profile in comoving frame with  $B/A = 5$ . As can be observed in Figure 5.21, the emergent intensity increases with the increase in sphericity owing to the dilution of the medium, here we observe that the result is true for any frequency point. The emergent intensity increases in the same extent for all velocity gradients. The asymmetry at the wing however remains the same indicating that the role of velocity field is not affected by the increase in curvature. The polarization profile in comoving frame remains the same as can be seen from Figure 5.3 and Figure 5.23. That means the anisotropy of the medium is not changed with the increase in curvature.

The  $l$  and the  $r$  components of the frequency independent source function in comoving frame are affected significantly with the increase in sphericity as can be seen from Figure 5.24. Towards the interior, the source function first increases slowly upto one third

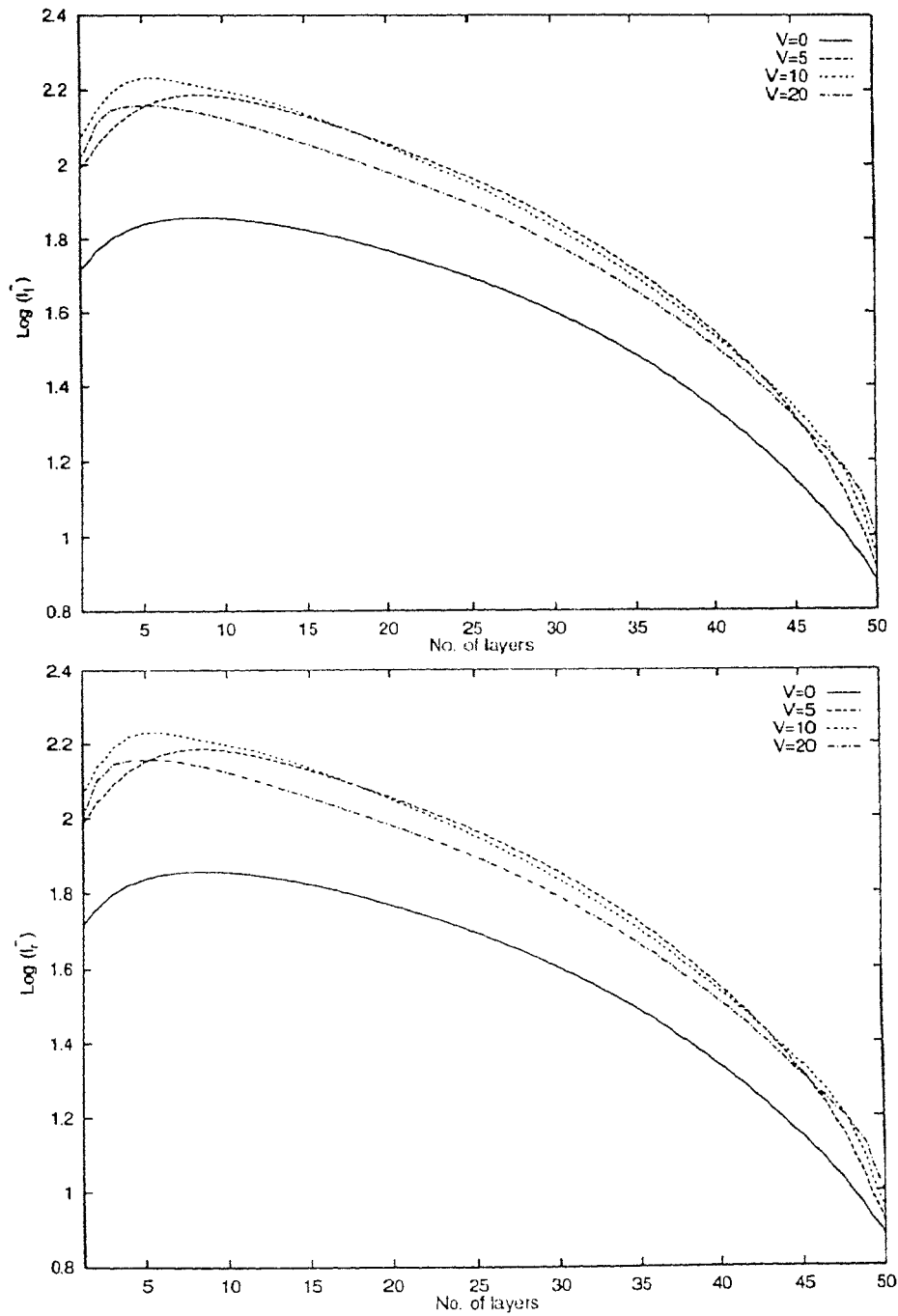


Figure 5.21:  $l$  and  $r$  components of the emergent intensity of radiation with the line center frequency at each shell along the direction  $\mu = 0.11$  in the comoving frame.  $\epsilon = \beta = 10^{-3}$ ,  $T = 10^3$ ,  $B/A = 5$  and  $\alpha = +0.9$ .



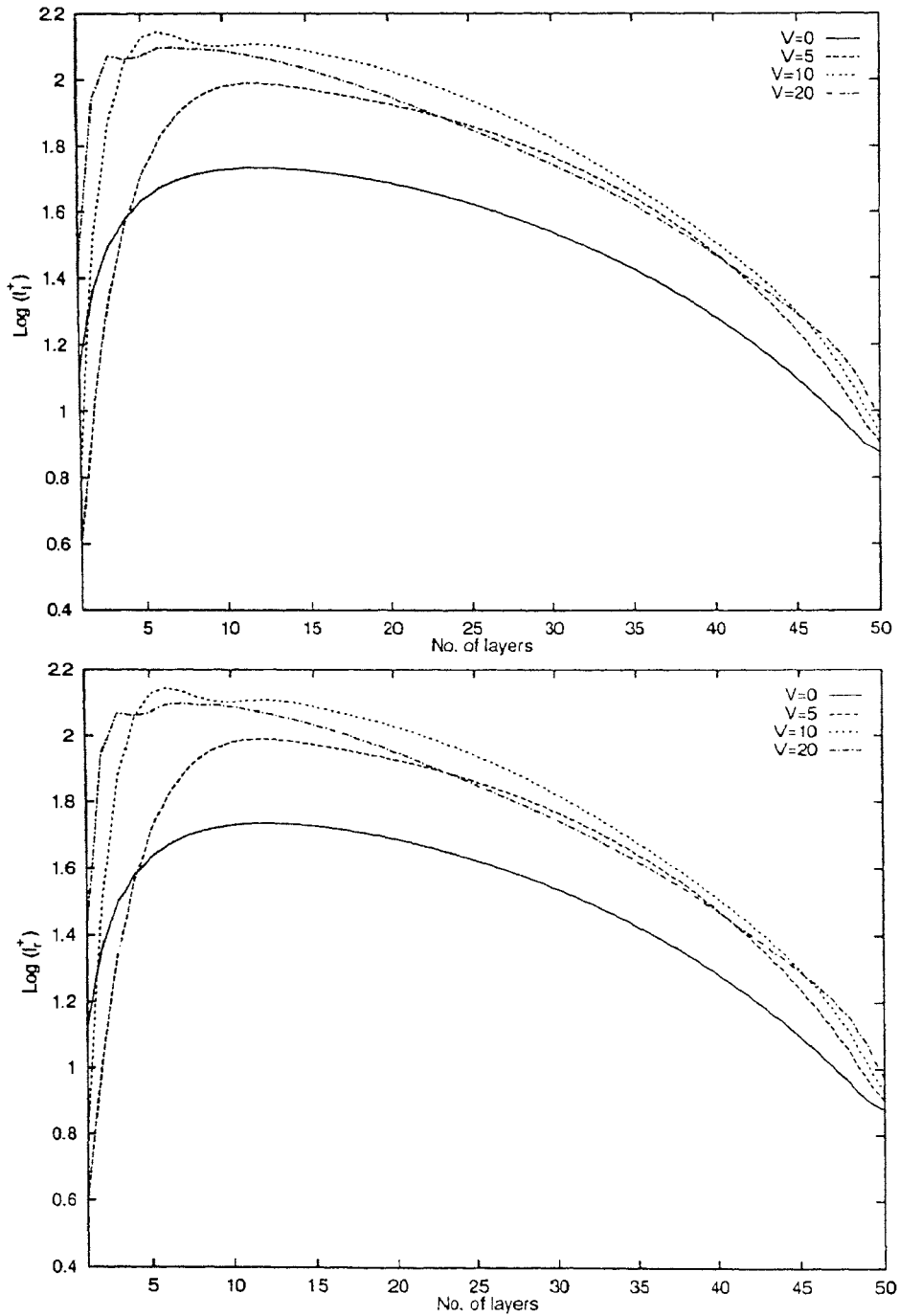


Figure 5.22:  $l$  and  $r$  components of the backscattered intensity of radiation with the line center frequency at each shell along the direction  $\mu = 0.11$  in the comoving frame.  $\epsilon = \beta = 10^{-3}$ ,  $T = 10^3$ ,  $B/A = 5$  and  $\alpha = +0.9$ .

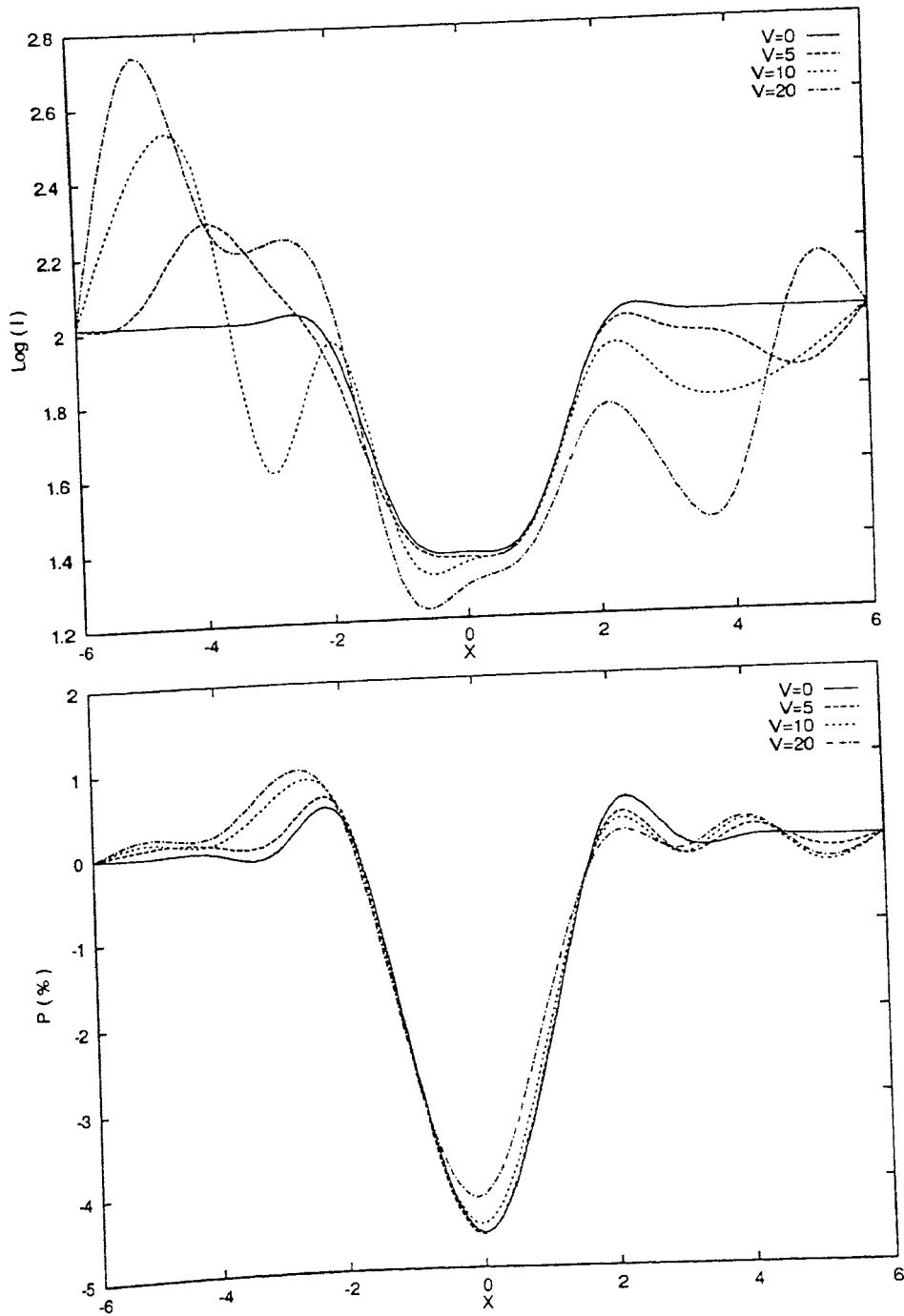


Figure 5.23: Emergent intensity and polarization profile along the direction  $\mu = 0.11$  in the comoving frame.  $\epsilon = \beta = 10^{-3}$ ,  $T = 10^3$ ,  $B/A = 5$  and  $\alpha = +0.9$ .

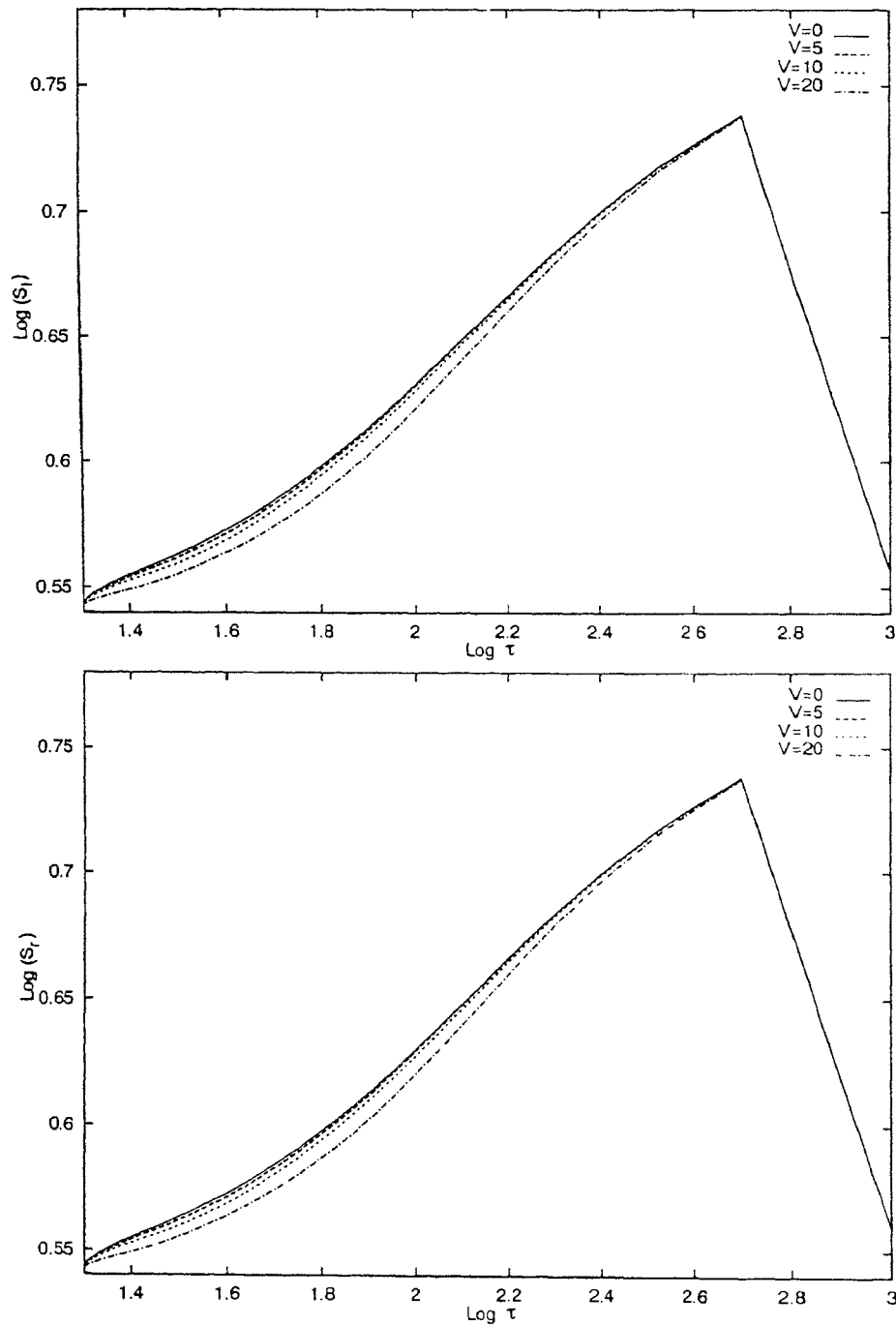


Figure 5.24:  $l$  and  $r$  components of the frequency independent source function along the direction  $\mu = 0.11$  in the comoving frame.  $\epsilon = \beta = 10^{-3}$ ,  $T = 10^3$ ,  $B/A = 5$  and  $\alpha = +0.9$ .

of the geometrical depth, then rises rapidly until it reaches the deepest region where it suddenly falls due to the adopted boundary condition. From the middle to the innermost region the source function is almost unaffected by the increase in  $B/A$  but due to the increase in the extension of the medium the outer region becomes more transparent and hence significant change in the source function takes place within this region. However the effect of velocity field remains the same with the increase in sphericity.

The dilutaion of the medium caused by the extension is clearly revealed in the emergent total flux profile along the line of sight as shown in Figure 5.25 wherein we observe a large increase in the amount of flux due to the increase in curvature. The profile becomes more oblate with large velocity gradient. With the increase in sphericity the emergent flux in observer's frame decreases significantly with the increase in velocity gradient and the decrease is maximum for large velocity gradient. Also the profiles for all velocity gradients tend to become more symmetric as the sphericity increases. With the increase in the extension of the medium, more energy from the opposite side of the core of the star where the expansion of the atmosphere is away from the observer, adds up to the net flux. Hence the net flux is contributed from both the blue-shifted and the red-shifted photons. In other words, as the extension increases the blockade to the radiation caused by the opaque core of the star becomes negligible and radiation from both the regions, moving away and moving towards the observer, contribute to the total flux in almost same extent. Hence, the asymmetry in the flux profile reduces significantly with the increase in the extension of the medium. The polarization profile in the observer's frame however shows no significant change implying that the degree of anisotropy of the atmosphere remains unaffected by the increase in sphericity.

## 5.4 Summary

The main features of the results are summarized as follows: With the introduction of sphericity and inhomogeneity, the polarization profile along the line of sight gets altered

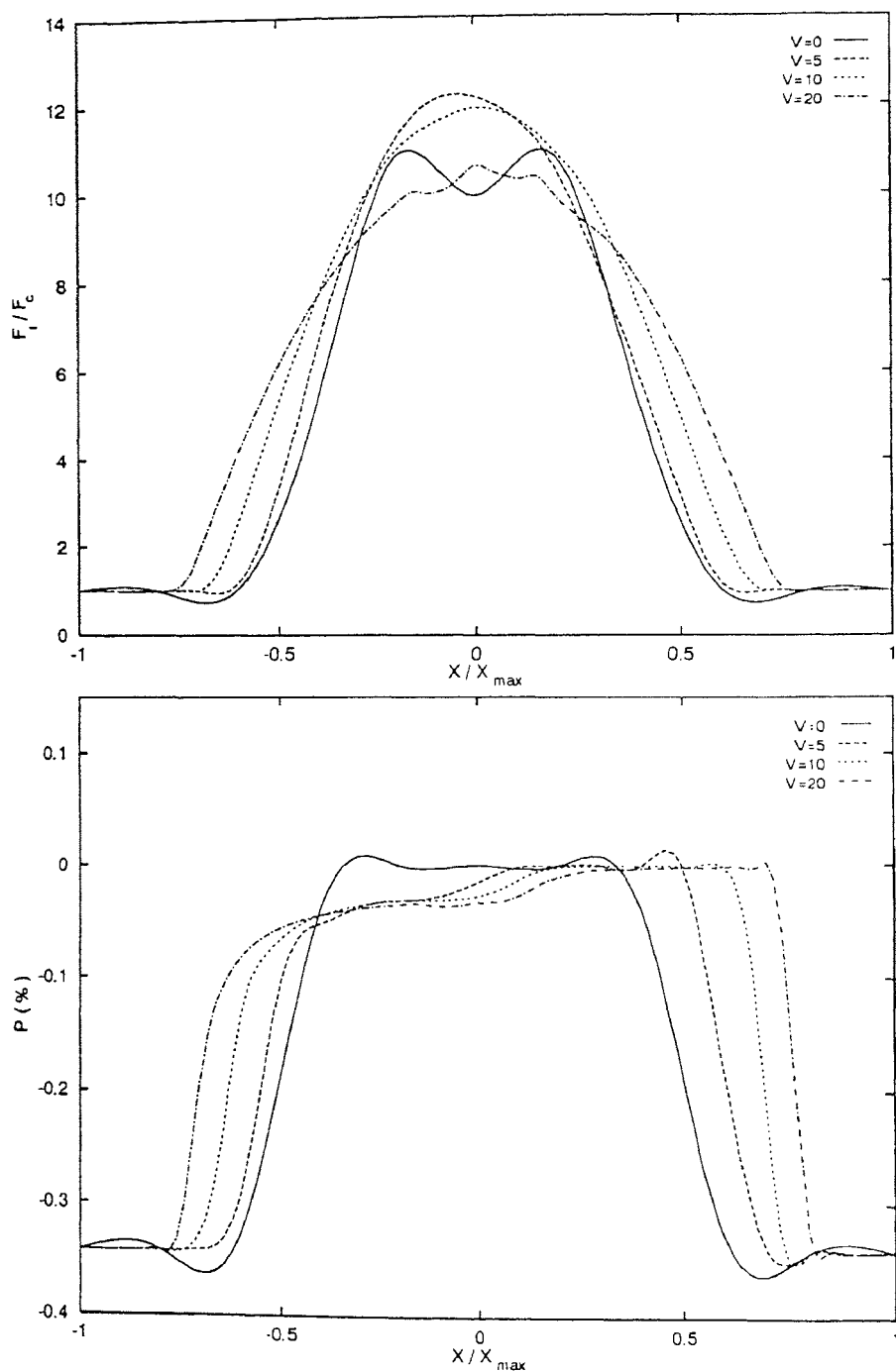


Figure 5.25: Emergent total flux and the polarization profile along the line of sight corresponding to Figure 5.24

significantly. The degree of polarization is almost negligible at the line but it increases rapidly towards the wings and take a constant value at the continuum for all the velocity gradients. The form of the velocity rule plays crucial role in the determination of the degree of polarization in observer's frame. When the value of the parameter  $\alpha$  in the velocity rule is -1.0, the rapid increase in the degree of polarization takes place from the near wing whereas this occurs from the far wing when  $\alpha$  is set as +0.9. The sign of the degree of polarization ( $F_Q/F_I$ ) is always negative in a spherically symmetric, inhomogeneous medium.

As the optical depth increases, the role of velocity field decreases significantly because the trapped photons cannot escape from an optically thick shell with the help of even large velocity gradient. As the sphericity increases the medium gets diluted due to the large extension of the atmosphere and hence the total flux increases in great extent. The flux profile becomes more symmetric as the extension of the atmosphere is increased. However the anisotropy of the medium remains almost unaffected either by the increase in total optical depth or by the increase in sphericity.

# Chapter 6

## Conclusions

---

The problem of constructing mathematical models of stellar atmospheres that provide a description of the physical structure of the atmosphere and of its emergent spectrum is one of enormous complexity, and presents both physical and mathematical difficulties even in its simplest form. The problem of obtaining solution of radiative transfer is basically a mathematical one. According to Synge "... the use of applied mathematics in its relation to a physical problem involves three steps :

- (1) a dive from the world of reality into the world of mathematics,
- (2) a swim in the world of mathematics and
- (3) a climb from the world of mathematics back into the world of reality, carrying the prediction in our teeth."

In the present work all these three steps have been followed to investigate the effect of differential radial expansion of stellar atmospheres on the formation of line polarization. Due to the formidable mathematical difficulties it has been necessary to make a number of simplifications, and to deal with idealized models that are rather high-order abstraction from reality. Nevertheless, such abstraction are useful inasmuch as they enhance our insight without overwhelming us with detail.

In the introductory chapter (the first chapter) I have presented a survey of the work done by various researchers that are relevant to the present investigation. When one re-

views the work on radiative transfer, one encounters an inexhaustable amount of literature because of the fact that each group of workers develop a distinctive set of techniques of varying generalities to suit its own needs. There is, however, hardly any cross fertilisation among these groups. As a consequence, it is not possible to mention each and every work although they are not less important than the work mentioned in the present survey. Only those work which are the most relevant and have been extremely useful for the present study have been mentioned.

In the second chapter, the basic concept of polarization of light and in particular the atomic processes that leads to resonance line polarization have been discussed. The special condition under which resonance line polarization becomes similar to the Rayleigh scattering has also been discussed in this context. The mathematical formulations of polarized radiation and the representation of it by Stokes parameters have been presented in detail. Since resonance line polarization is regarded as a quantum analogue of the well known Rayleigh scattering, a detail discussion on Rayleigh's law of scattering and its modification in order to incorporate it into the radiative transfer equation have been provided. The general and explicit form of the phase matrices that are used to describe the angular distribution of photons that undergo Rayleigh and resonance scattering have been presented in this chapter.

In the present work, plane parallel and spherically symmetric geometries have been considered. For both the cases, the axial symmetry of the radiation field requires that the plane of polarization be along the meridian plane or perpendicular to it. As a consequence, only two out of the four Stokes parameters are required to characterize the linearly polarized radiation field. The two-level atom line transfer equation governing the intensities  $I_l$  and  $I_r$  in rest frame with plane parallel and spherically symmetric geometries have been presented. Since accurate calculation of the scattering integral in the expression for line source function with a quadrature sum poses fundamental difficulties in rest frame calculation due to various reasons, the comoving-frame method has been adopted in the present work. The need for adopting comoving frame formalism in the



study of the transfer of radiation from expanding stellar atmospheres has been discussed in detail. Finally, the transfer equations for polarized radiation in comoving frame for both plane parallel and spherically symmetric stellar atmospheres have been presented along with the expressions for the absorption profile and the frequency redistribution function.

In the third chapter the numerical method for solving the transfer equations has been discussed in detail. The numerical method due to Peraiah has been employed to solve the plane parallel as well as the spherical radiative transfer problem in the comoving frame. The numerical method is based on the discrete space theory. The basic concept of the theory and its application to solve the radiative transfer equation have been explained. The generalization of all the steps of this finite-difference method for including the polarization state of the radiation has been described in detail. The main purpose has been to develop reflection and transmission operators that embody all the physical information contained in the problem. The medium under consideration is divided into a number of spherical shells. The transmission, reflection and source vectors are computed for all the shells. For a thick layer, the so-called star product, which is essentially a doubling algorithm, is used. The method can handle the problem arising out of the coupling of the comoving points across the line profile and the local velocity gradients. The stability of the solution is achieved by controlling the step-size, which arises in the discretization in radial, angle and frequency integrations. In the present work, two types of media have been considered; purely scattering medium and partially scattering medium with both line and continuum emission. The problem has been solved subject to two kinds of boundary conditions : (1) the radiation incident on either side of the atmosphere and (2) the frequency derivative appearing in the comoving term. The correctness of the numerical results has been checked by considering global flux conservation. It is found that the flux is conserved to up to nine decimal figure. The correctness check has also been performed by considering specular reflection at the inner boundary. The results for various velocity gradient have been provided in tabular form. Finally, the procedure for calculating the total flux and the polarization profiles

along the line of sight of an observer at infinity by using the components of the frequency independent source function calculated in the comoving frame has been described.

In the fourth chapter the effect of differential radial velocity on the distribution of line intensities and line polarization in a stellar atmosphere stratified in parallel planes has been presented in detail. The medium is assumed to be homogeneous and isothermal. Two different types of velocity rules have been adopted in this case with zero velocity at the innermost layer. The results have been compared with that of the static case. The line intensity profile and the polarization profile in the comoving frame as well as in the observer's frame are discussed in detail. It is found that in a purely scattering homogeneous and isothermal atmosphere, the amount of emergent and backscattered intensities of the radiation field is the same at each point along the geometrical depth, i.e., there is no change in photon energy at any layer of the atmosphere. This situation is altered significantly with the inclusion of a non-zero velocity field. With the inclusion of even a small velocity gradient, the intensity of the emergent radiation falls slowly from the innermost layer to the outermost layer. As the velocity gradient increases, the fall in the intensity towards the outer region is more rapid. The emergent intensity in the comoving frame decreases as the velocity increases with substantial asymmetry in the profile at the wing. Except for large velocity gradient the degree of polarization in comoving frame remains almost the same for any velocity gradient. In a purely scattering medium the flux profile along the line of sight becomes more and more asymmetric with absorption feature when a high velocity gradient is included. The amount of total flux in this case decreases with the increase in velocity gradient. The degree of polarization in the observer's frame is maximum for small velocity gradient and it decreases with the increase in velocity. In a partially scattering medium, the degree of polarization in comoving frame as well as in the observer's frame is substantially less compared to that in the purely scattering medium implying that a non-zero thermalization parameter decreases the anisotropy of the atmosphere. Unlike the case for a purely scattering medium, in a partially scattering medium the flux profile in the observer's frame is symmetric even with the inclusion of large velocity gradient. The results could be useful in obtaining a general idea about the

resonance line polarization in a radially expanding plane-parallel stellar atmosphere.

As the stellar radius increases the curvature effect plays a dominant role and a spherically symmetric geometry becomes more relevant in that case. In the fifth chapter the effect of differential radial velocity in the distribution of line intensities and line polarization for a spherically symmetric, inhomogeneous and isothermal medium is presented in detail. The atmospheric models could represent the photospheric layers of early type stars, giant and supergiant stars as well as luminous late type stars. In the case of a spherically symmetric stellar atmosphere, a fixed value of the thermalization parameter is taken in all models and the effect of differential radial expansion on line polarization under different optical depths as well as sphericity of the medium has been discussed in detail. Two different types of velocity laws have been adopted with zero velocity at the innermost shell. The velocity at the outermost shell has been taken 5, 10, 20 mean thermal units to study the effect of small, medium and large velocity gradients. The results have been compared with that of the static case. The emergent intensity in the comoving frame increases significantly with the inclusion of the velocity field. The change in the emergent intensity in the comoving frame is maximum when a small velocity gradient is included. The emergent total intensity profile in the comoving frame remains almost symmetric at the line but significant asymmetry is found at the wings. The asymmetry increases with the increase in the velocity gradient. The degree of polarization in the comoving frame decreases with the increase in the velocity gradient. The frequency independent  $l$  and the  $r$  components of the source function increase towards the inner region for all velocity gradients. The total flux profile along the line of sight for the static case is symmetric but with the inclusion of the velocity field it becomes highly asymmetric with the greatest change in the profile when a small velocity gradient is considered. As the velocity gradient increases, the amount of emergent flux decreases at the line. The important role of the velocity rule is revealed when a large velocity gradient is included. The degree of polarization in the observer's frame is negligible at the line where it is almost zero. It is found that the effect of different velocity rules is more important than that of the velocity gradient in the formation of the polarization profile along the line of sight. Significant changes in

both the intensity profile and the polarization profile in comoving frame are found when the total optical depth is increased. With the increase in total optical depth, the effect of velocity field on the emergent total intensity and the degree of polarization in comoving frame reduces. Although the increase in total optical depth reduces the effect of velocity field on the source function, the emergent total flux and the degree of polarization along the line of sight are not affected significantly. The emergent intensity in the comoving frame increases with the increase in sphericity. However the polarization profile remains unaltered. With the increase in sphericity, the total flux along the line of sight increases in great extent and the profile becomes more symmetric. The anisotropy of the medium remains almost unaffected and hence the degree of polarization remains the same with the increase in sphericity.

The net polarization of light emitted by a spherical star, however, is identically zero. Therefore a comparison with observational results are not possible at this stage. For that purpose one has to consider a distorted medium and to calculate the disc integrated flux and polarization profiles. This aspect is a topic which needs further study since it represents the closest situation to the feasibility of observations. Nevertheless, the present study can provide a reasonably good understanding of the basic features of the polarized line formation problem in a radially expanding and extended spherical stellar atmosphere.

## References

---

- Brukner, G., *Z. Astrophys.* 58 (1963) 73.
- Castor, J. I., *ApJ* 178 (1972) 779.
- Castor, J. I. and Lamers, H. J. G. L. M., *ApJS* 39 (1979) 481.
- Chandrasekhar, S., *ApJ* 102 (1945a) 402.
- Chandrasekhar, S., *Rev. Mod. Phys.* 17 (1945b) 138.
- Chandrasekhar, S., *Radiative Transfer* (Dover, New York 1960).
- Coyne, G. V., Magalhaes, A. M., Moffat, A. F. G., Schutte-Ladbeck, R. E., Tapia, S. & Wickramasinghe, D. T., eds., *Polarized Radiation of Circumstellar Origin* (Vatican Obs. Vatican City State and University of Arizona Press 1988).
- Dyck, H. M. & Sandord II, M. T., *Astron. J.* 76 (1971) 43.
- Faurobert, M., *A & A* 178 (1987) 269.
- Faurobert, M., *A & A* 194 (1988) 268.
- Faurobert, M., *A & A* 246 (1991) 469.
- Feautrier, P., *Ann. d'Astrophys.* 31 (1968) 257.
- Grant, I. P. and Hunt, G. E., *Proc. Roy. Soc. Lond.* A313 (1969a) 183.
- Grant, I. P. and Hunt, G. E., *Proc. Roy. Soc. Lond.* A313 (1969b) 199.

- Grant, I. P. and Peraiah, A., MNRAS 160 (1972) 239.
- Hamilton, D. R., ApJ 105 (1947) 424.
- House, L. L., JQSRT 11 (1971) 367.
- Kruszewski, A., Gekrels, T. & Serkowski, K., Astron. J. 73 (1968) 677.
- Lamb, F. K., Solar Phys. 12 (1970) 186.
- Landi degl'Innocenti, E., Solar Phys. 91 (1984) 1.
- Lindquist, R. W., Ann. Phys. 37 (1966) 487.
- Lucy, L., ApJ 163 (1971) 95.
- McKenna, S. J., Astrophys. Space Sc. 106 (1984) 283.
- McKenna, S. J., Astrophys. Space Sc. 108 (1985) 31.
- Mihalas, D., Kunasz, P. B. & Hummer, D. G., ApJ 202 (1975) 465.
- Mihalas, D., Shine, R. A., Kunasz, P. B. & Hummer, D. G., ApJ 205 (1976) 492.
- Mihalas, D., Kunasz, P. B. & Hummer, D. G., ApJ 210 (1976) 419.
- Mihalas, D., Stellar Atmospheres, 2nd Ed. (Freeman, Sanfrancisco 1978).
- Mitchell, A. C. & Zemanski, M. W., Resonance Radiation and Excited Atoms (Cambridge Univ. Press, Cambridge 1934).
- Nagendra, K. N., ApJ 335 (1988) 269.
- Noerdlinger, P. and Rybicki, G., ApJ 193 (1974) 651.
- Peraiah, A. and Grant, I. P., J. Inst. Maths. Appl. 12 (1973) 75.
- Peraiah, A., A & A 46 (1976) 237.
- Peraiah, A., J. Astrophys. Astron. 1 (1980a) 3.

- Peraiah, A., *Acta Astron.* 30 (1980b) 525.
- Peraiah, A., In Kalkofen, W., ed., *Methods in Radiative Transfer* (Cambridge Univ. Press, Cambridge 1984).
- Peraiah, A., *ApJ* 380 (1991) 212.
- Peraiah, A. & Varghese, B. A., *Kodaikanal Obs. Bull.* 12 (1993) 15.
- Preisendorfer, R. W., *Radiative transfer on discrete spaces* (Pergamon, Oxford 1965)
- Redheffer, R. M., *J. Math. Phys.* 41 (1962) 1.
- Rees, D. & Saliba, G., *A & A* 115 (1982) 1.
- Simonneau, E., *A & A* 29 (1973) 357.
- Stenflo, J. O., *Solar Phys.* 37 (1974) 31.
- Stenflo, J. O., *A & A* 46 (1976) 61.
- Stenflo, J. O., *A & A* 66 (1978) 241.
- Stenflo, J. O., *A & A* 84 (1980) 68.
- Stenflo, J. O. & Stenholm, L., *A & A* 46 (1976) 69.
- Stenflo, J. O., Bauer, T. G. & Elmore, D. F., *A & A* 84 (1980) 60.
- Voigt, H. H., *Z. Astrophys.* 28 (1951) 176.
- Warwick, J. W. & Hyder, C. L., *ApJ* 141 (1965) 1362.
- Wiehr, E., *A & A* 38 (1975) 303.
- Wiehr, E., *A & A* 85 (1981) 54.
- Zanstra, H., *MNRAS* 101 (1941) 273.